Probabilistic Risk-based Operation Planning for Wind Integrated Power Systems

by

Nguyen, Dinh Hieu

B.Eng. (Hanoi University of Science and Technology)

Submitted in fulfilment of the requirements for the degree of Doctor of Philosophy

School of Engineering & ICT

University of Tasmania

January 2016

Abstract

Operation planning studies are essential in maintaining and operating a reliable and secure power system. They are based on existing system elements and aim to identify the operating limits within which reliability criteria are satisfied. Traditionally these studies are performed using deterministic criteria. It requires that a power system must be able to withstand an outage of any single component without violating any operating limits. However, it has been recognised that the deterministic method may no longer be adequate to deal with modern power systems with high level of renewable energy penetration.

In particular, high variability and uncertainty of wind power generation may lead to significant load-generation imbalance resulting in large frequency deviations. This increases system operation risk, especially in small and isolated power systems which have low inertia and limited capabilities to provide frequency responses. Therefore, there is a need for investigating alternatives to current power system operation planning approaches to cope with the uncertain nature of the intermittent generation.

This thesis proposes a novel probabilistic risk-based approach to evaluate power system security quantitatively in short-term (e.g., hour/s up to a day) operation planning with significant wind power generation in order to help facilitate day to day system operation. The proposed approach deals with steady-state voltage and overload evaluations as well as frequency deviation analysis. Load flow calculation techniques are used to perform the steady-state voltage and overload evaluations for post-disturbance system conditions. An analytical method to approximate frequency deviations is developed in order to assess the consequence of these frequency events without performing dynamic simulations. As a result, the frequency deviation analysis can be run simultaneously with the steady-state voltage and overload evaluations in the proposed risk assessment. The system operation risk is defined as the product of the probability and severity of system operating states in terms of expected load interruption cost. The risk calculation takes into account both the randomness of contingencies as well as the uncertainty of operating conditions caused

by load and wind power generation forecast errors. The thesis also formulates a security constrained economic dispatch approach to determine operating reserve requirements in wind integrated power systems. This approach co-optimises operation risks resulted from inadequacy of system frequency responses and operation cost including energy price and cost of reserve provision. The effectiveness of the proposed approaches is illustrated by their application to a simplified model of Tasmanian power network, Australia under various system conditions and wind generation scenarios.

Declaration of Originality

This thesis contains no material which has been accepted for a degree or diploma by the University or any other institution, except by way of background information and duly acknowledged in the thesis, and to the best of my knowledge and belief no material previously published or written by another person except where due acknowledgement is made in the text of the thesis, nor does the thesis contain any material that infringes copyright.

Nguyen Dinh Hieu

15 January 2016

Authority of Access

The thesis may be made available for loan and limited copying and communication in accordance with the Copyright Act 1968.

Statement Regarding Published Work

The publishers of the paper comprising Chapters 4 hold the copyright for that content, and access to the material should be sought from the respective journal. The remaining non published content of the thesis may be made available for loan and limited copying and communication in accordance with the Copyright Act 1968.

Statement of Co-Authorship

The following people and institutions contributed to the publication of the work undertaken as part of this thesis:

Candidate: Dinh Hieu Nguyen – School of Engineering & ICT
Author 1: Michael Negnevitsky – School of Engineering &ICT
Author 2: Marian Piekutowski – Hydro Tasmania

Author details and their roles:

Paper 1: "Risk Assessment for Power System Operation Planning with High Wind Power Penetration," ***IEEE Transactions on Power Systems*****, vol. 30, no. 3, pp. 1359-1368, Aug. 2014.**
Located in Chapter 4
Candidate was the primary author and with author 2 and author 3 contributed to the idea, its formalization and development.

We the undersigned agree with the above stated "proportion of work undertaken" for the above published peer-reviewed manuscripts contributing to this thesis:

Signed:

	Michael Negnevitsky	
	Supervisor	Head of School
	School of Engineering & ICT	School of Engineering & ICT
	University of Tasmania	University of Tasmania
Date:	15.01.16	15.01.16

Acknowledgements

First of all, I would like to express my sincerest gratitude to my primary supervisor, Prof. Michael Negnevitsky, University of Tasmania, for his guidance, understanding and support guiding me towards the completion of my research. My recognition and gratitude goes to Dr. Marian Piekutowski, Hydro Tasmania, for his valuable advices, comments and help.

I would like to acknowledge Mr. Derek Jones and TasNetworks for their help and practical discussions. My gratitude goes to my colleagues and all academic staffs, especially Mrs. Mary Dixon and Mr. Justin Courtney, at School of Engineering, University of Tasmania, for giving me a warm and helpful research environment. Special thanks to Mr. Ahsan Latheef, Dr. Thanh Nguyen, Dr. Osman Haruni, and Mr. Koon Wong for their friendship and all the discussion, comments and ingenious ideas.

This thesis could not have been completed without the financial support I received from the Australian Agency for International Development. I greatly appreciate Mr. Chris Dillon and Mrs. Sharmila Prajit for their help and assistance during my study.

I would like to take this opportunity to gratefully acknowledge several friends including Dr. Tran Lam Dong, Dr. Nghiem Quynh Chi, and others from the Vietnamese Community in Hobart for their great friendship and support.

Most of all, I would like to express my deepest gratitude to my family. None of this would have been possible without the love, care, understanding, unconditional support and encouragement over the year of my parents, Nguyen Dinh Hoa, Nguyen Thi Le Thuy, Do Quang Thuy, Tran Thi Phuong and my beloved wife, Do Thi Phuong Chinh and son, Nguyen Duc Minh.

Nguyen Dinh Hieu

List of publications

Refereed journal publications

1. Michael Negnevitsky, Dinh Hieu Nguyen, and Marian Piekutowski, "Risk Assessment for Power System Operation Planning with High Wind Power Penetration," IEEE Transactions on Power Systems, vol. 30, no. 3, pp. 1359-1368, Aug. 2014.

Refereed conferences publication

2. Dinh Hieu Nguyen and Michael Negnevitsky, "Probabilistic Risk-based Security Assessment for Power Systems with Wind Power Generation", in *Proc of 2013 IEEE PES General Meeting,* 21-25 July 2013, Vancouver, BC, Canada, pp. 1-5.
3. Dinh Hieu Nguyen, Michael Negnevitsky, and Marian Piekutowski, "A Risk Assessment Approach for Power System with Significant Penetration Levels of Wind Power Generation", in *Proc of 2013 Australasian Universities Power Engineering Conference (AUPEC),* 29 Sept.-3 Oct. 2013, Hobart, TAS, Australia, pp. 1-6.
4. Dinh Hieu Nguyen and Michael Negnevitsky, "Probabilistic Security Assessment for Power System Operation with Significant Wind Penetration", *in Proc. Of 2012 International Conference on Power System Technology (POWERCON),* 30 Oct.-2 Nov. 2012, Auckland, New Zealand, pp. 1-6.
5. Dinh Hieu Nguyen and Michael Negnevitsky, "A Probabilistic Approach for Power System Security Assessment", *in Proc of 2012 Australasian Universities Power Engineering Conference (AUPEC),* 26-29 Sept. 2012, Bali, Indonesia, pp. 1-6.
6. Dinh Hieu Nguyen and Michael Negnevitsky, "A Review of Fault Ride Through Strategies for Different Wind Turbine Systems", in *Proc of 2010 Australasian Universities Power Engineering Conference (AUPEC),* 5-8 Dec. 2010, Christchurch, New Zealand, pp. 1-5.

Table of Contents

List of Figures

List of Tables

List of Acronyms

AEMO	Australian Energy Market Operator
AGC	Automatic Generation Control
BB	Busbar
CB	Circuit Breaker
CoE	Cost of Energy
CoPR	Cost of Primary Reserve
DFIG	Doubly-fed Induction Generator
EENS	Expected Energy Not Supplied
EFLC	Expected Frequency of Load Curtailment
ELIC	Expected Load Interruption Cost
ELNS	Expected Load Not Supplied
EOC	Expected Operation Cost
FCAS	Frequency Control Ancillary Services
FRI	Frequency Response Inadequacy
GDP	Gross Domestic Product
HVDC	High-Voltage Direct Current
HVRT	High Voltage Ride Through
LCC	Line-Commutated Converter
LVRT	Low Voltage Ride Through
MPC	Market Price Cap
MTTF	Mean Time to Failure
MTTR	Mean Time to Repair
NERC	North American Electric Reliability Corporation

ORR	Outage Replacement Rate
PFR	Primary Frequency Response
PLC	Probability of Load Curtailment
PLL	Phase Locked Loop
PMSG	Permanent Magnet Synchronous Generator
PV	Photovoltaics
RoCoF	Rate of Change of Frequency
TR	Transformer
UFLS	Under Frequency Load Shedding
UIC	Unit Interruption Cost
VOLL	Value of Lost Load
VSC	Voltage-Sourced Converter
WFSG	Wound Field Synchronous Generator
WPG	Wind Power Generation

Blank Page

Chapter 1

Introduction

1.1 Motivation

In an attempt to reduce greenhouse-gas emissions from electric power industry and deal with diminishing natural resources, many countries are increasing the installation of renewable energy, particularly wind power generation (WPG). World wind generation capacity has increased significantly in the last decades. By June 2014 wind power capacity has reached 336 GW and 4% of total worldwide electricity usage is supplied from wind power plants [1]. The total installed wind power capacity in the United States has increased to 62.3 GW by the third quarter of year 2014 and there are over 13.6 GW of wind under construction [2]. The European Union's total installed wind energy capacity reached 117.3 GW in 2013. It would be enough to supply 8% of the EU's electrical power consumption [3]. In Australia, the total installed wind capacity is 3.3 GW as in August 2014 [4] and is forecasted to increase to 11.5 GW by 2020 [5]. The increasing trend towards renewable forms of generation, and in particular wind, is creating new challenges for power system operators.

Operation planning studies are essential in maintaining a reliable and secure power system. These studies are based on existing system elements and aim to identify the operating limits within which reliability criteria are satisfied. Their timescale can vary from half an hour to a week, a month, or any specified period typically less than one year [6]. Security assessment is an important part of the operation planning studies. The assessment is performed for various expected operation states in the studied period [7].

Traditionally security assessment is performed based on deterministic criteria. The deterministic criterion, normally (N-1) criterion, requires that a power system must be able to withstand an outage of any single system component such as a generator, a transformer or a transmission line without violating any system operating

limits. Some utilities are also considering (N-2) or (N-1-1) criteria, which mean the system is required to withstand the removal of any single element due to maintenance and any other due to a failure. This is a worst-case scenario-based criterion – it provides a simple rule in system design and operation, and has satisfied the needs of the power industry for decades.

However, the basic weakness of this criterion is that it does not take into account the probabilistic nature of system behaviour, the uncertainty of demand and generation, and the probabilities of contingencies and network element failures. This may lead to results biased from reality and uneconomic decisions [7]. Moreover, in the deterministic assessment, operating conditions are only either secure or insecure. This method cannot quantify how secure the system is, and hence cannot represent the actual system risk which both utilities and customers are facing. It is also recognised that the deterministic method may no longer be adequate for modern power systems with market driven dispatch and high penetration of renewable energy and distributed generation [8]. Increasing installation of unobservable distributed and photovalics (PV) generation with unknown operating characteristics increases demand uncertainty and forecasting errors. This together with large-scale integration of WPG increases system variability and uncertainty due to wind intermittency and creates a number of technical challenges in the power system planning and operation. This raises a need to investigate new security assessment methods, which can cope with the uncertain behaviour of WPG as well as the probabilistic nature of system conditions and events in the operation planning studies.

In addition, one of the most important tasks of power system operators is to maintain the balance between the electrical power produced by generators and the power consumed by loads including system loses so that the system frequency is maintained at or very close to its nominal level. Power system operators often use scheduling techniques throughout the day to match generation and demand. Additional capacity (generation and responsive load availability) above that needed to meet actual demand is made available either on-line or on-standby so that it can be called on to assist if an imbalance between load and generation occurs resulting in a

frequency deviation. This capacity herein referred to as operating reserves. The way in which the system operators deploy and, especially, the way in which they plan for these reserves can significantly affect the security and efficiency of operating a power system with large amounts of variable generation. Power systems have developed their rules and practices based on a long-standing history of operations with the dominance of conventional synchronous generators. Operating reserve requirements are generally set using deterministic criteria based on system characteristics and tailored to achieve a desired level of risk in each power system. It may remain constant for all operating conditions during the year. One of the most common practices is to schedule the amount of operating reserves equal to the size of the largest online infeed so that the system will be able to withstand the outage of any single generating unit without the need of load shedding. However, many systems are now studying new ways to change these rules and practices where high penetrations of variable generation are becoming apparent. Recent studies that assess the impacts of high penetration of variable generation, particularly WPG, agree that power system operators must find alternative approaches for allocating and deploying operating reserves.

1.2 Scope of the work

Operating future “green” power systems with high penetration of intermittent renewable energy will be a challenging task. Large integration of WPG significantly increases the system variability and uncertainty as well as reduces the system frequency control capability. This leads to a need for larger flexibility from the remaining generation. This flexibility will need to come either from plants that are inherently less flexible or from alternative sources of flexibility. It is likely to increase the cost of wind integration and could potentially compromise the economic viability of power systems with large WPG.

Ensuring secure and cost-effective system operation requires major changes in system planning and operation methods. This thesis focuses on the development of a probabilistic approach to assess the system security in short-term (e.g., hour(s)-ahead)

operation planning with significant WPG in order to facilitate day to day system operation. A security-constrained economic dispatch approach is also developed for determining operating reserve to better cope with large integration of WPG to the grid.

To achieve these objectives, this thesis will address three major questions. These questions and corresponding answers which are also the main contributions of this thesis are outlined as follows.

Question 1: How does large penetration of wind generation affect system operation?

Answering this question requires:

- Understanding wind generation technology and its operating characteristics,
- Understanding how the system is currently operated and identify operation areas which will be affected by integration of WPG.

Question 2a: How to take into consideration the variable and uncertain characteristics of both system conditions (i.e., random contingencies and demand forecasting errors) and WPG in system security assessment?

The security of a power system can be defined as the degree of risk in its ability to withstand random contingencies without interruption to customer service [9]. Risk is a conceptual complement providing better measure of the security [10]. The higher the risk the lower the security, and vice-versa. Although risk cannot be eliminated fully due to unexpected fault events and probabilistic behaviours of power systems, it can be assessed and managed to an acceptable level in power system planning, design and operation activities [11].

A probabilistic approach based on risk assessment techniques is developed to evaluate power systems security quantitatively for short-term operation planning. The system security is represented by a risk index which is the product of probability and severity of system failure in terms of expected load interruption cost taking into account both the randomness of contingencies as well as the uncertainty of future

operating conditions caused by demand and WPG forecasting errors. The proposed approach is concerned with steady-state voltage and overload evaluations, as well as system frequency response adequacy. The adequacy of system frequency responses is defined as the system capability to prevent frequency from dropping below its operating limits [12].

Question 2b: How to incorporate the adequacy assessment of system frequency responses – a dynamic aspect with steady-state voltage and overload evaluations?

Since system frequency is a dynamic variable, adequacy assessment of system frequency responses often requires running dynamic simulations. However, dynamic simulations require dynamic models of system components as well as high computation resources and time. Therefore for fast evaluation of system frequency response adequacy, we develop a mathematical model to represent the dynamic frequency trajectories taking into account the system inertia and frequency control services in generation-load imbalance events. The consequences of these events are hence evaluated analytically in terms of expected load interruption cost. This evaluation is able to run with the steady-state voltage and overload evaluations simultaneously in the main security assessment. A case study will be performed to evaluate the performance of the proposed approach.

Question 3: What is a cost-effective solution for determining operating reserve requirements in the presence of significant WPG?

This thesis develops an optimization approach based on risk assessment techniques to find a cost-effective solution for system operating reserve determination. Firstly, the adequacy of system frequency responses is assessed in terms of operation risk - expected load interruption cost. The resulted risk will then be used to determine the reserve requirements by co-optimizing with energy in a security-constrained economic dispatch in order to minimise total operation cost which is the sum of cost of energy, cost of reserve, and operation risk. As discussed, a number of studies have been done investigating the impact of large scale integration of WPG on system secondary and tertiary frequency control. Therefore, the focus of this thesis is system primary frequency control. A case study will be performed to

evaluate the performance of the proposed approach.

1.3 Thesis structure

Based on the objectives presented and the approach proposed, this thesis is organised as follows.

Chapter 2 discusses operation challenges associated with large scale integration of wind energy. The overview of WPG technology, its operating characteristics, and literature review of wind integration challenges will be presented.

Chapter 3 presents the basic elements of power system risk assessment. The evaluation procedure, system component outage models, and fundamental methods for the risk evaluation will be presented.

Chapter 4 presents a novel approach to quantitative risk evaluation of wind integrated power systems for short-term operation planning. A case study will be performed to evaluate the effectiveness of the proposed approach.

Chapter 5 presents the development of mathematical models of system frequency in load-generation imbalance events, taking into account system inertia and frequency control ancillary services. The mathematical models are used in the proposed risk assessment approach presented in Chapter 4 and Chapter 6.

Chapter 6 presents the probabilistic risk-based approach to determine the operating reserve requirements in the presence of significant WPG. A case study is performed to evaluate the performance of the proposed approach.

Chapter 7 presents the conclusions from this work and proposes directions for future work.

Appendix A present the basic probability concepts used in power system risk assessment.

Appendix B shows the single line diagram of the Tasmanian power network which is used in the case studies presented in Chapter 4 and Chapter 6.

Chapter 2

Operation Challenges of Wind Integrated Power Systems

2.1 Introduction

Developing an assessment approach to the system security for operation planning with significant wind energy requires the understanding of operation challenges caused by large integration of WPG into the system. This chapter presents the overview of WPG technology, its operational characteristics and challenges. It then provides an in-depth literature review of existing system operation procedures and methodologies dealing with these operation challenges.

2.2 Overview of wind power generation

2.2.1 Wind power generation technology

There are four main types of wind turbines:

1. **Type 1**: the type 1 wind turbine uses induction generators directly connected to the grid. It is normally referred to as a constant/fixed speed wind turbine as its rotor speed often varies within a very small range, such as 1% to 2% of the rated speed. Fig. 2.1 shows the main structure of the type 1 wind turbine.
2. **Type 2**: the type 2 wind turbine also uses induction generators directly connected to the grid but are equipped with variable rotor resistance (controlled by power electronics). By changing the rotor resistance, the torque/speed characteristic of the generator is shifted and the rotor speed can vary up to 10% from the nominal rotor speed. Therefore, the type 2 wind turbine is normally referred to as semi-variable speed systems. Fig. 2.2 shows the main electrical and mechanical components of the type 2

wind turbine.

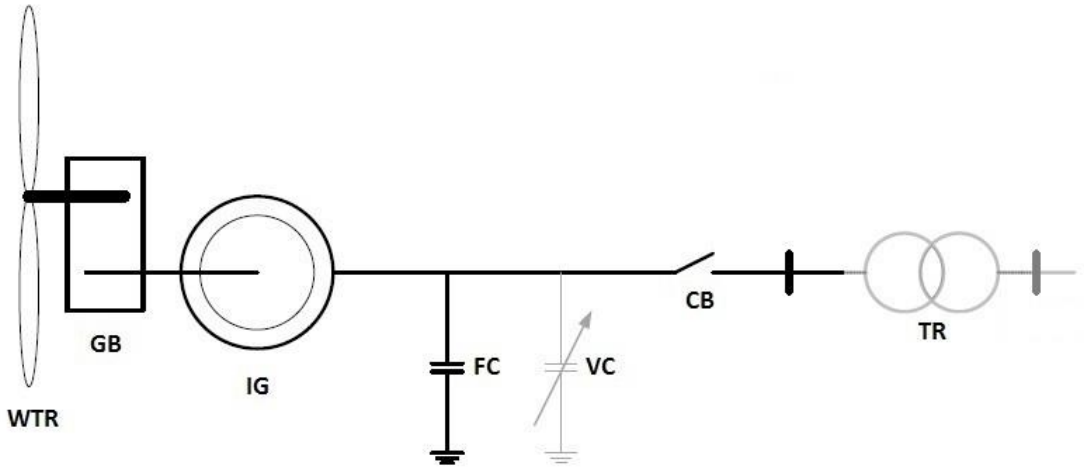

Fig. 2.1. Structure of type 1 wind turbine.

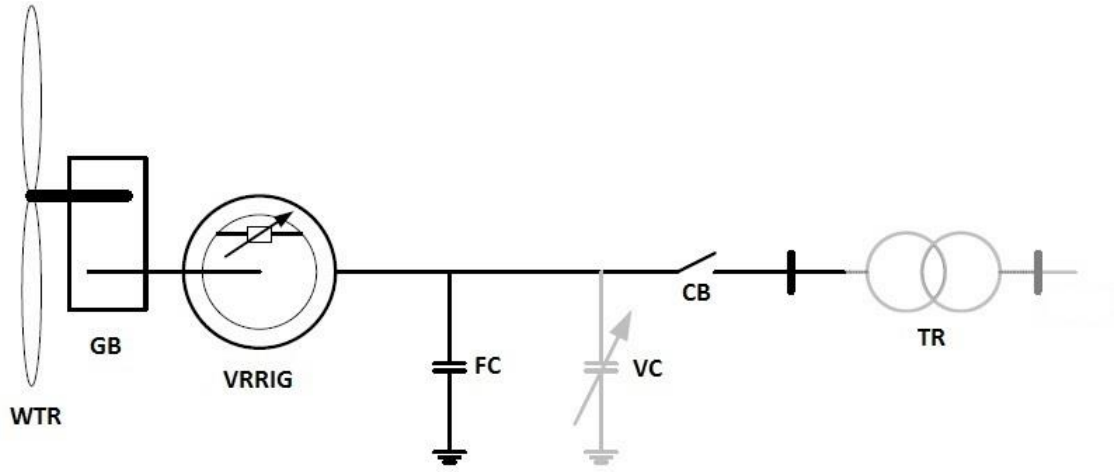

Fig. 2.2. Structure of type 2 wind turbine

3. **Type 3**: the type 3 wind turbine is equipped with a doubly-fed induction generator (DFIG) where the stator is directly connected to the grid and the rotor is connected through a back-to-back power electronics converter. The main structure of the wind turbine is illustrated in Fig. 2.3. The type 3 wind turbine is often considered as a limited variable speed wind turbine with its rotor speed varying around ±30% of the rated speed.
4. **Type 4**: the type 4 wind turbine utilises either synchronous or induction

generators connected to the grid through a full scale power converter. Therefore, it is referred to as a fully variable speed wind turbine. The main mechanical and electrical components of the type 4 wind turbine are shown in Fig. 2.4. Some type 4 wind turbines use direct drive synchronous generators such as permanent magnet synchronous generator (PMSG) or wound field synchronous generator (WFSG), and hence have no gearbox.

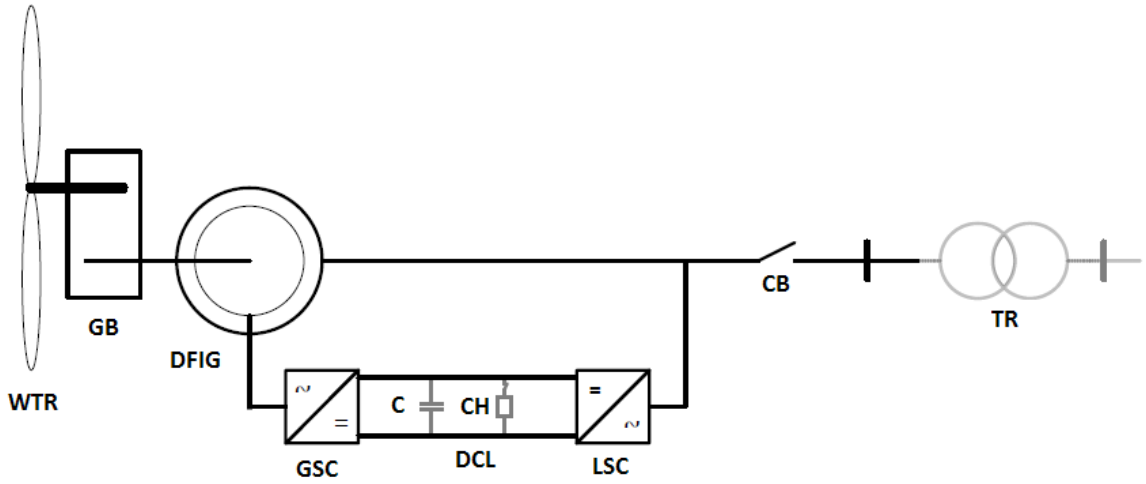

Fig. 2.3. Structure of type 3 wind turbine

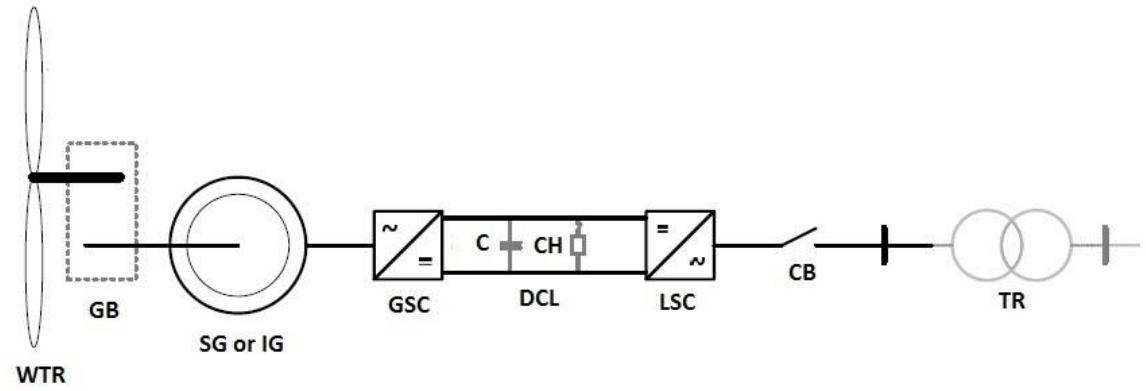

Fig. 2.4. Structure of type 4 wind turbine

The advantage of a constant speed or semi-variable speed wind turbine (Type 1 and 2) is that it is relatively simple and its price is low compared to variable speed wind turbines (Type 3 and 4). However, the type 3 and 4 wind turbines are the most common WPG system nowadays thanks to their superior controllability and operating

performance such as low voltage ride through (LVRT), high voltage ride through (HVRT), frequency support, and power quality to comply with new grid codes for WPG worldwide which are becoming more and more strict.

2.2.2 Characteristics of wind power generation

Wind energy is characterised by high **variability** and **uncertainty**. Variability is the expected changes in power system variables whereas uncertainty is the changes in power system variables that are unexpected. As with other intermittent renewable energy technologies (such as tidal, wave, and solar) WPG has an availability limit that varies over time (variability) due to its dependence on the uncontrolled wind resource. This variability occurs on all time frames of power system planning and operation (seconds to years), with perhaps the most important variations occurring in the 10-minute, 1-hour, and 1-day time frames. However, the impact and possible incurred cost of these variations on the power system depends upon several factors, such as the penetration level and characteristics of the WPG, the characteristics of the system load and generation, and the market flexibility [13]. In addition to being variable, wind energy cannot accurately be predicted (uncertainty) as accurate prediction of future wind speed is not an easy task and the error increases with the forecast time horizon. The uncertainty in wind forecasts can be significant and must be accounted for in system planning and operation. The error inherent in wind power production forecast will impact the system reliability and operation cost as will inaccuracies in assumptions about the forecast errors. Fig. 2.5 shows an example of the variability and uncertainty of WPG output [14].

The uncertainty in WPG output due to wind forecast errors increases the system overall uncertainty. Large WPG forecast errors combined with load forecast errors are much more common and can be more severe compared to load forecasts alone [14]. This may lead to significant load-generation imbalances resulting in large frequency deviations, which in turn, may cause unwanted load shedding (or, in some cases, lead to a system black-out). Meanwhile the variability of wind energy changes the daily commitment of conventional generation. It increases the variability in the system net demand which will require more frequent plant start/stop, partial load operation

(generators running off their peak efficiency points), and ramping capability. In order to cover for the variability and uncertainty of WPG, more operating reserves may need to be scheduled. Fig. 2.6 shows an example of impacts of WPG variability and uncertainty on system operating reserves.

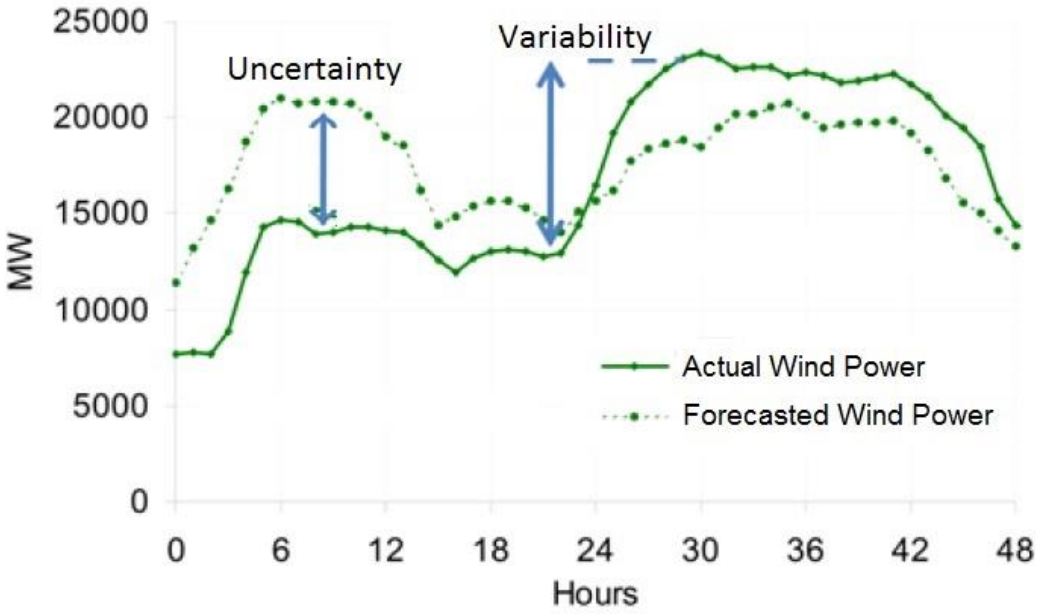

Fig. 2.5. Example of wind energy variability and uncertainty.

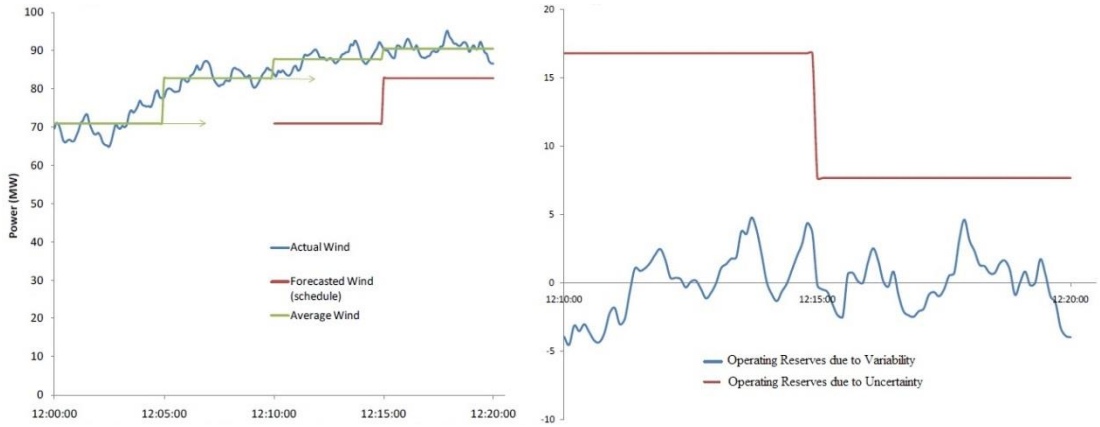

Fig. 2.6. Example of impacts of WPG variability and uncertainty on system operating reserves.

In addition, modern WPG units, particularly electronics converter-based variable-speed wind turbines, also have different mechanism for regulating their output and reacting to changes from the grid, such as voltage or frequency disturbances, compared to conventional thermal and hydropower generating units (**asynchronism**). Firstly, the moving parts of a wind turbine are not synchronised with the system frequency. As a result, the kinetic energy stored in a wind turbine is independent of system frequency. In other words, the contribution of a wind turbine to system inertia is low to zero. Secondly, since wind turbines are normally operated to extract maximum power from wind while wind is an uncontrollable energy source, wind turbines power output cannot be increased in response to a frequency drop like synchronous generators equipped with a governor. Thus, the integration of wind power will reduce the average system inertia and governor ramping capability per unit of installed capacity. Especially, if this integration results in the decommission of conventional power plants, it will reduce the total system inertia and governor ramping capability significantly leading to lower frequency nadirs and higher rate of change of frequency (RoCoF). This may cause unwanted load curtailment due to under-frequency load-shedding and trip of generators triggering by their RoCoF protection relay. Fig. 2.7 shows an example illustrating the effect of large integration of WPG on system frequency.

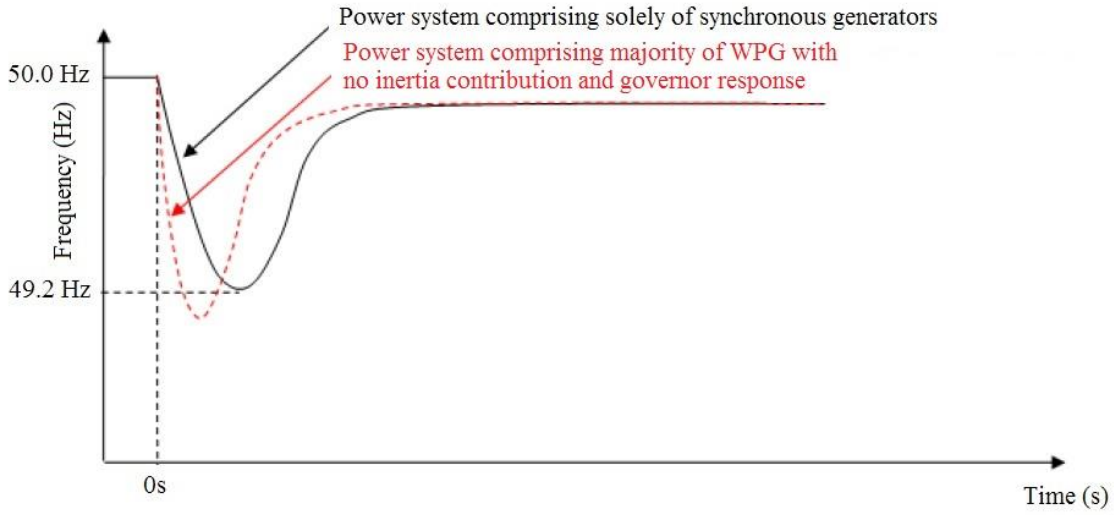

Fig. 2.7. The effect of large integration of WPG on system frequency.

Moreover, modern wind turbines are often equipped with fault-ride-through devices to prevent tripping during low-voltage faults. If a frequency disturbance is accompanied by depressed system voltage, wind generation output is significantly reduced for a short period of time (from about 0.5s to 3s), which increases the magnitude of the frequency excursion [13]. For example, in a small power system, a forced outage of a large generator may lead to a large frequency excursion due to sympathetic trips of unobservable generation. This may also draw voltages throughout the network down. Wind turbines reduce their active power output during and after the fault proportionally to the voltage drop at their terminals due to fault-ride-through operation as shown in Fig. 2.8. This reduction dramatically increases the RoCoF and the maximum dynamic frequency deviation, and hence may lead to under-frequency load-shedding. Detailed description of this phenomenon can be found in [15].

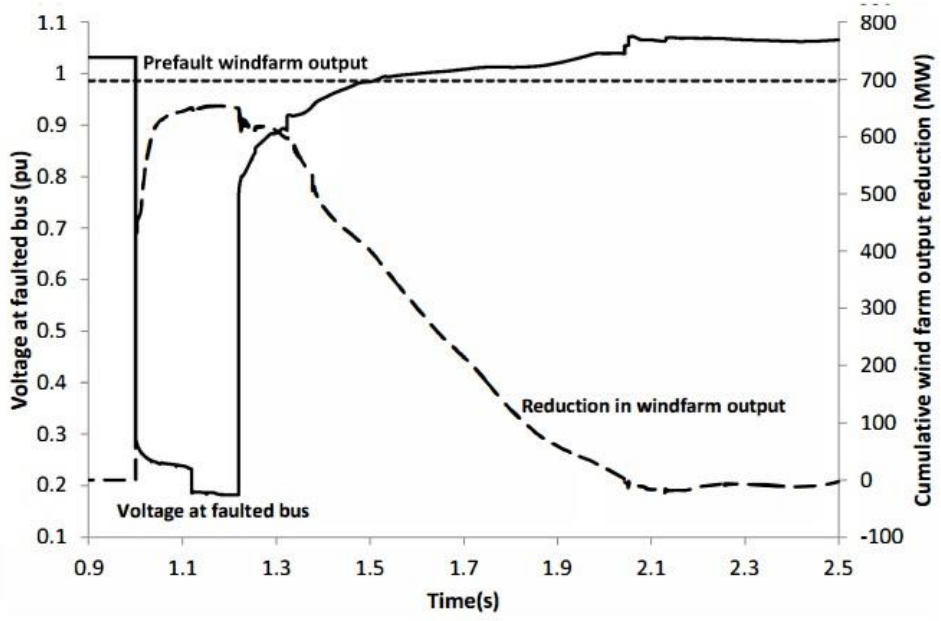

Fig. 2.8. Power reduction of a wind farm during a voltage dip.

These three characteristics – **variability**, **uncertainty**, and **asynchronism** – can cause challenges for maintaining a reliable and secure power system. Many studies have been performed to better analyse these system impacts. Improved strategies to better integrate wind and other variable generation are also being developed by

system utilities, balancing area authorities, regional reliability organizations, and independent system operators. Demand response, energy storage, and improved wind power forecasting techniques have often been described as potential mitigation strategies. In recent years, there is also ongoing research to study the use of WPG units to support power system frequency control capability by providing active power control at fast timescales [16]-[22]. A number of wind power manufacturers have implemented frequency response control algorithms to their turbines.

Although converter-based wind turbines have no inherent inertial and governor responses like synchronous generators do, they are capable of injecting more active power into the grid by utilizing their converter controller in frequency deviation events. There are two types of frequency responses a wind turbine can provide: synthetic inertial and governor (frequency droop) responses. The former utilises the kinetic energy stored in the wind turbine (e.g., gearbox and blades). The release of kinetic energy from a wind turbine can be controlled independently from the RoCoF. In theory it can thus even deliver a larger inertial response than a traditional synchronous generator. However, if the wind turbine is operating below its rated wind speed and hence power output, there will be a recovery period in which the turbine power output needs to reduce for the turbine re-acceleration [23]. This phenomenon is shown in Fig. 2.9 [24]. Whereas the wind turbine governor response requires it to operate at a power output level less than that possible with the available wind speed (wind power curtailment). This means the turbine needs to operate at a sub-optimal operating point which represents a cost that needs to be considered. Therefore, further study is still required to better assess the benefit of the frequency response of wind turbines and its consequences before it can be widely implemented in power system operating schemes and considered as a new ancillary service market design.

2.3 Literature review

Since it is well recognised that the traditional deterministic approach may no longer be adequate to deal with modern power systems with increased variability and uncertainty, probabilistic methods are becoming more attractive because they can

take all variable and uncertain factors into consideration as well as combine consequences and probabilities together to truly represent the system security level. Allan and Billinton [25] reviewed different reliability evaluation methods and their use in modern power systems. The authors proved that probabilistic reliability analysis is promising and would become increasingly common and used in practice. Billinton and Mo [26] illustrated the rigidity of the deterministic criteria and proposed a probabilistic approach to assess variable risks associated with the loss of generation and transmission system components. An integrated probabilistic cost-benefit analysis is proposed in [27] for making system operational decisions. It enhances economic efficiency whilst maintaining the system security.

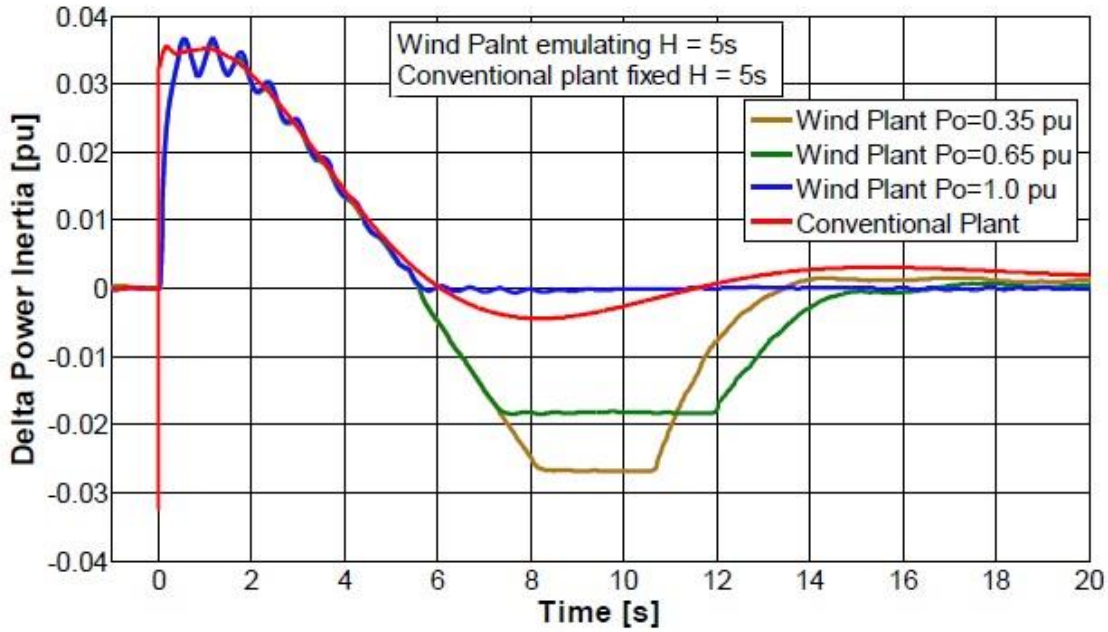

Fig. 2.9. Inertial response of wind power plant.

A probabilistic steady-state security assessment using Monte Carlo approach is presented in [28] introducing performance indices which are used to assess the impact of contingencies on power system security. These indices allow assessing accurately the influence of overloads, voltage limit violations and voltage stability problems in the power system. The authors developed a probabilistic software package based on the proposed approach. Ma *et al.* [29] presented a probabilistic approach based on the

power flow analysis and voltage distribution to evaluate the power system vulnerability in terms of voltage magnitudes and loading of transmission lines. The proposed probabilistic analysis is conducted without Monte Carlo simulation to avoid computational time-consuming problems especially for large scale power systems. In [30], a comprehensive power system reliability assessment based on probabilistic approach is presented. This integrated approach addressed the issues of component reliability as well as the system reliability. Both an enumerative approach and Monte Carlo simulation were used. The study also introduced a probabilistic approach for estimating available transfer capability.

A comprehensive series of papers in probabilistic risk-based approaches for a various type of security assessment have been published by McCalley and his associates [8], [10], [31]-[39]. These assessment approaches take into account the probability of a predefined set of contingencies, normally N-1 contingencies, as well as the uncertainty of future load. The consequence of these contingencies is measured in terms of the violation of operating constraints that these contingencies would cause. However, although both elements of the risk assessment are taken into consideration, the result is only an indirect quantification of the system risk faced by network users [14]. The relation between the estimated risk values and the impact of contingencies on these users such as cost of load interruption or price of electricity generation is not clear. A severe constraint violation with high severity value does not necessarily indicate a large load interruption and vice-versa.

Another approach to the probabilistic risk-based security assessment has been developed by Kirschen and his associates [40]-[43]. In these works, the authors generate system contingencies at random instead of using a predefined list of contingencies. The impact of these random events is measured in terms of load not served and then translated into energy not supplied using a model of load restoration process. The value of energy not supplied is multiplied by the estimated value of lost load to form the expected cost of an outage that is used to assess the system risk level. The weakness of this approach is that it requires a significant amount of computing resources as it relies on Monte Carlo simulations.

In [44], the authors presented a stochastic model capturing the uncertainties in the system load at the wind generator bus to approximate the randomness experienced by the system. This stochastic assessment investigates the security and stability of a WPG system on an electrical utility to quantify the operational limits of the system. Wind power integration is also studied in [45] using probabilistic approach. This study investigates different stochastic characteristics in the wind energy integration including wind resource availability, generation facility outage, and transmission availability. The proposed probabilistic approach can assess the reliability capacity cost for wind energy integration with the power system for maintaining system reliability.

A stochastic mixed integer linear optimization scheduling model is built in [46] to minimise system operation costs; load and wind power production were treated as stochastic inputs. The model is used to study operational impacts of future high wind penetrations in Ireland. Risk assessment techniques are also used in [47], [48] for short-term wind power commitment and operation planning of wind integrated power systems. A comprehensive review of probabilistic and risk-based approaches in power system planning is presented in [6]. This review identifies the motivations, current status, gaps, and future directions of probabilistic and risk-based planning methods. New innovative reliability and risk evaluation methods in power system planning and operation with high penetration of WPG are also presented in [49].

Probabilistic methods are also used to determine operating reserve requirements in order to cope better with the increased system variability and uncertainty caused by large integration of WPG. Bouffard *et. al.* [50]-[52] used probabilistic methods and stochastic programming to formulated a short-term forward electricity market-clearing problem with stochastic security capable of accounting for non-dispatchable and variable WPG. The proposed stochastic approach allows the improvement of the economic performance of the market by taking advantages of the freely-available wind power and by reducing reserve scheduling and hydro-thermal generation unit commitment costs. The stochastic approach also permits the expansion of the feasible

space of the security-constrained market-clearing problem and hence allows greater wind power penetration without sacrificing security.

Doherty and O'Malley [53] proposed an approach to set spinning reserve requirements based on a predefined minimum system reliability level considering the installed wind capacity. However, setting a single level of reliability to be achieved at all periods of the optimization horizon results in suboptimal solutions as the cost and benefit of the reserve provision depends on several factors such as system demand, WPG output and units committed. In [54] the authors considered the wind forecast uncertainty and set the reserve requirements at 3.5 times of the standard deviation of the net demand (demand minus WPG) error to capture more than 99.7% of system imbalances. However this approach ignores the probability and extent of the system's contingencies and simply set larger amounts of spinning reserves as the total WPG production increases. Dany [55] studied the impact of WPG on primary, secondary and tertiary reserves. He concluded that these reserve requirements increase proportionally to the installed WPG capacity. However, this conclusion does not take into account the cost of providing reserves.

Persaud *et. al.* [56] concluded that the spinning reserve requirements are inversely proportional to the net demand forecasting accuracy. Therefore, when WPG is integrated to a power system, larger amounts of reserve would be required to maintain the same level of system security. However, this conclusion is drawn on the assumption that the reserve requirement is set based on a predefined security index. As a result the authors do not consider the balance that should be attained between the cost of and benefit of spinning reserves for an efficient economic operation. Ortega-Vaquez and Kirschen [57], [58] proposed a probabilistic method to estimate the optimal spinning reserve requirements and operating costs in a power system with significant WPG. Probabilistic techniques are used in [59], [60] to determine system reserve requirements for wind power integration. A probabilistic framework for optimal reserve scheduling and N-1 secure daily dispatch of systems with significant wind power is also proposed in [61]. It is generally agreed that large integration of WPG will result in an increase in the required amount of operating reserves to

maintain system reliability. System operators should use the available information to estimate the system operating risk, and then schedule operating reserves accordingly. In addition, the cost of providing reserves is far from negligible and should be taken into account when determining the reserve requirements [58].

However, most of these studies assume that WPG fast fluctuations can be compensated by conventional generation units and the variations in the time frame of primary control reserve is small compared to the load variations and outages of large conventional units. Therefore, the impact of large scale WPG integration on primary reserve requirements and performance is negligible [52], [58]-[61]. These studies mainly focus on the steady state behaviour of the secondary and tertiary frequency control to estimate the expected social cost of load interruptions due to insufficient operating reserves. None of them consider dynamic frequency responses in determining the reserve requirement. Only few recent studies focus on the impact of WPG on the adequacy of primary frequency response (PFR) [62], [63]. While this assumption is usually valid in large systems with high inertia and primary control reserves, this may not be true in small and isolated power systems, which have low inertia and limited capabilities of providing fast frequency responses. As discussed, in these power systems, large scale integration of WPG may significantly reduce the system inertia and governor ramping capability as well as increase the rate of change of frequency. In addition, with increasing penetration of WPG, a sudden change in residual load (demand minus wind generation) caused by unforseen sudden changes in demand and/or wind generation may lead to large load-generation imbalances. These may lead to significant frequency deviations, which in turn, may cause unwanted load shedding or, in some cases, lead to a system black-out. Even in large power systems, if the penetration of renewable energy reaches a certain level replacing a large portion of synchronous generators, this may reduce the system frequency security [64]. Therefore, it is necessary to re-assess the system primary frequency control capability and the methods of determining reserve requirements in the presence of high penetration of WPG.

Chapter 3

Power System Risk Assessment

3.1 Introduction

This chapter presents the basic elements of power system risk assessment including the evaluation procedure, system component outage models, and fundamental evaluation methods.

Reliability is one of the most important aspects of power system planning and operation. Reliability is defined as "the degree to which the performance of a power system could results in power being delivered to consumers within accepted standard and desired amount" according to the North American Electricity Reliability Council (NERC). The performance of a power system in reacting to component failures or sudden disturbances can be judged acceptable or unacceptable by reliability criteria. Reliability of power systems in much of the literature is divided into two different concepts: adequacy and security [65]. Adequacy criteria is defined as reliability criteria in terms of violations of static failure conditions while reliability criteria based on dynamic factors are called security criteria. However, in practice and many research works, the term security is often used to cover both aspects of reliability. It is an umbrella word to capture both static and dynamic failure conditions that help to identify the limits of acceptable operating conditions for a power system. These include overload, under-voltage, voltage instability, transient instability, transient voltage dip, and oscillatory instability [8]. Reliability/security analyses involve evaluating numerous system contingencies at different operating conditions; analysing their consequences to customers, transmission system and generation utilities; revealing the most influential factors affecting reliability; identifying the operating limits within which reliability criteria are satisfied; and the finding the most efficient/economical ways to enhance system reliability [66].

Over the last decades, the application of risk assessment in reliability analyses has drawn ever-increasing interest in the electric utility industry, particularly since large power outage events happened across the globe in recent years. Risk and reliability can be considered to have identical implication. They are the two facets of the same fact [11]. Risk can be considered as a conceptual complement providing better measure of reliability/security [10]. The higher the risk the lower the security, and vice-versa. The root origin of risk is the probabilistic behaviour of power systems. Random failures of system components are generally out of control of power system operators. There are always uncertainties in load forecast. Power flows, energy exports and imports under the deregulation environment depend on the volatile energy market. The integration of intermittent renewable energy sources such as wind and PV also introduce other uncertain factors into power systems. Risk assessment and management has become more and more challenging and an essential part in power system design, planning and operation today.

There are three main tasks in risk assessment and management [11]. The first task is performing quantitative risk evaluation. The objective of this evaluation is to create the quantitative risk indices which should recognise not only the probability of failure events but also the severity of their consequences. Secondly, measures to reduce risk need to be determined. In order to do this, both the impact of the measures on risk reduction and the cost associated with the measures should be quantified. The third task is to justify an acceptable risk level. A very important point to be recognised is that zero risk can never be achieved as random contingencies are unpredictable and uncontrollable. In many situations, a risk level has to be accepted as long as it is technically and financially justified.

Risk management has become ever-increasingly important since the introduction of the deregulation framework in the electrical power industry. The new competitive operation framework forces utilities to plan and operate their system closer to the limit leading to deterioration is system reliability [11]. The large scale integration of intermittent energy sources which brings more uncertainties to the

system also emphasise the importance of proper risk management in order to maintain a reliable and secure power system.

3.2 Quantitative risk evaluation

Random contingencies caused by outages of system components such as generators, transformers and transmission lines are unavoidable and uncontrollable in power system operation. They represent the main causes of a system failure state and system risks. The first step in system risk evaluation is to develop component outage models and then calculate the probabilities of these events. Component failures are classified into two categories: independent and dependent outages. They can be further classified according to the outage models such as repairable forced outages or planned outages. The probabilities of component outages depend on several factors including weather conditions, environment, equipment age, and operating conditions.

The second step is to select system failure states and calculate their probabilities. There are two main methods to do this: state enumeration and Monte Carlo simulation. Both methods have advantages and disadvantages. The former one is generally more efficient if complex operating conditions are not considered while Monte Carlo method is more preferable when complex operating conditions are considered and the number of severe events is large.

The third step is to conduct the analysis for system failure states and evaluate their consequences. The type of analysis is determined by the system under study. It could be a simple power balance calculation, or a complex calculation process including power flow, optimal power flow, or even dynamic, transient and stability evaluation. In order to perform a quantitative risk analysis, an index/indices truly representing system risk should be created. The indices will serve as risk indicators that reflect a number of factors such as load/generation profiles and forecast uncertainties, component outages, and operational conditions.

A power system consists of three fundamental functional zones: generation, transmission, and distribution. Performing a risk evaluation for the whole system is often impractical as such a system is too enormous to handle in terms of study scale,

computing capacity, and accuracy requirements. In this case, risk assessment is conducted in each functional zone, or composite generation and transmission systems. By doing so, the assessment is more realistic.

In power system risk evaluation, collecting reliability data is as important as developing evaluation methods. The required data are the parameters of component outage models. They are normally calculated from historical statistics of system components. The data must be sufficient to ensure the quality of the risk assessment as well as restrictive enough so that unnecessary data are not collected. For a simple model, the data of failure and restoration process of system components are needed. For a more complex model, the data related to transitions rates between different states of the components is required. It is very important to note that the ability to include a complex model and high degree of precision in calculation should not override the unavoidable uncertainty in the data.

3.3 Component outage models

As mentioned earlier, components outages can be generally classified into two categories: independent and dependent. The independent outages can be further broken down to 4 subcategories which are planned, forced, semi-forced outages, and partial failures. There are also various types of dependent outages such as common-cause outage or cascading outage. A typical example of common-cause outages is a simultaneous failure of two overhead lines on the same tower due to tower failure or lightning strikes. Malfunction protection coordination may result in failure of several components leading to a cascading outage. These dependent outages often lead to much more severe consequences than independent outages. In addition, the typical characteristic of dependent outages is that an outage state includes more than one component failure. The probability of this dependent outage state is often larger than the probability of concurrent independent failures of the same components. Therefore, system risk associated with dependent outages is often much higher than the one caused by independent outages.

3.3.1 Independent outages

3.3.1.1 Planned outage

Planned outages are scheduled by personal for maintenance, replacement, or an operational requirement. Two methods can be applied to model a planned outage. The first method assumes that the failure and recovery time of a planned outage follow given distributions. The distribution parameters are estimated from historical data of planned outage activities. In the first method, a planned outage is considered as a random event. Its state transition diagram is shown in Fig. 3.1.

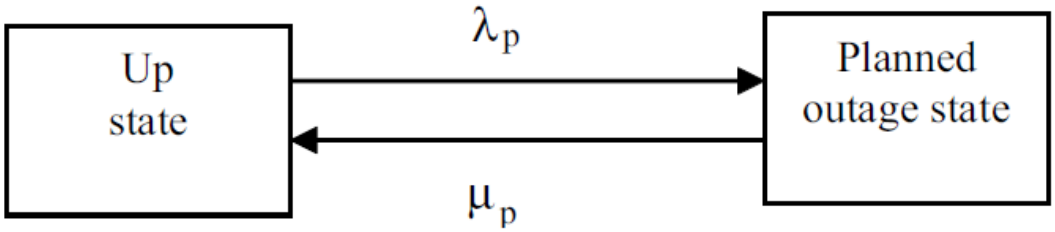

Fig. 3.1. State transition diagram for planned outages.

Therefore, the average unavailability due to planned outage is

$$U_p = \frac{\lambda_p}{\lambda_p + \mu_p} = \frac{MTTR_p}{MTTF_p + MTTR_p} = \frac{f_p \times MTTR_p}{8760} \tag{3.1}$$

where λ_p, μ_p, and f_p are the failure rate (failures/year), the repair rate (repairs/year), and the average failure frequency (failures/year) due to planned outages, respectively. $MTTR_p$ is the mean time to repair (hours) and $MTTF_p$ is the mean time to planned outage (hours). From Equation (3.1), the following relationships can be obtained.

$$\mu_p = \frac{8760}{MTTR_p} \tag{3.2}$$

$$\lambda_p = \frac{8760}{MTTF_p} = \frac{f_p}{1 - f_p/\mu_p} \tag{3.3}$$

$$f_p = \frac{8760}{MTTF_p + MTTR_p} = \frac{\lambda_p}{1 + \lambda_p/\mu_p} \tag{3.4}$$

It is important to note that λ_p and f_p are two different terms as this can be seen from Equations (3.3) and (3.4). In most cases, they are numerically close as normally $MTTR_p \ll MTTF_p$. However $MTTR_p$ can be quite large in some certain cases, such as the repair time for a sub-marine cable.

The second method is to recognise a planned outage as the scheduled event that occurs at pre-determined intervals but not a random event. For example, an overhead line is scheduled to be out of service for three days for maintenance. This planned outage will be defined by its start and end dates and can be easily modelled by taking out the component during the planned outage period in the simulation process.

3.3.1.2 Forced outage

Force outages occur randomly and are uncontrollable. Most of forced outages in power systems are repairable, whereas some fatal failure events which are non-repairable can also happen. Similar to planned outages, repairable forced outages can be modelled by a state transition diagram shown in Fig. 3.2.

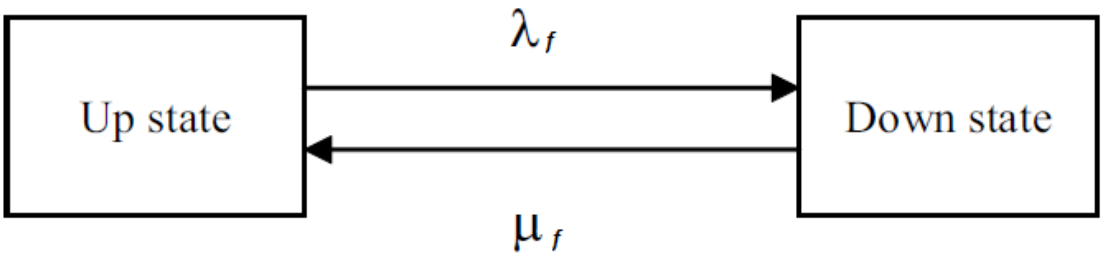

Fig. 3.2. State transition diagram for repairable forced outages.

and the component unavailability due to repairable forced outage is

$$U_f = \frac{\lambda_f}{\lambda_f + \mu_f} = \frac{MTTR_f}{MTTF_f + MTTR_f} = \frac{f_f \times MTTR_f}{8760} \tag{3.5}$$

where λ_f, μ_f, f_f, $MTTR_f$, and $MTTF_f$ are the failure rate (failures/year), the repair rate (repairs/year), the average failure frequency (failures/year), the mean time to repair (hours), and the mean time to failure (hours), respectively.

We also can combine Fig. 3.1 and Fig. 3.2 to create a state space diagram for a system component with both planned and repairable forced outage as shown in Fig. 3.3.

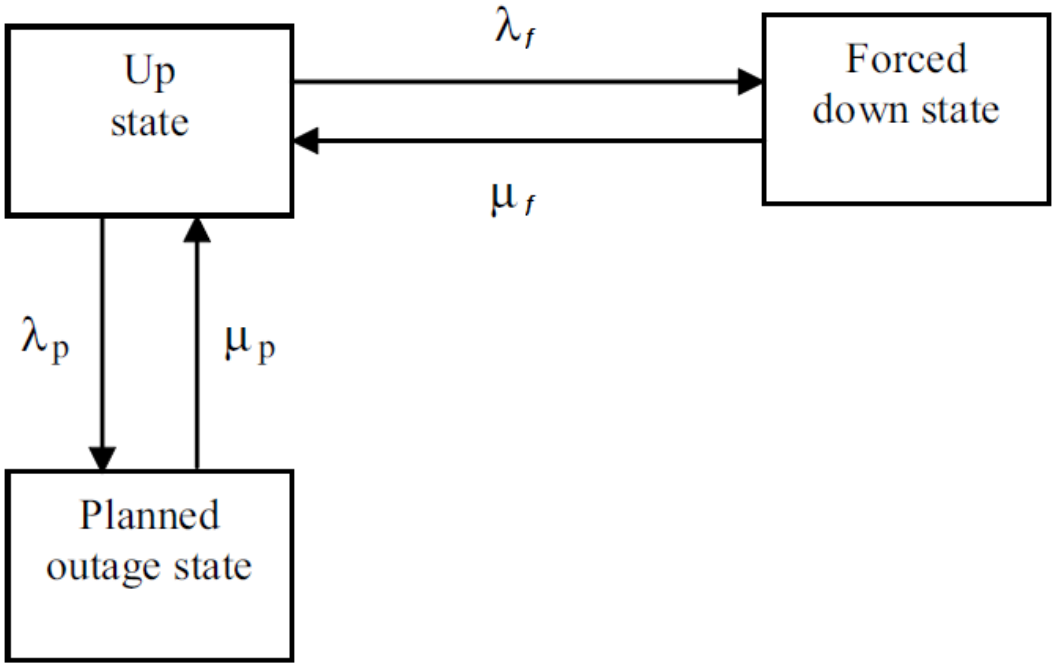

Fig. 3.3. State space diagram for both planned and repairable forced outages.

Applying Markov method [11] to the above state diagram we have

$$f_p = \frac{\lambda_p \mu_p \mu_f}{\lambda_p \mu_f + \lambda_f \mu_p + \mu_p \mu_f} \tag{3.6}$$

$$f_f = \frac{\lambda_f \mu_f \mu_p}{\lambda_p \mu_f + \lambda_f \mu_p + \mu_p \mu_f} \tag{3.7}$$

$$P_p = \frac{\lambda_p \mu_f}{\lambda_p \mu_f + \lambda_f \mu_p + \mu_p \mu_f} = \frac{f_p}{\mu_p} \tag{3.8}$$

$$P_f = \frac{\lambda_f \mu_p}{\lambda_p \mu_f + \lambda_f \mu_p + \mu_p \mu_f} = \frac{f_f}{\mu_f} \tag{3.9}$$

$$P_{up} = \frac{\mu_p \mu_f}{\lambda_p \mu_f + \lambda_f \mu_p + \mu_p \mu_f} = \frac{f_p}{\lambda_p} = \frac{f_f}{\lambda_f} = \frac{f_p + f_f}{\lambda_p + \lambda_f} = \frac{f}{\lambda} \tag{3.10}$$

where P_p, P_f, and P_{up} are the probabilities of the planned outage, repairable forced outage and up states of the component, respectively. The total failure probability is

$$U_{total} = P_p + P_f = \frac{\lambda_p \mu_f + \lambda_f \mu_p}{\lambda_p \mu_f + \lambda_f \mu_p + \mu_p \mu_f} \tag{3.11}$$

However, in reality the outage frequencies and repair times of components are recorded instead of the outage rates. Therefore, it is often assumed that planned outages and repairable forced outages of a system component are not mutually exclusive in order to reduce the complexity in collecting input data. The planned and repairable forced outages are then represented using two separate two-state models as shown in Fig. 3.1 and 3.2. In this case, the total failure probability is

$$U_{total} = 1 - (1 - U_p)(1 - U_f) = \frac{\lambda_p \mu_f + \lambda_f \mu_p + \lambda_p \lambda_f}{\lambda_p \mu_f + \lambda_f \mu_p + \lambda_p \lambda_f + \mu_p \mu_f} \tag{3.12}$$

The difference between Equations (3.11) and (3.12) is only associated with the term of $\lambda_p \lambda_f$ in both the denominator and numerator. As generally $\lambda_p \ll \mu_p$ and $\lambda_f \ll \mu_f$ the difference is negligible.

3.3.1.3 Semi-forced outage

Semi-forced outages refer to the case in which a system component sustains a physical issue leading to an outage with a time delay that depends on a forced reason but can be scheduled. For example, a transformer with oil leakage does not immediate fail but will do so within a limited time. This time delay depends on several factors such as the severity of leakage, the availability of manpower for repair, or the possibility of reducing the leakage by some temporary measures. Therefore, semi-forced outages are generally included in risk assessment for short-term operation planning but excluded in long-term system planning. It is also important to note that although a semi-force outage can be scheduled, it cannot be treated as a planned outage because its time delay is limited. It also cannot be considered as a deterministic event since the issue happens randomly. The state space diagram for a semi-forced outage is shown in Fig. 3.4.

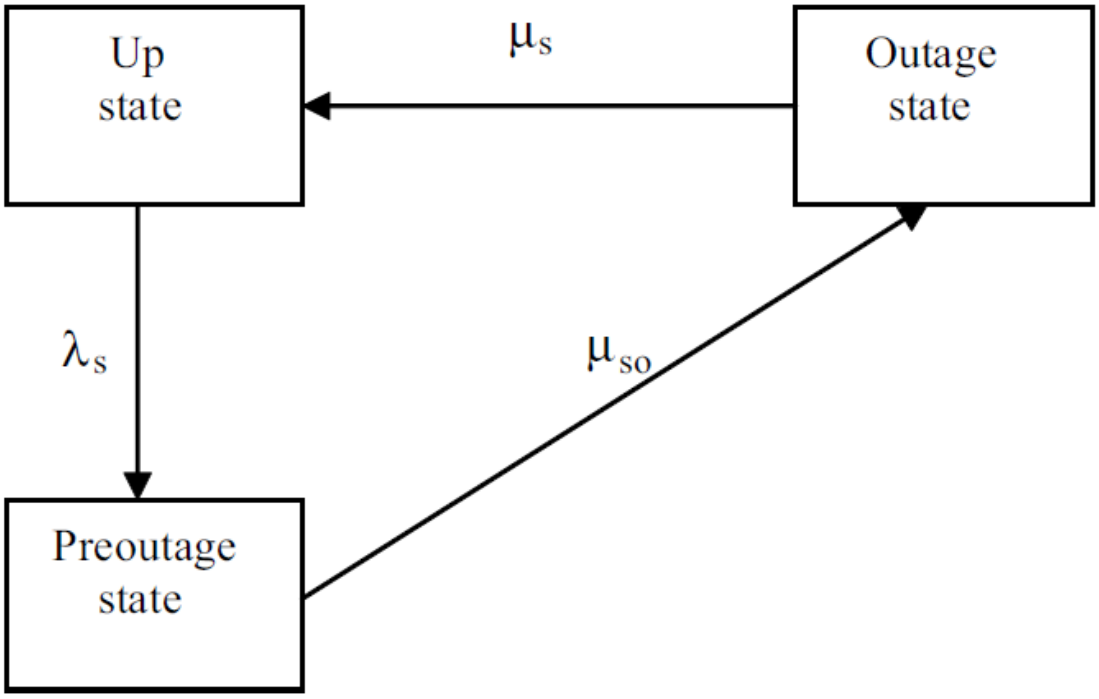

Fig. 3.4. State space diagram for a semi-forced outage.

Applying Markov approach to the model we can obtain the following formulas:

$$f_s = \frac{\lambda_s \mu_s \mu_{so}}{\lambda_s \mu_s + \lambda_s \mu_{so} + \mu_s \mu_{so}} \tag{3.13}$$

$$P_{sp} = \frac{\lambda_s \mu_s}{\lambda_s \mu_s + \lambda_s \mu_{so} + \mu_s \mu_{so}} = \frac{f_s}{\mu_{so}} \tag{3.14}$$

$$P_{so} = \frac{\lambda_s \mu_{so}}{\lambda_s \mu_s + \lambda_s \mu_{so} + \mu_s \mu_{so}} = \frac{f_s}{\mu_s} \tag{3.15}$$

$$P_{su} = \frac{\mu_s \mu_{so}}{\lambda_s \mu_s + \lambda_s \mu_{so} + \mu_s \mu_{so}} = \frac{f_s}{\lambda_s} \tag{3.16}$$

where λ_s, μ_s, and μ_{so} are the transition rate from the up state to the pre-outage state, the repair rate which is the reciprocal of the repair time, and the transition rate from the pre-outage state to the outage state which is the reciprocal of the time delay, respectively. f_s is the frequency of the issue occurrence per year. P_{sp}, P_{so}, and P_{su} are the probabilities of the pre-outage, outage, and up states of the component. Generally, there are three steps to calculate these probabilities. Firstly, historical data or an

engineering analysis could be used to estimate the average values of f_s, the repair time (μ_s), and the time delay (μ_{so}). Secondly, λ_s is calculated using Equation (3.13). The third step is to use Equations (3.14) to (3.16) to calculate the three state probabilities of the semi-forced outage.

3.3.1.4 Partial failure

A partial failure of a system component is when the component sustains a non-severe problem leading but can still operate in a derated state. Fig. 3.5 shows a three state transition diagram of a component with partial failure. However, in reality, a repair is often carried to bring the component back to the full-up state but not the derated state. Therefore, it is reasonable to ignore the transitions between the derated and full-down states. The new simplified state space diagram is shown in Fig. 3.6.

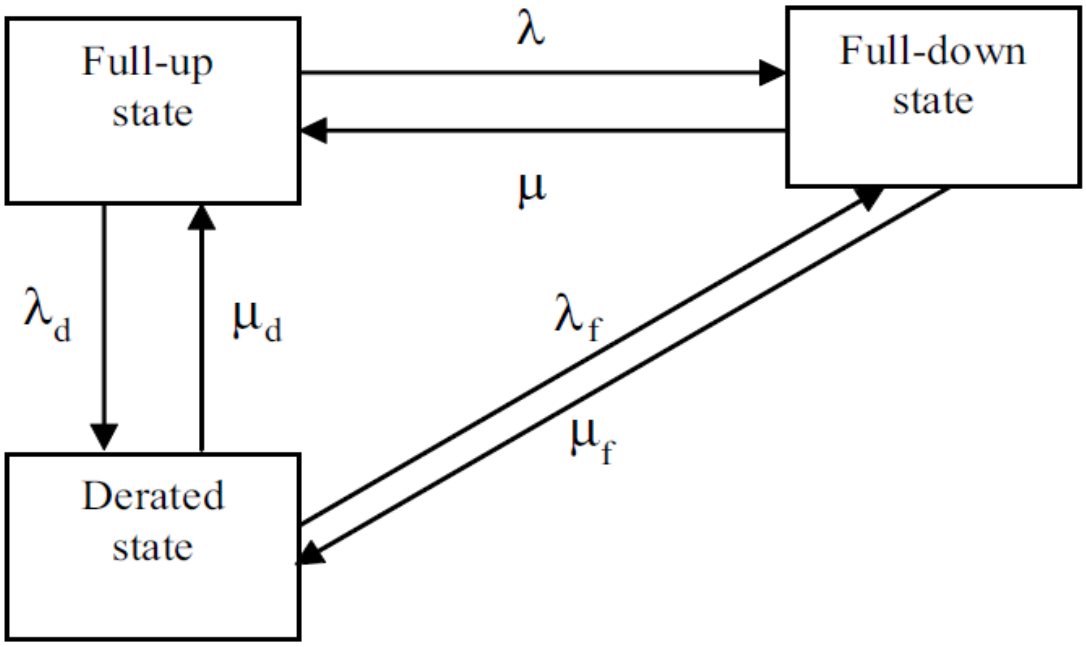

Fig. 3.5. State space diagram for a component with a derated state.

Applying Markov method to the above state diagram we have

$$f = \frac{\lambda\mu\mu_d}{\lambda\mu_d + \lambda_d\mu + \mu\mu_d} \tag{3.17}$$

$$f_d = \frac{\lambda_d \mu_d \mu}{\lambda \mu_d + \lambda_d \mu + \mu \mu_d} \tag{3.18}$$

$$P_{down} = \frac{\lambda \mu_d}{\lambda \mu_d + \lambda_d \mu + \mu \mu_d} = \frac{f}{\mu} \tag{3.19}$$

$$P_{derated} = \frac{\lambda_d \mu}{\lambda \mu_d + \lambda_d \mu + \mu \mu_d} = \frac{f_d}{\mu_d} \tag{3.20}$$

$$P_{up} = \frac{\mu \mu_d}{\lambda \mu_d + \lambda_d \mu + \mu \mu_d} = \frac{f}{\lambda} = \frac{f_d}{\lambda_d} \tag{3.21}$$

where λ and μ are the transition rates between full-up and full-down states; , λ_d and μ_d are the transition rates between full-up and derated states; f and f_d are the frequencies of full failure and derating events. P_{down}, $P_{derated}$, and P_{up} are the probabilities of full failure, derated and up states of the component, respectively.

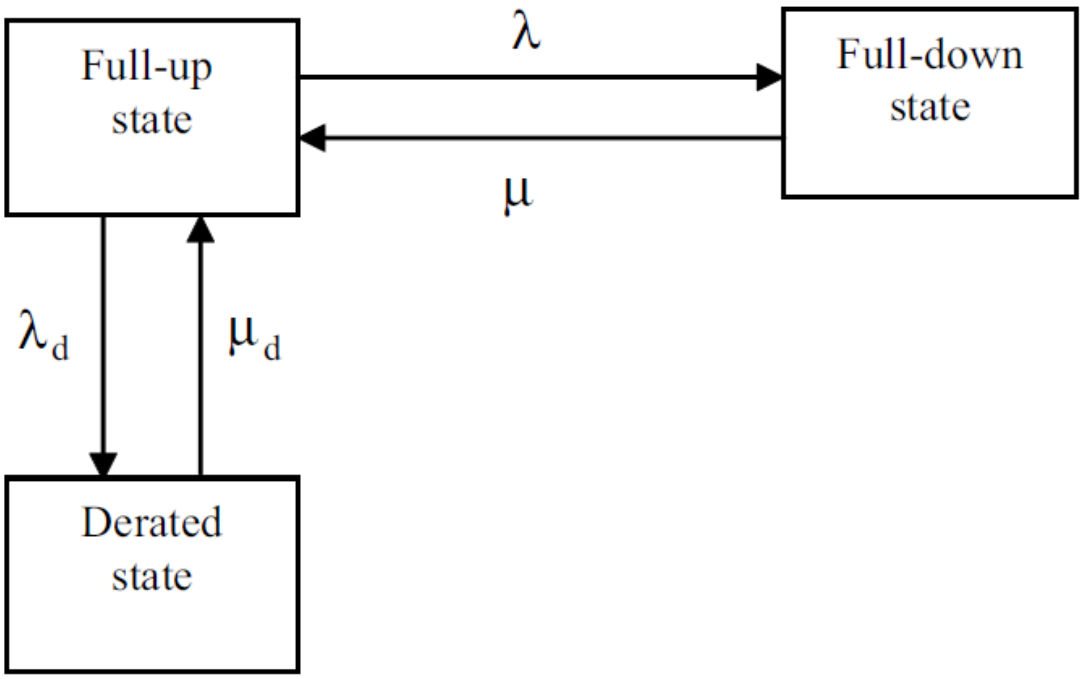

Fig. 3.6. Simplified state space diagram for a component with a derated state.

3.3.2 Dependent outages

3.3.2.1 Common-cause outage

A common-cause outage refers to coincident failures of various components due to a common cause. Typically, a common-cause outage is combined with independent outages into a composite state space model [66]. An example of two components is shown in Fig. 3.7.

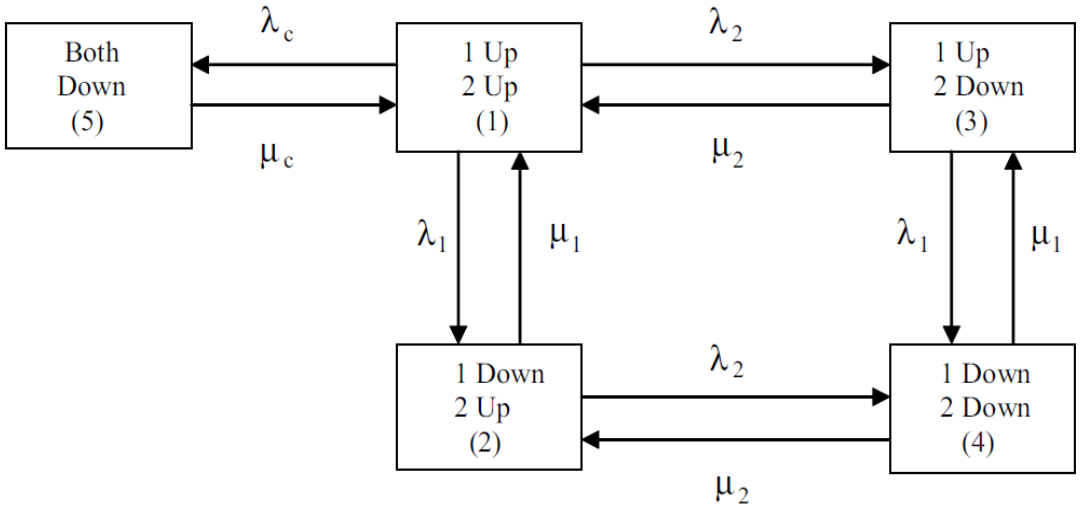

Fig. 3.7. State space diagram for a common cause outage including two components.

The above composite model has been widely used for years. However, it has two disadvantages. Firstly, it assumes that an independent outage and a common-cause outage are mutually exclusive but this is not always the case. Let's consider the model of two overhead lines on the same tower. An independent failure of the lines can happen at the same time as the tower failure. The second advantage is the complexity of the composite model if there are more than two components. The number of states in the model increases exponentially with the number of components.

There is another approach to model common-cause outages. It is to use the individual two-state models for the common-cause failure and each independent failure, and the intersection concept for combinations of the failures. These outages are independent and not exclusive from each other. This approach is shown in Fig. 3.8.

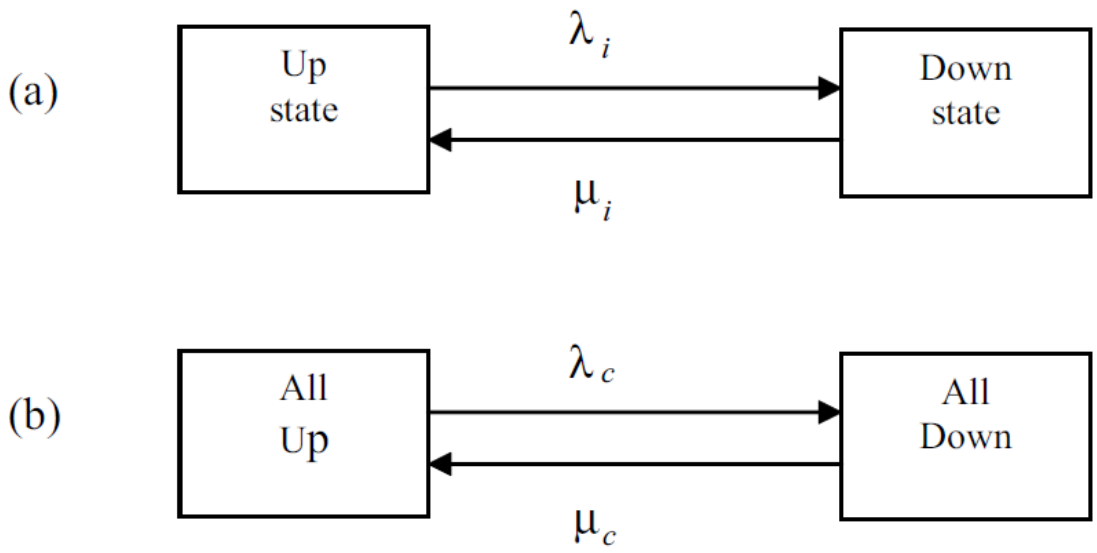

Fig. 3.8. Two-state individual models for independent (a) and common-cause (b) failures.

The individual models can be represented using the following equations:

$$\lambda_i = \frac{f_i}{1 - f_i/\mu_i} \qquad (i = 1, \dots, n) \tag{3.22}$$

$$P_{iD} = \frac{\lambda_i}{\lambda_i + \mu_i} \qquad (i = 1, \dots, n) \tag{3.23}$$

$$P_{iU} = \frac{\mu_i}{\lambda_i + \mu_i} \qquad (i = 1, \dots, n) \tag{3.24}$$

$$\lambda_c = \frac{f_c}{1 - f_c/\mu_c} \tag{3.25}$$

$$P_{cD} = \frac{\lambda_c}{\lambda_c + \mu_c} \tag{3.26}$$

$$P_{cU} = \frac{\mu_c}{\lambda_c + \mu_c} \tag{3.27}$$

where λ_i, μ_i and f_i are the failure rate (failures/year), repair rate (repairs/year), and the failure frequency (failures/year) of the *i*th component (there are *n* components in

total); P_{iD} and P_{iU} are the probabilities of the *i*th component in the down and up states; λ_c, μ_c and f_c are the failure rate, repair rate, and the failure frequency of the common-cause outage of the *n* components; P_{cD} and P_{cU} are the probabilities of the common-cause outage happening and not happening.

3.3.2.2 Component-group outage

When a component in a group consisting of several components fails leading to concurrent outages of all the components, this is called a component-group outage. It is similar to and can be considered as a specific case of the common-cause outage. The only difference is that any component associated with the common-cause failure can also have its independent failure, whereas in the component-group outage all the components always go to outage state together. Therefore, the two-state model shown in Fig. 3.8(b) and Equations (3.25) to (3.27) can be used for a component-group outage. Fig. 3.9 shows an example of the group failure. It is a simple network with two lines transferring power from a generator through a transformer. There is a circuit breaker (CB) at the end of each line. These two breakers (CB1 and CB2), busbar (BB) and transformer (TR) form a group of four components. A short-circuit on any of the components will result in their simultaneous outages.

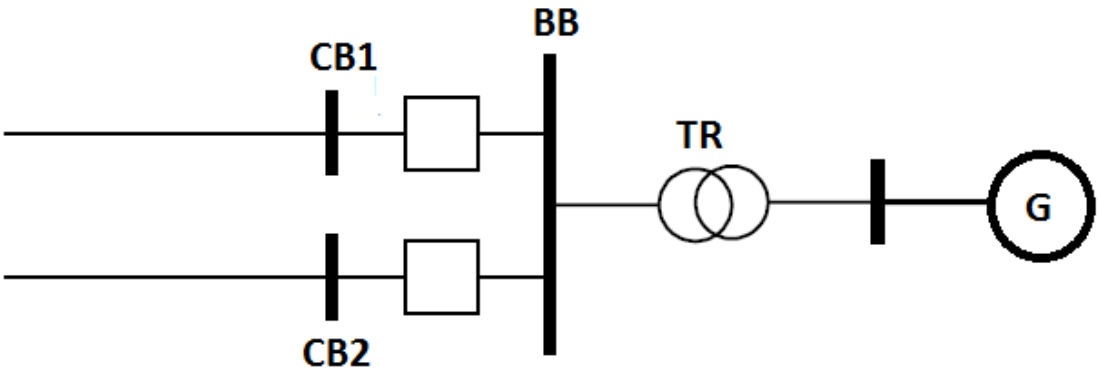

Fig. 3.9. An example of a component-group outage.

3.3.2.3 Cascading outage

A cascading outage is defined as an event in which a component failure leads to consecutive failures of other components. The first component failed is called the

cascading outage trigger. A cascading outage is often the main reason for a whole system blackout. The state space diagram for a cascading outage is shown in Fig. 3.10.

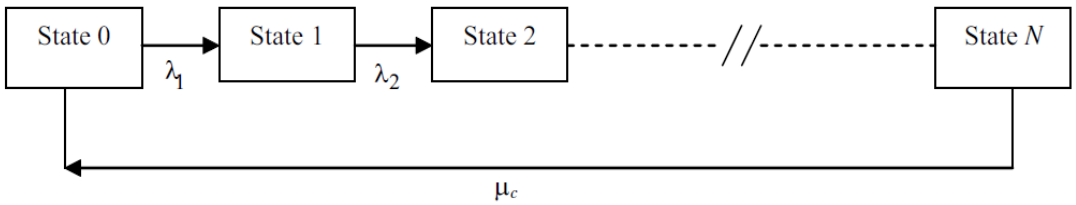

Fig. 3.10. State space diagram for a cascading outage.

where State 0 indicates the normal state; State 1 corresponds to the failure of the trigger component; State 2 to the second component's outage; and so on. It is assumed that all the failed components would return to service (normal state) at the same time. A set of equations for the model can be obtained using Markov method as this has been done for the previous outage models. However, in real systems only State 0 and *N* are considered as the transition from a state *i* to state *i+1* is very fast that no action can be carried out. This assumption allows use of the simple model between State 0 and *N*, which is similar to that for the common-cause outage shown in Fig. 3.8(b). State 0 indicates that all the components are up, whereas all of them are down in State *N*. Failure and repair rates between the two states are those of the trigger component.

3.4 Risk evaluation methods

There are four fundamental methods in power system risk evaluation [11]: the probability convolution, series and parallel networks, Markov equations, and frequency-duration approaches. The main objective of these methods is to calculate risk indices. The methods are selected from a number of general reliability techniques since they are important concepts and can be directly applied to simple power system risk assessment. For example, Markov equations and the series network concept have been used to develop the outage models of individual components as shown in previous sections.

For risk assessment of large and complex power systems, selection of system states and calculation of their probabilities are two key processes. There are two main methods to select system states as mentioned earlier: state enumeration and Monte Carlo simulation. Both methods have advantages and disadvantages. The former one is generally more efficient if outage probabilities of components are quite small and complex operating conditions are not considered. Monte Carlo method is more preferable when complex operating conditions are considered and/or the number of severe events is large.

3.4.1 Probability convolution

The mathematical definition of convolution is as follows. Assuming that two independent random variables *X* and *Y* have the probability density functions *g(x)* and *h(y)*, respectively. The probability function *s(z)* of the random variable *Z=X-Y* is the following integral, which is called convolution:

$$s(z) = \int_{-\infty}^{+\infty} g(w) \times h(w - z) dw \tag{3.28}$$

In some simple cases, a risk assessment is nothing more than the probability convolution. For example, the core function of a generation system risk assessment is calculation of the difference between the generation capacity and the load level as two random variables following probability distributions. This is the concept of probability convolution.

In power system risk assessment, a risk index is often the mean value of the random variable Z. The mean can be theoretically calculated with the probability density function *s(z)*. However, as Equation (3.28) is not suitable for use in actual application, it is better to develop the discrete expression of the difference between the two random variables. Given the two random variables *X* and *Y* with the following discrete probability density function

$$\begin{cases} p(X = X_i) = p_i & (i = 1, \dots, n) \\ p(Y = Y_j) = p_j & (j = 1, \dots, m) \end{cases} \tag{3.29}$$

the mean value of the random variable *Z* is

$$\bar{Z} = \sum_{i=1}^{n}\sum_{j=1}^{m}(X_i - Y_j)p_i p_j \tag{3.30}$$

A risk index is often the mean value of Z under a given condition. For example, if X represents the load level and Y represent the generation capacity, the expected load not supplied (ELNS) should be the mean of Z under the condition of $X>Y$. It is easy to incorporate this condition in the discrete convolution as shown below:

$$\bar{Z} = \sum_{i=1}^{n}\sum_{j=1}^{m} max(0, X_i - Y_j)p_i p_j \tag{3.31}$$

3.4.2 Series and parallel networks [67]

The series and parallel network is defined here as the logical relationship between the failure/success of the network and the failure/success of its components. A series network is defined as a network in which a failure of any of its components leads to the network failure or all the components must be up for the network success. In contrast, a parallel network is a network in which all the components must fail for the network failure or only one of its components needs to be up for the network success.

The series or parallel network does not refer to a topological structure of power system components, even though it is often consistent with the topology of a physical system. A radial distribution system generally can be modelled as a series network. A transmission line with double circuits can be modelled as a parallel network. A simple transmission system consists of towers and double overhead lines or a simple substation configuration can be represented as a network including series and parallel branches.

3.4.2.1 Series network

Let us consider the case of two repairable components in series as shown in Fig. 3.11. From the definition of the series network, we can have the following equations:

$$U_{series} = U_1 + U_2 - U_1 U_2 \tag{3.32}$$

$$\lambda_{series} = \lambda_1 + \lambda_2 \tag{3.33}$$

$$A_{series} = A_1 A_2 \tag{3.34}$$

where A indicates the availability, U the unavailability, and λ the failure rate; the subscripts *1*, *2* and *series* represent Components 1, 2, and the equivalent series network, respectively. For a repairable system, combining Equations (3.1) and (3.34) we have

$$(1 - \frac{\lambda_{series}}{\lambda_{series} + \mu_{series}}) = (1 - \frac{\lambda_1}{\lambda_1 + \mu_1})(1 - \frac{\lambda_2}{\lambda_2 + \mu_2}) \tag{3.35}$$

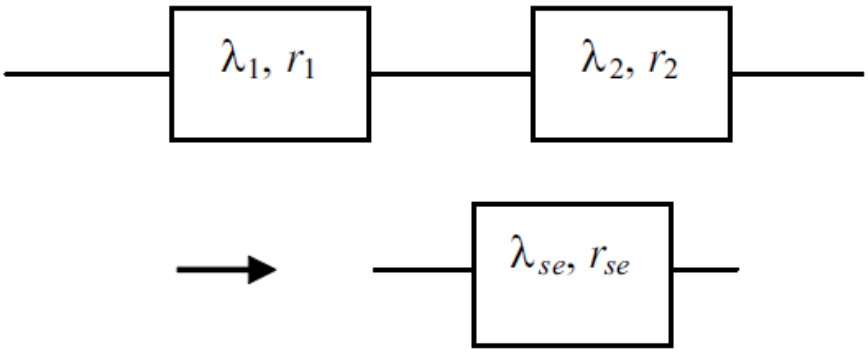

Fig. 3.11. Equivalent series network of two repairable components.

By substituting Equation (3.33) into (3.35) and the relationship between r the repair time and μ the repair rate, the equivalent repair time and the failure frequency for the series network can be calculated by

$$r_{series} = \frac{\lambda_1 r_1 + \lambda_2 r_2 + \lambda_1 r_1 \lambda_2 r_2}{\lambda_1 + \lambda_2} \tag{3.36}$$

$$f_{series} = f_1(1 - f_2 r_2) + f_2(1 - f_1 r_1) \tag{3.37}$$

Equations (3.32) to (3.34), (3.36), and (3.37) are used to calculate risk indices of the series network. Although these equations are derived from the network of two components, it is also straightforward to apply them to a series network of several components. Firstly, it is applied to any two components. Then the equivalent series network of the first two components is considered as a single component and combined with the third component, and so on.

3.4.2.2 Parallel network

The equivalent parallel network of two repairable components is shown in Fig. 3.12.

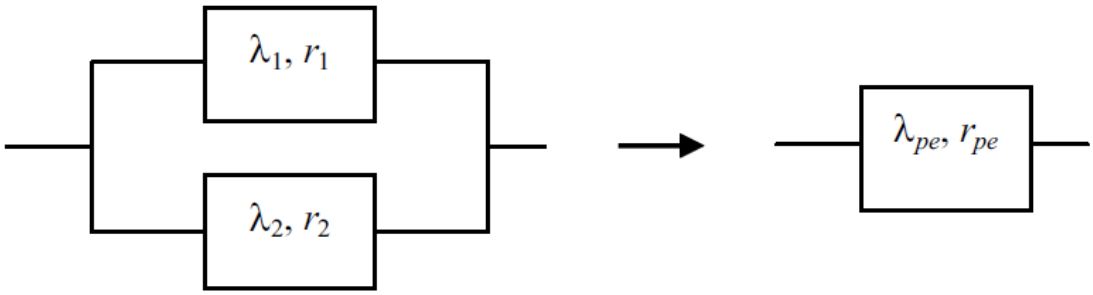

Fig. 3.12. Equivalent parallel network of two repairable components.

From the definition of parallel network, we have:

$$U_{parallel} = U_1 U_2 \tag{3.38}$$

$$\mu_{parallel} = \mu_1 + \mu_2 \tag{3.39}$$

$$A_{parallel} = A_1 + A_2 - A_1 A_2 \tag{3.40}$$

$$r_{parallel} = \frac{r_1 r_2}{r_1 + r_2} \tag{3.41}$$

All the symbols are the same as those defined in Section 3.4.2.1 except the subscript *parallel* represent the equivalent parallel network. For repairable components, using Equations (3.1) and (3.38) gives

$$\frac{\lambda_{parallel}}{\lambda_{parallel} + \mu_{parallel}} = \left(\frac{\lambda_1}{\lambda_1 + \mu_1}\right)\left(\frac{\lambda_2}{\lambda_2 + \mu_2}\right) \tag{3.42}$$

Substituting Equation (3.41) into (3.42), we get

$$\lambda_{parallel} = \frac{\lambda_1 \lambda_2 (r_1 + r_2)}{1 + \lambda_1 r_1 + \lambda_2 r_2} \tag{3.43}$$

Applying Equations (3.41) and (3.43) we obtain

$$f_{parallel} = f_1 f_2 (r_1 + r_2) \tag{3.44}$$

Equations (3.38) to (3.41), (3.43), and (3.44) are used to calculate risk indices of the parallel network. Similarly these equations can be repeatedly applied to a parallel network of multiple components. A network consisting of both series and parallel branches can be assessed through combinations of the equations derived in Section 3.4.2.1 and 3.4.2.2.

3.4.3 Markov equations [67]

The Markov equation method is based on a state space diagram. It is very useful in modelling the failures of individual components as shown in Section 3.3. The Markov approach can be used to solve both the time dependent and limiting state probabilities. The former is represented by a set of differential equations while the latter by a set of algebraic equations. In power system risk assessment, there are often limiting state probabilities and hence only the Markov equations for limiting state probabilities is considered.

The main advantage of this technique is the clear picture of all states and transitions between them. However, it is difficult to apply the method to a large system since the number of system states increases exponentially with the number of components. For a system with N two states (up and down) components, the number of system states is 2^N. When N is large, it is impossible to draw a state space diagram.

Let us use the system consisting of two repairable components as an example to explain the Markov method. There are 6 steps:

1. Step 1: Build a state space diagram according to the transitions of component states. Fig. 3.13 shows the four states and their transitions for the system.
2. Step 2: Build the transition matrix based on the state space diagram. The number of columns and rows of the matrix are the same as the number of system states. Or in other words, each system state corresponds to one row and one column. If there is a transition from State *i* to State *j*, the transition rate is filled as the element at the *i*th row and *j*th column. Otherwise, the element is filled by zero. The diagonal element in each row is filled by a

value so that the sum of all elements in this row is *1.0*. For the given system with two repairable components, the transition matrix is

$$\boldsymbol{T} = \begin{bmatrix} 1-(\lambda_1+\lambda_2) & \lambda_1 & \lambda_2 & 0 \\ \mu_1 & 1-(\mu_1+\lambda_2) & 0 & \lambda_2 \\ \mu_2 & 0 & 1-(\lambda_1+\mu_2) & \lambda_1 \\ 0 & \mu_2 & \mu_1 & 1-(\mu_1+\mu_2) \end{bmatrix} \tag{3.45}$$

It should be noted that the transition matrix $\boldsymbol{T}$ given by Equation (3.45) is not a probability matrix as λ and μ are not probabilities.

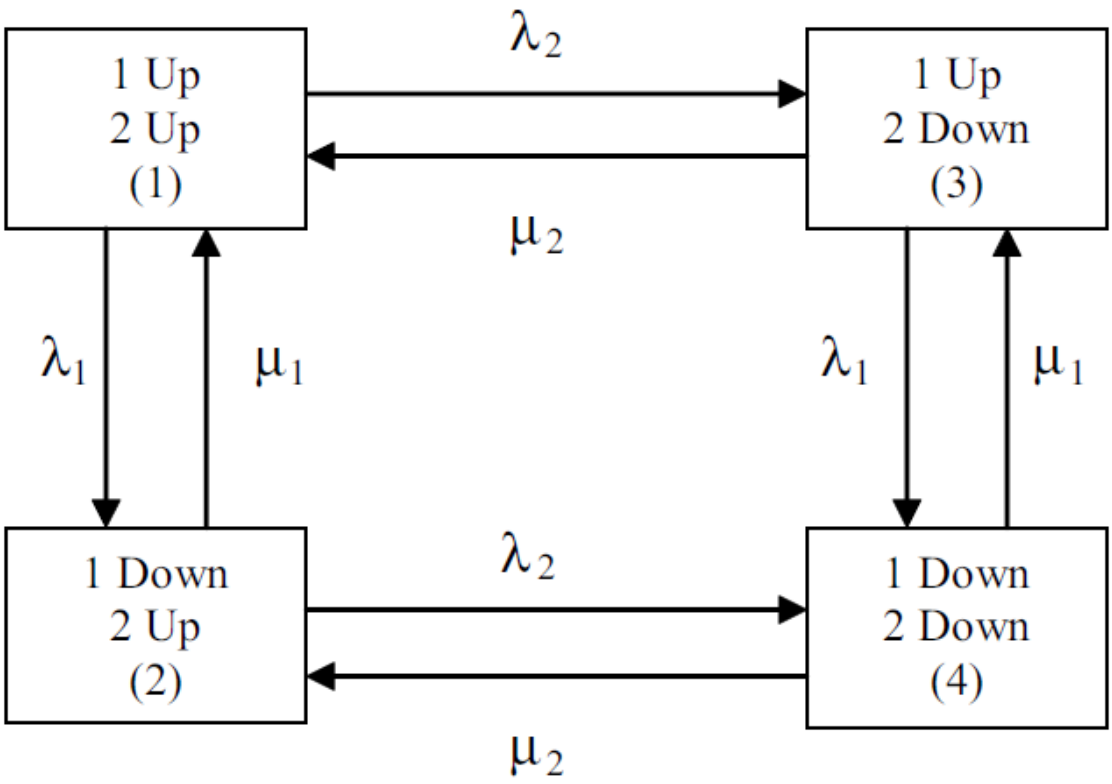

Fig. 3.13. State space diagram of two repairable components.

3. Step 3: Apply the Markov method which states that the limiting state probabilities would not change in the further transition process. It can be expressed as

$$\boldsymbol{PT} = \boldsymbol{P} \tag{3.46}$$

where $\boldsymbol{P}$ is the limiting state probability vector. Equation (3.46) can be rewritten as

$$\boldsymbol{P}(\boldsymbol{T}-\boldsymbol{I})=\boldsymbol{0} \tag{3.47}$$

where $\boldsymbol{I}$ is the unit matrix. For the given system, Equation (3.47) is expressed in a full matrix form as follows

$$[P_1 \quad P_2 \quad P_3 \quad P_4]\begin{bmatrix}-(\lambda_1+\lambda_2) & \lambda_1 & \lambda_2 & 0\\ \mu_1 & -(\mu_1+\lambda_2) & 0 & \lambda_2\\ \mu_2 & 0 & -(\lambda_1+\mu_2) & \lambda_1\\ 0 & \mu_2 & \mu_1 & -(\mu_1+\mu_2)\end{bmatrix}$$
$$=[0 \quad 0 \quad 0 \quad 0] \tag{3.48}$$

Equation (3.48) can be rewritten as

$$\begin{bmatrix}-(\lambda_1+\lambda_2) & \mu_1 & \mu_2 & 0\\ \lambda_1 & -(\mu_1+\lambda_2) & 0 & \mu_2\\ \lambda_2 & 0 & 1-(\lambda_1+\mu_2) & \mu_1\\ 0 & \lambda_2 & \lambda_1 & 1-(\mu_1+\mu_2)\end{bmatrix}\begin{bmatrix}P_1\\P_2\\P_3\\P_4\end{bmatrix}=\begin{bmatrix}0\\0\\0\\0\end{bmatrix} \tag{3.49}$$

4. Step 4: Add the full probability condition – the sum of the probabilities of all system states should be 1.

$$[P_1+P_2+P_3+P_4]=1 \tag{3.50}$$

The Markov matrix equation obtained in Step 3 has a rank of *N-1*, where *N* is the number of system states. In other words, only *N-1* equations are independent and the full probability condition has to be added. In the given example, Equation (3.50) will replace any one of the four equations in Equation (3.49) in order to solve the four system state probabilities. If the first equation in (3.49) is replaced by Equation (3.50) we have

$$\begin{bmatrix}1 & 1 & 1 & 1\\ \lambda_1 & -(\mu_1+\lambda_2) & 0 & \mu_2\\ \lambda_2 & 0 & 1-(\lambda_1+\mu_2) & \mu_1\\ 0 & \lambda_2 & \lambda_1 & 1-(\mu_1+\mu_2)\end{bmatrix}\begin{bmatrix}P_1\\P_2\\P_3\\P_4\end{bmatrix}=\begin{bmatrix}1\\0\\0\\0\end{bmatrix} \tag{3.51}$$

5. Step 5: Solve the Markov matrix equation obtained in Step 4 using a linear algebraic algorithm. For the given example, the solution is as follows:

$$P_1 = \frac{\mu_1\mu_2}{(\lambda_1+\mu_1)(\lambda_2+\mu_2)} \tag{3.52}$$

$$P_2 = \frac{\lambda_1\mu_2}{(\lambda_1+\mu_1)(\lambda_2+\mu_2)} \tag{3.53}$$

$$P_3 = \frac{\mu_1\lambda_2}{(\lambda_1+\mu_1)(\lambda_2+\mu_2)} \tag{3.54}$$

$$P_4 = \frac{\lambda_1\lambda_2}{(\lambda_1+\mu_1)(\lambda_2+\mu_2)} \tag{3.55}$$

6. Step 6: The frequency and duration can be calculated if necessary using the frequency-duration method described in the next subsection.

3.4.4 Frequency-duration approaches [67]

The frequency-duration method is a technique to calculate the frequency and duration from the state probabilities and transition rates. The frequency of encountering State *i* is calculated by

$$f_i = P_i \sum_{k=1}^{M_d} \lambda_k = \sum_{j=1}^{M_e} P_j\lambda_j \tag{3.56}$$

where P_i is the probability of State *i*, P_j is the probability of a state directly communicating to State *i*, λ_k or λ_j is the transition (failure or repair) rate, M_d is the number of the rates departing from State *i*, and M_e is the number of the rates entering State *i*. Equation (3.56) also indicates the basic concept in the frequency balance method, that is the frequency of leaving a state is equal to the frequency of entering the state for any state in an ergodic system. For example, the frequency of leaving or entering State 1 in Fig. 3.13 is

$$f_1 = P_1(\lambda_1+\lambda_2) = P_2\mu_1 + P_3\mu_2 = \frac{\mu_1\mu_2(\lambda_1+\lambda_2)}{(\lambda_1+\mu_1)(\lambda_2+\mu_2)} \tag{3.57}$$

The frequency of transition from State *i* to State *j* is calculated by

$$f_{ij} = P_i\lambda_{i-j} \tag{3.58}$$

where P_i is the probability of State *i* and λ_{i-j} is the transition rate from State *i* to State *j*. Generally, $f_{ij} = f_{ji}$ if there are both transitions from State *i* to State *j* and vice versa in an ergodic system. For example, the two transition frequencies between State 1 to State 2 in Fig. 3.13 are

$$f_{12} = f_{21} = P_1\lambda_1 = P_2\mu_1 = \frac{\mu_1\mu_2\lambda_1}{(\lambda_1 + \mu_1)(\lambda_2 + \mu_2)} \tag{3.59}$$

The mean duration of staying in a state is the reciprocal of the sum of all departure rates and can be calculated directly from the state space diagram:

$$d_i = \frac{1}{\sum_{k=1}^{M_d} \lambda_k} \tag{3.60}$$

where d_i is the mean duration of staying in State *i*. λ_k and M_d are the same as defined in Equation (3.56). For State 1 in Fig. 3.13, the mean duration is

$$d_1 = \frac{1}{\lambda_1 + \lambda_2} \tag{3.61}$$

3.4.5 State enumeration

State enumeration is based on the expansion of the following expression:

$$(P_1 + Q_1) \times (P_1 + Q_1) \times \ldots \times (P_N + Q_N) \tag{3.62}$$

where P_i and Q_i are the success and failure probabilities of the *i*th component and *N* is the number of components in the system. The probability of a system state is given by

$$P(s) = \prod_{i=1}^{N_f} Q_i \prod_{j=1}^{N-N_f} P_j \tag{3.63}$$

where N_f and $N - N_f$ are the numbers of failed and non-failed components in State *s*, respectively. $N_f = 0$ in the normal state in which all the components are up. Then Equation (3.63) becomes

$$P(s) = \prod_{i=1}^{N} P_i \tag{3.64}$$

Based on the concepts given in Section 3.4.4, the system state frequency and the mean duration are calculated as follows

$$f(s) = P(s) \sum_{i=1}^{N} \lambda_i \tag{3.65}$$

$$d(s) = \frac{1}{\sum_{i=1}^{N} \lambda_i} \tag{3.66}$$

where λ_i is the departure rate of the *i*th component in State *s*. It is the failure rate if the component is up, and is the repair rate if the component is down.

As can be seen from Equation (3.63), all the enumerated system states are mutually exclusive. Therefore, the cumulative failure probability is the direct sum of the probabilities of all failure states:

$$P_f = \sum_{s \in \boldsymbol{S}} P(s) \tag{3.67}$$

where $\boldsymbol{S}$ is the set of all system failure states. The cumulative failure frequency is given by

$$F_f = \sum_{s \in \boldsymbol{S}} f(s) - \sum_{i,j \in \boldsymbol{S}} f_{ij} \tag{3.68}$$

where f_{ij} is the transition frequency from State *i* to State *j*. Since it is almost impossible to calculate these transition frequencies in the state enumeration approach, they are often neglected in practical application. This assumption is generally acceptable as the transitions between system failure states are very rare, whereas the transitions between the normal and failure states are dominant in real application. Equation (3.68) can be rewritten as

$$F_f = \sum_{s \in \boldsymbol{S}} f(s) \tag{3.69}$$

The mean duration of residing in the set of system failure states is

$$D_f = \frac{P_f}{F_f} \tag{3.70}$$

For each system failure state, any risk index function such as load curtailment, *C(s),* can be obtained through system analysis techniques. The mathematical expectation of the index function for all system failure states is given by

$$E(C) = \sum_{s \in \boldsymbol{S}} C(s)P(s) \tag{3.71}$$

A very important note is that it is not computationally feasible to enumerate all system states for a system consisting of a large number of components as the number of states increase exponentially with the number of components. It is common to stop at a given enumeration depth. Another common criterion is to determine a suitable cut-off threshold of system state probability. The system states whose probability is lower than the threshold would be ignored. It should be noted that compared to Monte Carlo approaches, state enumeration is more effective for a system with a relatively small number of components and/or low outage probabilities. State enumeration also cannot model time-dependent events.

3.4.6 Nonsequential Monte Carlo simulation [68, 69]

Nonsequential Monte Carlo simulation is widely used in power system risk evaluation. It is often called the state sampling approach. The main concept is that a system state is a combination of all component states and each component state can be determined by sampling the probability of the component occurring in that state. The main difference between nonsequential Monte Carlo simulation and state enumeration is how to select system states and how to calculate individual state probabilities.

Each component is modelled using a uniform distribution between [0, 1]. Assume that each component has two states including failure and success, and component outages are independent of each other. Let s_i represents the state of the *i*th

component and Q_i its failure probability. Produce a random number R_i following a uniform distribution between [0, 1] for the *i*th component:

$$s_i = \begin{cases} 0 & (success) \quad if\ R_i > Q_i \\ 1 & (failure) \quad if\ 0 \le R_i \le Q_i \end{cases} \tag{3.72}$$

The state of the system containing *N* components is represented by the vector *s*:

$$s = (s_1, \dots, s_i, \dots, s_N) \tag{3.73}$$

After selecting a system state in the sampling, the system analysis is conducted to determine whether it is a failure state or not, and a risk index for that state would be assessed.

When the number of samples, *M*, is sufficiently large, the sampling frequency of the system state *s* can be used as an unbiased estimation of its probability:

$$P(s) = \frac{m(s)}{M} \tag{3.74}$$

where *m(s)* is the number of occurrences of the system state *s* in the sampling. The same formulas as those in Equations (3.65) to (3.71) can be used to calculate the system failure probability, failure frequency, mean system failure duration, and other risk indices.

It is important to note that the Monte Carlo simulation is a fluctuating process. As a result, the estimated risk indices always come with a confidence band. Although this confidence band decreases as the number of samples increases, it cannot be guaranteed that a few more samples will definitely result in a smaller error. An appropriate convergence criterion is vital to assure the accuracy of a Monte Carlo simulation. The coefficient of variance is often used as the stopping rule in the sampling process. Another approach is to determine a maximum number of samples as the stopping rule.

The state sampling not only applies to random component outages but also can be used to sample the states for other uncertain factors in power system risk evaluation such as load levels, intermittent generation, and weather states. Compared to the state enumeration, the nonsequential Monte Carlo approach is more preferable

when a large system or a system with high failure probabilities of components is studied. However, similar to the state enumeration techniques, the state sampling method cannot model time-dependent events

3.4.7 Sequential Monte Carlo simulation [68]

Sequential Monte Carlo approach refers to a simulation process over a chronological time span. It is often called the state duration sampling. It is based on sampling a probability distribution of component state duration and contains 5 steps:

1. Step 1: Specify initial states of all components. Typically, they are assumed to be in the up state initially.
2. Step 2: Sample the duration of each component residing in its present state. The probability distribution of the state duration should be assumed. For example, the sampling value of the state duration distributed exponentially is given by

$$D_i = \frac{1}{\lambda_i} \ln R_i \tag{3.75}$$

   where R_i is a random number between [0,1] following a uniform distribution corresponding to the *i*th component. λ_i is either the failure rate of the *i*th component if the present state is up, or the repair rate if the present state is down.

3. Repeat Step 2 in the considered time span and record sampling values of each state duration for all components. The chronological state transition processes of each component in the given time span can be obtained as shown in Fig. 3.14.
4. Step 4: Create the chronological system state transition cycle by combining the state transition processes of all components as shown in Fig. 3.15.
5. Step 5: Perform the system analysis for each system state to calculate the risk indices. Equations (3.76) to (3.78) are the three general formulas of the risk indices:

$$P_f = \frac{\sum_{k=1}^{M_{dn}} D_{dk}}{\sum_{k=1}^{M_{dn}} D_{dk} + \sum_{j=1}^{M_{up}} D_{uj}} \tag{3.76}$$

$$F_f = \frac{M_{dn}}{\sum_{k=1}^{M_{dn}} D_{dk} + \sum_{j=1}^{M_{up}} D_{uj}} \tag{3.77}$$

$$D_f = \frac{\sum_{k=1}^{M_{dn}} D_{dk}}{M_{dn}} \tag{3.77}$$

where P_f, F_f, and D_f are the system failure probability, frequency, and mean duration, respectively; D_{dk} is the duration in the kth down state and D_{uj} is the duration in the jth up state; M_{dn} and M_{up} are the numbers of occurrences of system failure and success states. Generally these two numbers are the same.

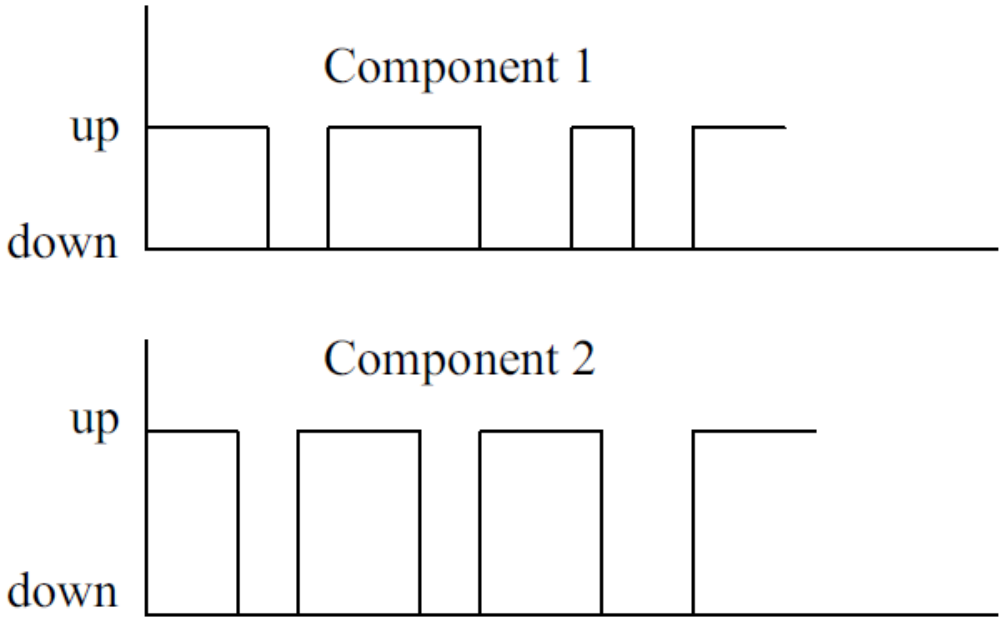

Fig. 3.14. Chronological state transition processes of components.

Similar to nonsequential Monte Carlo simulation, the sequential approach is a fluctuating process, and hence an appropriate convergence criterion is required such as the coefficient of variance rule. The main advantages of the state duration sampling are accurate evaluation of frequency and duration indices, flexibility of modelling any

state-duration distribution, and the capacity to calculate statistical probability distributions of system risk indices. The main disadvantage on the sequential Monte Carlo approach is high computational capacity.

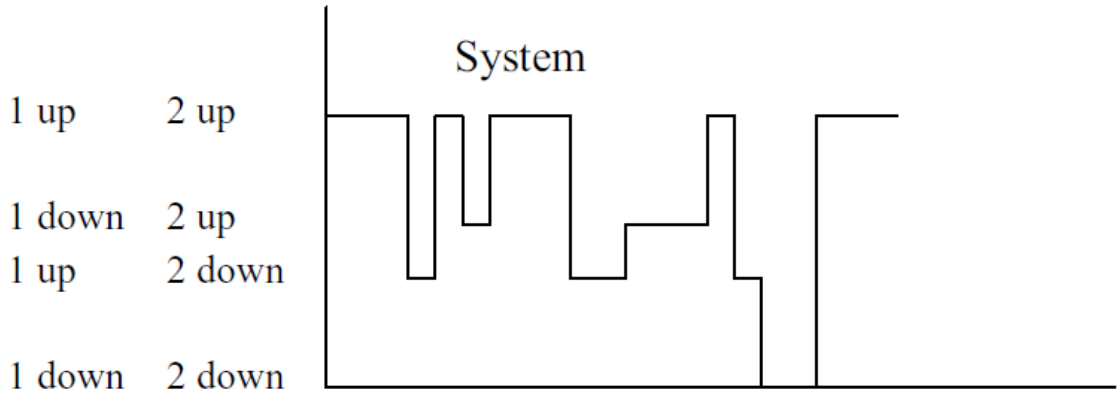

Fig. 3.15. Chronological system state transition process.

3.5 Conclusion

This chapter has presented the basic elements of power system risk assessment including the evaluation procedure, the component outage models, the fundamental methods used in the risk assessment. There are three steps in a power system risk assessment. The first step in system risk evaluation is to develop component outage models and then calculate the probabilities of these events. The second step is to select system failure states and calculate their probabilities. The last step is to conduct the analysis for system failure states, evaluate their consequences, and then calculate risk indices.

The failure models of system components are the vital part of power system risk assessment. They are classified into two categories: the independent and dependent outages. In the former one, the two-state, repairable forced-outage model is of the most importance and has been extensively used in the risk evaluation. The semi-forced outage concept is based on actual conditions such as transformer with oil leakage. It is often represented using a three-state model. A planned outage can be modelled using two modelling methods. For short-term operation planning, it is often represented using a simplified two-state model similar to a repairable forced outage.

The partial failure concept is also considered to represent the derated states of generating units. In the dependent outages, the most popular one is the common-cause outage. There are two methods can be applied to model a common-cause outage. The first method is using a composite model which is theoretically approximate and requires relatively complex calculations. The second one is to use individual models which are not only much simpler but also more accurate compared to the composite model. The component-group and cascading outages are also addressed in this chapter.

There are four fundamental methods that have been used in power system risk assessment. They are the probability convolution, series and parallel networks, Markov equations, and frequency-duration approaches. The four methods are often used for simple systems. For the risk evaluation of large-scale systems, two primary methods have been presented. They are state enumeration and Monte Carlo simulation. The former one is often used for systems with small number of components and/or low component outage probabilities. The latter one is further divided into nonsequential or state sampling and sequential or state duration sampling approaches. The Monte Carlo simulation method is preferable for large and complex systems with high failure probabilities of system components.

Chapter 4

Risk Assessment for Operation Planning of Wind Integrated Power Systems

4.1 Introduction

This chapter presents a novel approach to quantitative risk evaluation of wind integrated power systems for short-term operation planning. Firstly, it introduces the risk evaluation techniques used in system operation planning. It then presents the probabilistic approach to assess the operation risk of a wind integrated power system taking into different system uncertainties. A case study is also performed to evaluate the effectiveness of the proposed approach.

System operation planning studies are essential in maintaining and operating a reliable and secure power system. There is a fundamental difference between system development planning and operation planning. The former is associated with system reinforcement in a long time frame (years), whereas the latter is associated with operational measures in a short term usually less than 1 year. Long-term planners need to determine the necessary facilities and make a decision that is whether or not to strengthen the existing facilities to fulfil the system reliability criteria. In contrast, system operators need to identify the acceptable operating regions within which security criteria are met and make a decision that is whether or not to take actions to modify the operating conditions.

The traditional approaches used in system operation planning are based on the deterministic principle. The deterministic criterion, normally *N-1* criterion, requires that a power system must be able to withstand an outage of any single system component such as a generator, a transformer or a transmission line without violating any system operating limits. Some utilities also study a few *N-2* or *N-1-1* events in their operation planning. In recent decades, probabilistic risk assessment has become an important part of the operation planning studies. There are several reasons for this.

1. Any system, even if it satisfies the N-1 criterion, still has operational risk due to higher failure levels caused by multiple component outages.
2. There are often a number of operation modes that all meet the deterministic criteria. It is necessary to identify the lowest-risk or the most economical operation mode.
3. In recent years, large-scale integration of WPG significantly increases system variability and uncertainty due to wind intermittency and creates a number of technical challenges in the power system planning and operation. The deterministic criteria do not take into account the probabilistic nature of system behaviour, the uncertainty of demand and generation, and the probabilities of contingencies and network element failures. This may lead to results biased from reality and uneconomic decisions [7]. Probabilistic risk evaluation provides risk indices that take into account consequences of all possible failure operation states and probabilities of their occurrence. This is a valuable enhancement to the deterministic operation criteria.

It is very important to appreciate that the introduction of probabilistic risk assessment into system operation planning is not to replace but to enhance the existing deterministic operation criteria.

4.2 Risk evaluation in system operation planning

Power systems are divided into three functional zones: generation, transmission, and distribution. Generation (or generation-demand) system risk evaluation is concerned with only generation facilities and is called the hierarchical level one (HL1) study. Both generation and transmission equipment are included in the hierarchical level 2 (HL2), whereas all the three function zones are considered in the hierarchical level 3 (HL3). In risk evaluation for system operation planning, the HL2 will be studied. Depending on different requirements and study purposes, there are three possible cases in this risk assessment:

1. General cases: the failures of both generation and transmission components are considered.
2. Transmission system risk evaluation: only the failures of transmission components are considered, whereas all generating units are assumed to be 100% reliable.
3. Generation system risk evaluation: only the failures of generating units are considered, whereas all transmission components are assumed to be 100% reliable. Please note that this case is different from the generation-demand system risk assessment since the constraints due to the transmission network such as transmission line loading constraints are still considered in the evaluation.

4.2.1 Basic procedure

Operation planning risk evaluation has four main aspects: determination of component outage and load curve models, selection of system operation states, identification and analysis of system problems, and calculation of risk indices. Both the state enumeration and Monte Carlo simulation approaches can be applied to the risk evaluation. The two approaches select system operation states and calculate operation risk indices differently but use the same techniques to identify and analyse operation problems in a system state. The basic procedure is shown in Fig. 4.1.

4.2.2 Component outage models

Generating units are represented using the two-state (up and down) or multiple-state (including derated states) model. There might be several generators connected to one bus. If the Monte Carlo simulation is used, the states and state transitions of all generators can be directly sampled and hence no simplification is needed. If the state enumeration approach is used, to reduce the computational effort, a generation capacity probability table for each generation bus can be created. Instead of using the state probabilities of individual generators, the probabilities of generation capacity

levels in the table are enumerated. Or in other words, the generators on the same bus are aggregated into one generator with multiple generation levels.

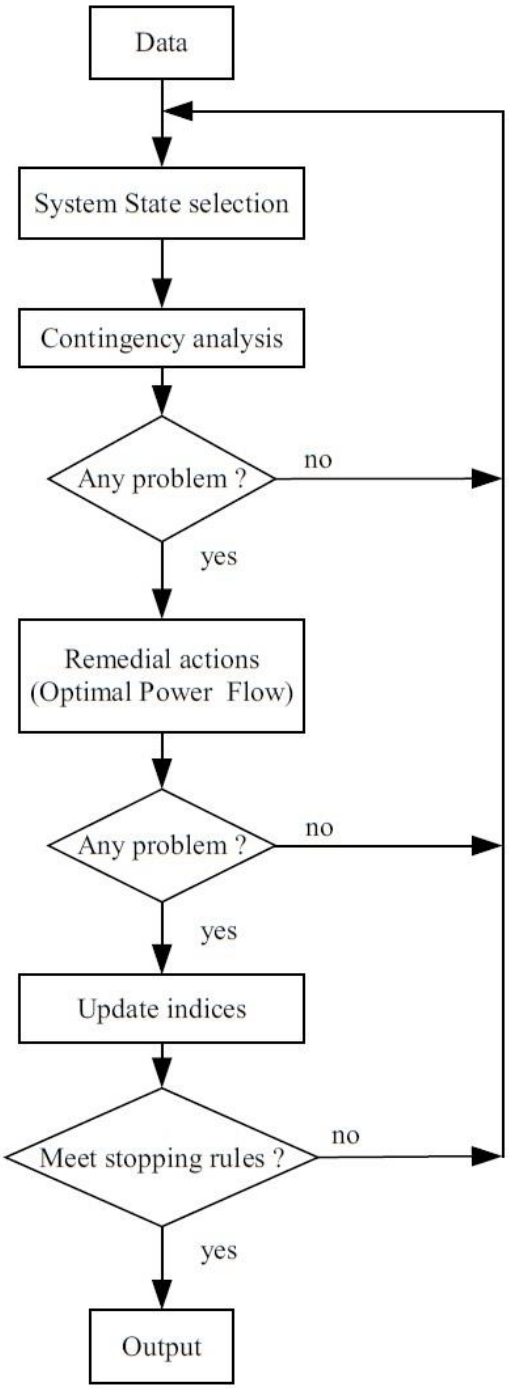

Fig. 4.1. Basic procedure of risk assessment for operation planning.

For example, consider a generation bus with two 30 MW and two 20 MW generating units which have the unavailability of 0.03 and 0.04, respectively. All the generation capacity levels with their probabilities are enumerated and shown in Table 4.1.

Table 4.1 Generation capacity and probability

Capacity (MW)		Probability
Available	Outage	
100	0	0.97×0.97×0.96×0.96 = 0.86713
80	20	0.97×0.97×0.96×0.04×2 = 0.07226
70	30	0.97×0.96×0.96×0.03×2 = 0.05363
60	40	0.97×0.97×0.04×0.04 = 0.00150
50	50	0.97×0.96×0.03×0.04×4 = 0.004470
40	60	0.96×0.96×0.03×0.03 = 0.00083
30	70	0.97×0.03×0.04×0.04×2 = 0.00009
20	80	0.96×0.03×0.03×0.04×2 = 0.000069
0	100	0.03×0.03×0.04×0.04 = 0.0000014

Transmission components include overhead lines, cables, transformers, capacitors, and reactors. They are often represented by a two-state model (up and down). The common-cause outage model is used for overhead lines on the same right of way or a set of components controlled by the same protection logic. The tap-connection structure in a transmission line is represented by a component-group

outage model. For details of the component outage models, please refer to Section 3.3.

4.2.3 Load curve models

If the state enumeration or nonsequential Monte Carlo approach is applied, a non-chronological load duration curve is used. If the sequential Monte Carlo simulation is used, a chronological load curve is utilised. There are three types of load model:

1. A single load curve is considered and loads at all buses are scaled proportionally to follow the shape of the considered load curve. A multiple-step model can be created to represent the load duration curve such as the one shown in Fig. 4.2.

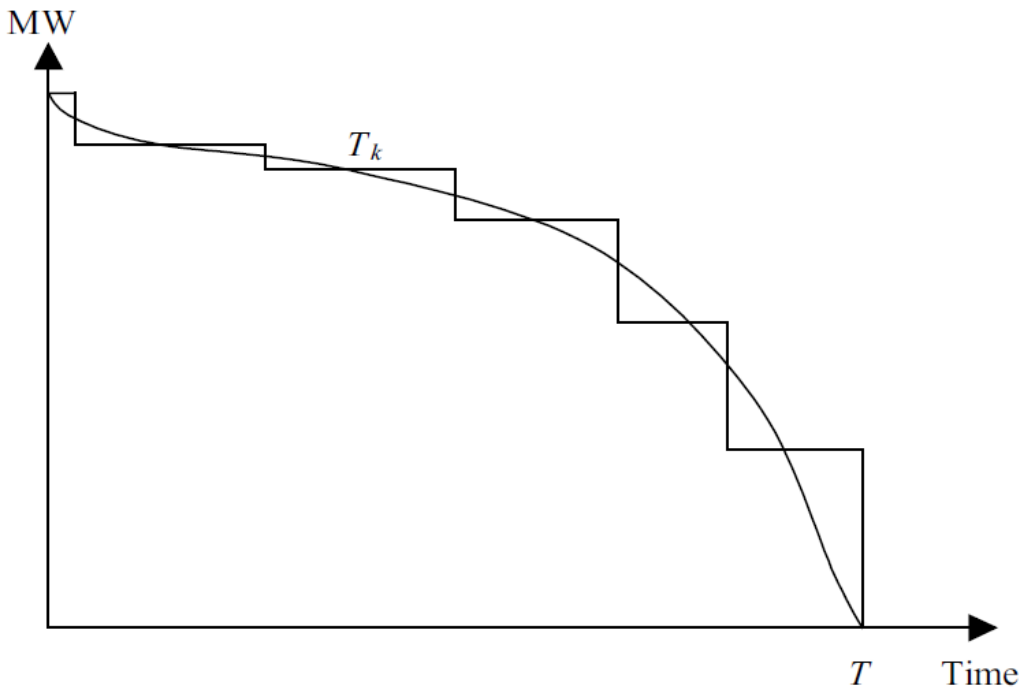

Fig. 4.2. Multiple-step model for a load duration curve [11].

2. Loads at some buses do not change such as an industrial customer with the same power demand every hour, whereas other bus loads follow a load curve.

3. Loads are classified into different bus groups with varied load curves. In this case, several load duration curves have to be included and each curve represents a bus group. The multiple step load model has to capture the correlation between all the load curves.

4.2.4 Contingency analysis

The contingency analysis for generating units is straightforward. If the remaining generation capacity at each generation bus can compensate the unavailable capacity due to loss of generator(s) at the same bus, load curtailment is not required. Otherwise, a generation rescheduling should be carried out. However, if dynamic phenomena are considered such as frequency deviations caused by load-generation balance, the analysis will be much more complex.

The contingency analysis for transmission components is more complex. The purpose is to calculate line loading levels and bus voltages following one or more component outages, and identify if there is any line overloading, voltage violation, or isolated bus. There are two basic transmission contingency analysis approaches: AC power-flow-based sensitivity technique and DC power-flow-based contingency analysis.

4.2.5 State enumeration method

State enumeration method is often used for power systems with low component failure probabilities. The basic concept of the state enumeration method has been described in Section 3.4.5. In the state enumeration approach, the probability of a system operation state is given by

$$P(s) = \prod_{i=1}^{n_d} PF_i \prod_{i=1}^{n_r} PP_i \prod_{i=1}^{n-n_d-n_r} (1 - PF_i - PP_i) \qquad (4.1)$$

where n_d and n_r are the numbers of components unavailable (down state) and partially unavailable (derated state) in the operation state *s*; *n* is the total number of

components in the system; PF_i is the outage probability of component *i*; and PP_i is the probability of component *i* in the derated state.

Some common risk indices used in the state enumeration method for operation planning risk assessment are shown as follows:

1. Probability of load curtailment (PLC):

$$PLC = \sum_{i=1}^{NL} \left(\sum_{s \in F_i} P(s) \right) \frac{T_i}{T} \tag{4.2}$$

where $P(s)$ is the probability of state *s*; F_i is the set of all the failure system states at the *i*th load level in the multiple-step load model; T_i is the time length (in hours) of the *i*th load level; NL is the number of load levels; T is the total time period of the load curve (in hours), it can be hours, days, weeks or months for operation planning.

2. Expected frequency of load curtailment (EFLC – failures/period):

$$EFLC = \sum_{i=1}^{NL} \sum_{s \in F_i} \left(P(s) \sum_{j=1}^{m(s)} \lambda_j \right) \frac{T_i}{T} \tag{4.3}$$

where λ_j is the *j*th departure rate of the components in state *s*; *m(s)* is the total number of the transition rates departing from state *s*.

3. Expected energy not supplied (EENS – MWh/period):

$$EENS = \sum_{i=1}^{NL} \left(\sum_{s \in F_i} P(s) \times C(s) \right) T_i \tag{4.4}$$

where $C(s)$ is load curtailment (MW) in state *s*.

All the three indices can be used for individual buses, areas, or the overall system.

4.2.6 Nonsequential Monte Carlo method

The nonsequential Monte Carlo method is often used in complex power systems. The basic concept of the state sampling approach is described in Section 3.4.6. Selecting a system operation state using the state sampling approach is associated with random determination of bus loads and component states. Random variables following a normal distribution are used to capture uncertainties of bus loads, whereas random variables distributed uniformly represent component states (up, down, or derated). The risk indices are calculated as follows:

1. Probability of load curtailment:

$$PLC = \sum_{i=1}^{NL} \left(\sum_{s \in F_i} \frac{n(s)}{N_i} \right) \frac{T_i}{T} \tag{4.5}$$

where $n(s)$ is the number of occurrences of state *s* in the sampling; N_i is the total number of samples; F_i is the set of all the failure system states at the *i*th load level in the multiple-step load model; T_i is the time length (in hours) of the *i*th load level; NL is the number of load levels; T is the total time period of the load curve (in hours), it can be hours, days, weeks or months for operation planning.

2. Expected frequency of load curtailment (failures/period):

$$EFLC = \sum_{i=1}^{NL} \sum_{s \in F_i} \left(\frac{n(s)}{N_i} \sum_{j=1}^{m(s)} \lambda_j \right) \frac{T_i}{T} \tag{4.6}$$

where λ_j is the *j*th departure rate of the components in state *s*; *m(s)* is the total number of the transition rates departing from state *s*.

3. Expected energy not supplied (MWh/period):

$$EENS = \sum_{i=1}^{NL} \left(\sum_{s \in F_i} \frac{n(s)}{N_i} \times C(s) \right) T_i \tag{4.7}$$

where $C(s)$ is load curtailment (MW) in state *s*.

It can be seen from Equations (4.2) to (4.7) that the difference between the formulas for the risk indices in the state enumeration and nonsequential Monte Carlo approaches is the estimation of the system operation state probabilities.

4.3 Proposed risk assessment approach for operation planning of wind integrated power systems

Recent global trend indicates a rapid growth in grid-connected renewable generation particularly wind energy in the coming decades. However, planning and operating a power system with high wind penetration face a number of technical challenges due to variability and uncertainty associated with wind. Wind energy conversion systems cannot be scheduled and dispatched in the traditional way. They also regulate their output and react to grid changes such as voltage or frequency disturbances differently compared with conventional synchronous generators. Moreover, the correlation between WPG output and load may be negative due to the variable nature of wind. Wind generation forecast also introduces an additional uncertainty factor to the system. As a result, in order to analyse a power system with significant wind generation, it is necessary to take into account the uncertainty of WPG.

4.3.1 Risk index

To perform power system risk assessments, a risk index needs to be defined. Since risk refers to "the effect of uncertainty on objective" and "is often expressed in terms of a combination of the consequences of an event and the associated likelihood of occurrence" [6], a risk index can be defined as the sum of products of probabilities and quantified consequences as shown below [7]:

$$Risk = \sum_{j}\sum_{i} P(C_i) \times P(S_j) \times Q(C_i, S_j) \tag{4.8}$$

where $P(C_i)$ is the probability of the *i*th contingency C_i; $P(S_j)$ is the probability of system operating condition S_j; and $Q(C_i, S_j)$ is the quantified consequence of the

contingency C_i in the operating condition S_j. An operating condition includes different components, such as load and generation levels, network configuration, and possible operation measures. Some components are random with a specified probability distribution. The probability of the operating condition is based on the probability distribution of these components. The quantified consequence can be determined as the amounts of limit violation, load curtailments, or socio-economic losses due to contingencies, depending on the purpose of the risk assessment [7].

Equation (4.8) is a generic representation of the risk index. This equation can be used for both the evaluation of the real-time operational risk and operational planning. In this paper, the risk assessment method is proposed for operational planning. Therefore, in calculating probabilities of contingencies and operating conditions, initial conditions are assumed known (a component is assumed operational in initial condition; it may fail in the future with the probability as a function of the lead time).

System operational risks at a given time *t* in the planning period are estimated by summing the products of probabilities and quantified consequences of possible contingencies and operating conditions in this time period. The details of this estimation are presented in the following sections.

4.3.2 Contingency probability

Random contingencies caused by outages of system components such as generators, transformers and transmission lines are unavoidable and uncontrollable in power system operation. They represent the main causes of the system operational risks. The probabilities of these events depend on several factors including weather conditions, environment, equipment age, and operating conditions.

To calculate the event probabilities, we assume that the failure/repair cycle of a single unit is represented by a two-state Markov model and its transitions follow an exponential probability distribution. Thus, the probability of failure of a single unit

during a time period *T*, given that the repair process is neglected, can be determined by [66]:

$$P = 1 - e^{-\lambda T} \tag{4.9}$$

where λ is the failure rate of the given unit. For short time period of up to several hours $\lambda T \ll 1$, then Equation (4.9) becomes $P \approx \lambda T$, which is known as outage replacement rate (ORR) representing the probability that a unit fails and is not replaced during the time period *T* [66]. The probability of a random contingency $P(C_i)$ in Equation (4.8) is determined by Equation (4.9).

4.3.3 Wind forecast uncertainty

Due to the intermittent nature of wind, predicting WPG output accurately on the time scale of interest (e.g., hourly, daily) represents a real challenge for power system planners and operators. There are various factors contributing to WPG forecast errors such as the forecast accuracy of individual wind plant outputs and the correlation between different wind farms. WPG output also depends on atmospheric factors such as wind speed and direction, or air density which are hard to predict accurately. The uncertainty in WPG forecasts can be relatively large, resulting in significant impacts on the reliability, security, and economic performance of wind integrated power systems.

The forecast horizon will have a significant impact on the WPG forecast error. For very short time scales (e.g., seconds to minutes), wind variation and forecast error is small given that there is significant diversity in WPG output. Larger time scales from minutes to several hours can lead to higher forecast errors due to the higher probability of WPG output changes for longer forecast horizon [70], [71]. Fig. 4.3 shows the probability density function of wind forecast errors over four different time scales (from half an hour to 4 hours). These errors are obtained using a sample of wind historical data in the UK and persistence based forecast techniques [72]. The forecast errors of WPG output are expressed as percentages of the total installed wind capacity.

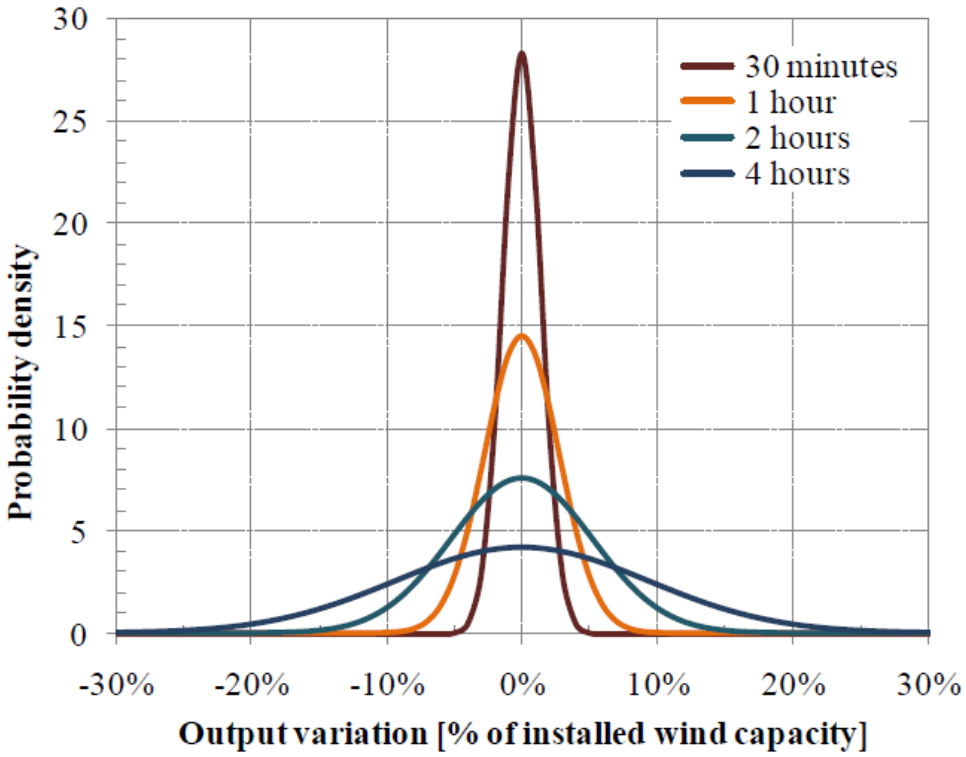

Fig. 4.3. Forecast errors of WPG output over different forecast time horizon [69].

As can be seen in Fig. 4.3, the variance and/or standard deviation of the WPG forecast error increases remarkably with the forecast horizon. The probability density functions of WPG forecast errors have the form of a "Bell-shaped curve" but with thicker "tail" than normal distribution.

However, for simple illustration purpose it is assumed in this thesis that WPG forecast errors can be modelled as a zero-mean normally-distributed random variable [52]. The WPG output at time *t*, wp^t, is the sum of the forecast wind generation, wp_f^t, and the forecast error, ε_{wp}^t. The standard deviation, σ_{wp}^t, is given by [73]:

$$\sigma_{wp}^t = \left(\alpha + \beta \times wp_f^t\right) WP_I \tag{4.10}$$

where α and β are forecast parameters depending on the forecast horizon and the size of the region where wind farms are located, wp_f is the forecast output of wind generation in per unit, and WP_I is the total installed WPG capacity. Although in

practice, statistical data show that the WPG prediction errors do not fit a normal distribution [60], [72], this assumption can be justified by the invocation of the central limit theorem due to the large number and geographical dispersion of wind turbines [52]. Moreover, although the normal distribution is used in this work to represent WPG forecast errors, other probability distribution models can be applied.

4.3.4 Load forecast uncertainty

Similarly, the load forecast error is represented as a zero-mean normally-distributed random variable. The load level at time *t*, l^t is the sum of the forecast load, l_f^t, and the forecast error, ε_l^t. The standard deviation of load forecast error, σ_l^t, is given by [58]:

$$\sigma_l^t = \frac{a}{100} l_f^t \tag{4.11}$$

where *a* is the constant representing the load forecast accuracy.

In addition, to reduce computation time, instead of using the continuous normal probability distribution, the typical seven-interval discretization of the zero-mean continuous normal-distributed function shown in Fig. 4.4 is used. This is a discrete distribution made up of seven one-standard-deviation-wide slices. The discrete probabilities of this approximation are given in Table 4.2.

Both load and WPG forecast errors are considered in calculating the probability of an operation condition $P(S_j)$ in Equation (4.8). At a given time *t*, there are seven possible load levels and seven possible WPG output levels. Their probabilities are:

$$\begin{cases} P(l_i^t) = P\left(l_{f,i}^t + \varepsilon_{l,i}^t\right) = P(\varepsilon_i)\ for\ i\ =\ 1,\ldots,7 \\ P\left(wp_j^t\right) = P\left(wp_{f,j}^t + \varepsilon_{wp,j}^t\right) = P(\varepsilon_j)\ for\ j\ =\ 1,\ldots,7 \end{cases} \tag{4.12}$$

As a result, there are forty-nine possible operating conditions at time *t* and their probabilities are:

$$P\left(S_{i,j}^t\right) = P(l_i^t) \times P\left(wp_j^t\right) \qquad for\ i,j\ =\ 1,\ldots,7 \tag{4.13}$$

Table 4.2. Discrete probabilities of seven-interval representation of forecast errors

	Forecast error	Probability
ε_1	-3σ	0.0062
ε_2	-2σ	0.0606
ε_3	-1σ	0.2417
ε_4	0σ	0.383
ε_5	1σ	0.2417
ε_6	2σ	0.0606
ε_7	3σ	0.0062

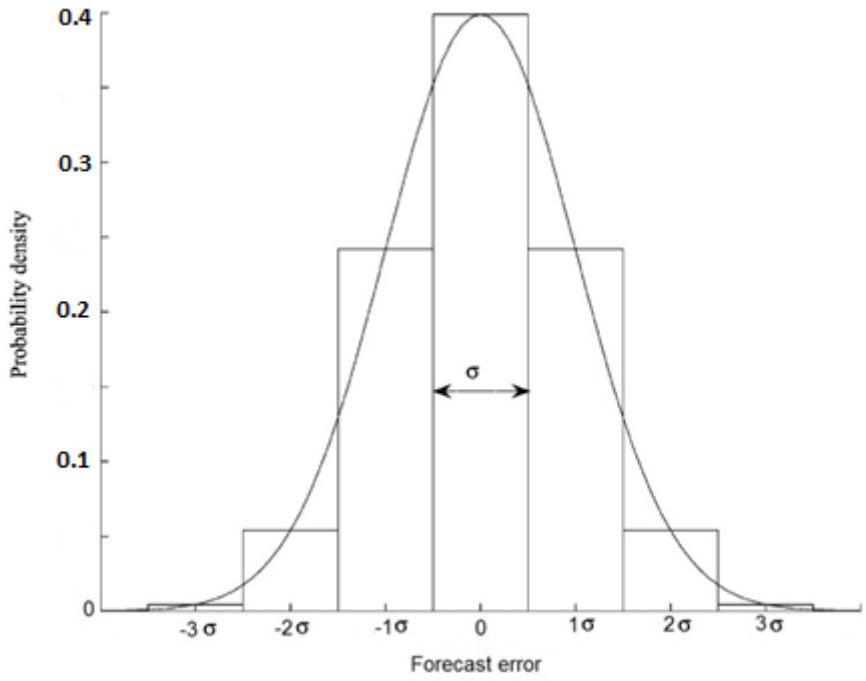

Fig. 4.4. Discrete seven-interval representation of normal.

4.3.5 Quantifying the consequence of a contingency in an operation state

The consequence of a contingency in an operating condition is quantified by the amount of expected load interruption cost (ELIC), which is the product of the unit interruption cost (UIC) or the value of lost load (VoLL) in $/kWh and the EENS. The unit interruption cost can be estimated by several methods [74] including:

1. Method based on customer damage functions obtained from customer surveys and relevant statistical analysis. For example, the average UIC in Canada is from $4/kWh to $10/kWh [11], whereas $12.5/kWh – the market price cap (MPC) is used as the unit interruption cost in reliability studies in Australia [75]. This is the average social damage cost due to the interruption of power supply. It is very important to admit that the UIC is region-, country-, and system-specific.
2. Method based on capital investments. For a power system utility, any capital investment for system reinforcement improves system reliability. In other words, there is a quantifiable relationship between the capital investment and the system risk. Therefore, the average unit interruption cost can be obtained.
3. Method based on gross domestic product (GDP). The GDP for a region or country divided by the total annual electric energy consumption of the region or country results in a dollar value per kWh. This number reflects the average economic damage cost due to loss of 1 kWh electrical power in that region or country.

The EENS is estimated based on the amount of load curtailments to clear post-disturbance system security violations including steady-state voltage and line overload violations and frequency response inadequacy (FRI). This estimation is done using the heuristic load restoration process presented in [42]. It consists of two phases:

1. The control phase: is the period for the operator to perform corrective actions to try to bring the system back to a stabilised state and to decide a restoration strategy.
2. The load restoration phase: involves the reconnection of the load that was interrupted.

The duration of the first phase, t_1, is calculated as follows:

$$t_1 = T \times \frac{P_{shed}}{P_T} \tag{4.14}$$

where T is the expected duration of this first phase for a total system blackout (assumed to be 30 minutes based on the French blackout of 19 December 1978); P_{shed} and P_T are the interrupted and the total load of the system, respectively. The second phase is estimated using the load restoration rates given in Table 4.3.

Table 4.3 Load restoration rates

Time period min	Restoring rate MW/min
0-30	10.0
30-60	33.3
60-90	66.6
>90	83.3

To quantify the consequences of the steady-state security violations including violated voltage constraints and equipment overload after a contingency occurs, the post-disturbance system condition is checked via power flow solutions. If any equipment such as a transmission line or a transformer is overloaded and/or voltage at any bus is out of the allowable range, the load located at or near the violated element

is disconnected in small blocks until these violations are cleared. In practice, these system violations can be solved by various corrective actions such as generation re-scheduling, distribution network re-configuration, and dynamic line ratings. In fact, load shedding is used only as the last resort. However, because a general indicator is needed to quantify the consequence of a system contingency, load shedding is commonly used in probabilistic benchmarking studies [40].

To quantify consequences of the frequency response inadequacy, instead of using dynamic simulations we propose an analytical method. Firstly, a mathematical model is developed to approximately represent frequency trajectories during frequency excursion events. Secondly, using the developed frequency trajectories, we determine consequences of the frequency events in terms of load curtailments. By using this analytical method, the frequency response adequacy assessment can be run simultaneously with the steady-state voltage and overload evaluations. The detail of this analytical method will be presented in the next chapter.

Fig. 4.5 shows the flow chart illustrating how the system operation risk given by is calculated for each operating point in our study. As discussed above, load shedding is the only corrective action which has been considered.

4.4 Case study

4.4.1 Case description

To demonstrate the performance of the proposed risk assessment method it is applied to a nine-bus power system shown in Fig. 4.6. The model represents a power system with characteristics similar to the Tasmanian power system. The Tasmanian system is connected to the main Australian power network via a single monopolar HVDC link with a capacity to export 630 MW from and import 480 MW to Tasmania. The total installed generation capacity of the system is 2.9 GW with 2.2 GW of hydro, 400 MW of gas, and 300 MW of wind generation. The power demand in Tasmania is approximately in the range of 800-1700 MW [76].

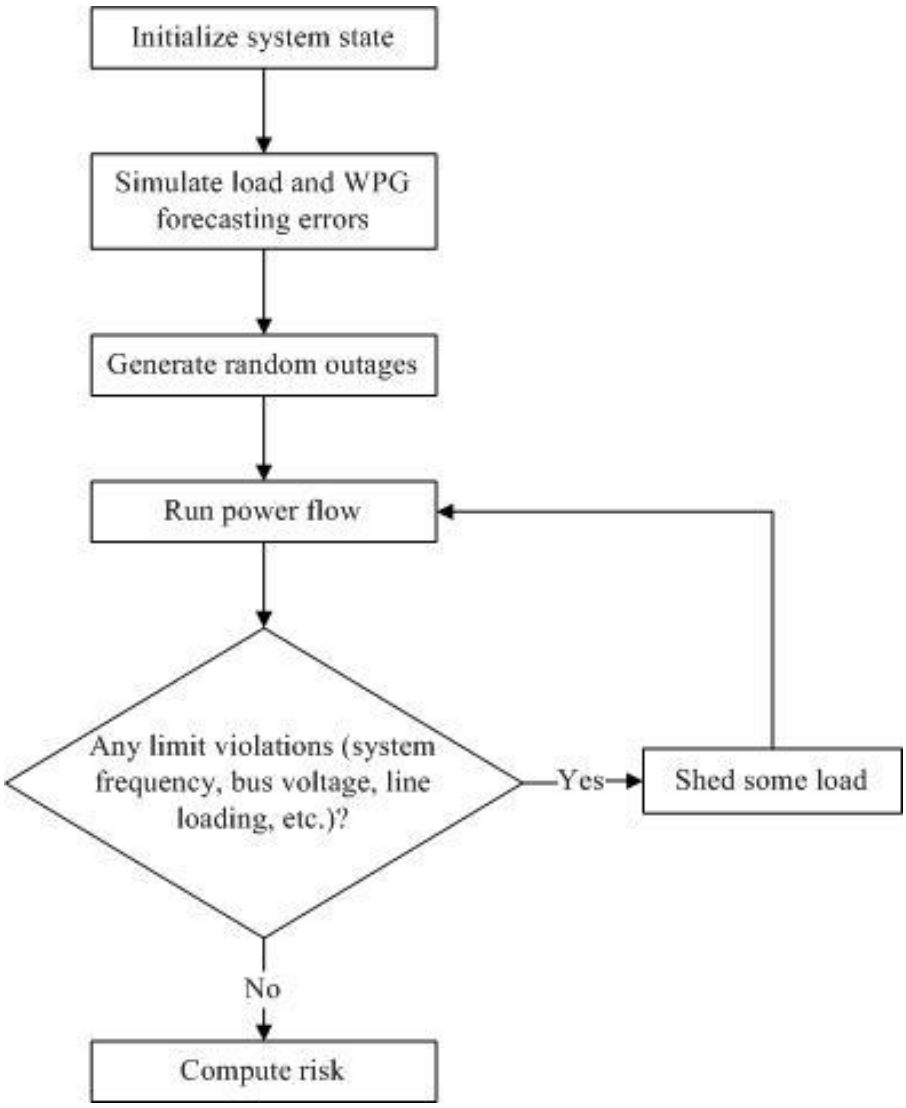

Fig. 4.5. Risk calculation flow chart.

Data of the nine-bus system are shown in Table 4.4. It has nine buses, six double circuit transmission lines, three single circuit lines and 17 conventional generating units with the same capacity of 150 MW. There are two wind farms connected to Bus 2 and Bus 9, respectively, with the installed capacity of 150 MW each. The system load is between 900 MW and 1800 MW. The system also has an interconnection line to an external grid with a capacity of 600 MW exporting and 450 MW importing.

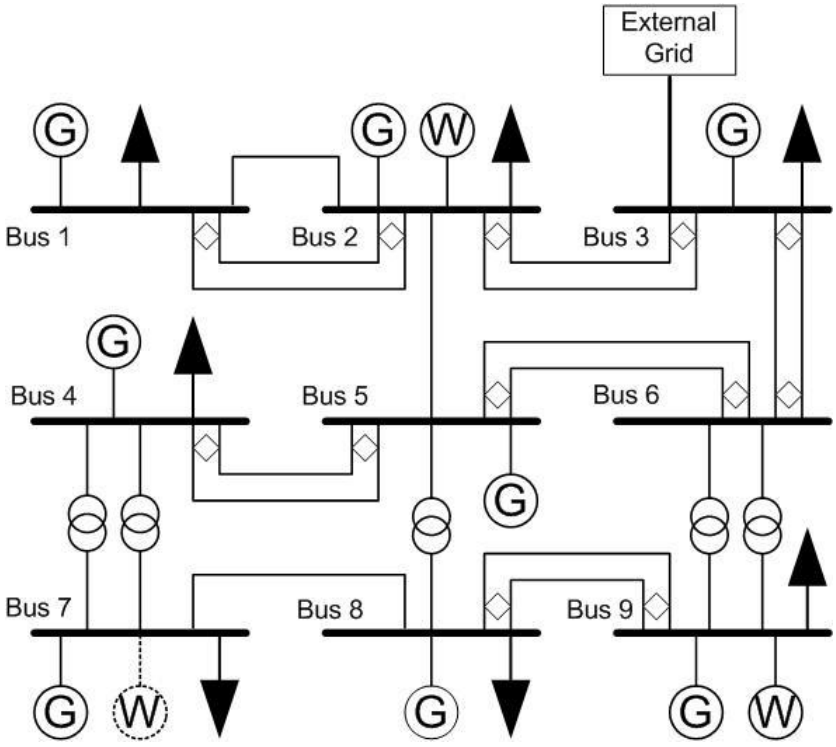

Fig. 4.6. The nine-bus power system.

A number of system operation planning studies using the proposed risk assessment method are performed for six consecutive hours with varying system conditions and wind generation levels. Load and WPG hourly forecast data are given in Table 4.5. Load forecast errors are given by Equation (4.11) with a = 1. Wind generation forecast errors are given by Equation (4.10) with $\alpha = 0.01$ and $\beta = 0.16$ based on the data of one-hour WPG forecast in a region with a diameter of 360 km [73]. In the case study, it is assumed that the wind conditions at both wind farms are the same at any given time interval. This assumption is usually valid for geographically small power systems, such as the Tasmanian system, that display little or no diversity between locations. However, the proposed method can easily be adopted for cases when wind farms are far away from each other and have different wind conditions.

The contingencies considered in the planning studies include:

- outage of a single conventional generator;

- outage of a single wind farm;
- outage of a single circuit (i.e., one circuit of a double circuit line or a single circuit line); and
- outage of both circuits of a double circuit line.

Table 4.4 System data

Bus	Conventional generation (MW)	Wind generation (MW)	Maximum load (MW)
1	600	0	75
2	300	150	240
3	300	0	450
4	600	0	360
5	150	0	0
6	0	0	0
7	300	0	420
8	150	0	45
9	150	150	210
Total	2550	300	1800

Table 4.5 Hourly load and WPG forecast data for the next six hours

Time t (h)	1	2	3	4	5	6
Load (MW)	1000	1400	1600	1600	1800	1200
WPG (p.u.)	0.6	0.8	0.6	0	0.2	0.5

The contingency probabilities are calculated as explained in Section 4.3.2. The outage replacement rates of the system components are calculated from the reliability

data of the Tasmanian power network provided by Transend Networks. Security violations caused by random contingencies and forecast errors are line overloads and frequency response inadequacy (no voltage violations have been recorded in the studies).

In this study, it is assumed that the secondary and tertiary reserves are sufficient to restore the frequency back to its nominal value and hence, we consider only the system primary frequency control capability when evaluating frequency response inadequacy risks. There are three under-frequency relay settings for the period of the primary control, as shown in Table 4.6 (the nominal frequency is 50 Hz).

Table 4.6 Under frequency relay setting

Relay	Load shedding block size (%)	Frequency threshold 1 (Hz)	Time delay 1 (s)	Frequency threshold 2 (Hz)	Time delay 2 (s)
1	10	47.8	0.2	-	-
2	10	47.5	0.2	47.8	10
3	10	47.2	0.2	47.5	2

These settings are similar to the automatic under-frequency load shedding configuration used in [77]. The system primary reserve is set at 150 MW that is the size of the largest generator. It will be activated once the system frequency drops below 49.85 Hz and takes 6 seconds to reach its maximum value of 150 MW. This is similar to the fast (R6) rise frequency control response in Australia [78]. The load relief factor k = 1. The system aggregate effective inertia is the sum of the inertia of all online generating units. All conventional generators have the same effective inertia of 750 MWs. It is assumed that the system load does not contribute to the system aggregate inertia. The wind generators are connected to the grid via electronic converters and hence, are also assumed to provide no inertial response.

The unit interruption cost is \$12.5/kWh, which is the MPC often used in reliability studies in Australia [75]. The simulations (stead-state power flow calculations) were conducted using DIgSILENT PowerFactory. The simulation

procedure follows the flow chart shown in Fig. 4.5. The state enumeration approach is used to select system operation states and calculate the risk index. Generation-load imbalances are taken care by the generator inertial and governor responses.

4.4.2 Result evaluation

4.4.2.1 Risk-based operation planning

We first investigate the operational risks in the planning hours assuming the system operates in the islanding mode (the interconnection flow is 0). The operational risks are shown in Fig. 4.7. As can be seen, the overload risks are almost zero in the planning period except at time interval t = 5 when the system load reaches its maximum value of 1800 MW. In the meantime, the operational risks associated with frequency response inadequacy are very high during time intervals t = 1 and t = 2, but are reduced considerably in the subsequent four hours. It indicates that the FRI risks are high under low demand and high wind generation conditions. This can be explained by the fact that when the load level is low and the wind generation is high, the number of online conventional generators is small and hence, the system inertia is reduced, which, in turn, makes the system more vulnerable to frequency deviations. In addition, when the wind generation output is high, the wind forecast error also increases, as shown in Equation (4.10), leading to larger load-generation imbalances, which are the main causes of FRI risks.

We now examine how the proposed risk assessment method can assist system operators in their operation planning studies. For example, let us consider the operation planning study for the system at time interval t = 2 (Fig. 4.7). The goal is to determine limits for the interconnection power flow and required levels of wind power curtailment so that the operational risk remains below a certain threshold. Wind power generation is often considered as non-scheduled generation and modelled as negative loads. However, high penetration of WPG may result in the WPG curtailment under some conditions in order to prevent violations of operation constraints [79]. In Australia, from 2008 large intermittent generators such as wind farms, which have generating capacity equal or larger than 30 MW, must be classified

as semi-scheduled generators; they are required to participate in the central dispatch process. In some dispatch intervals, semi-scheduled generators are required to limit their output to a level below the dispatch level based on constraints in the central dispatch process [80].

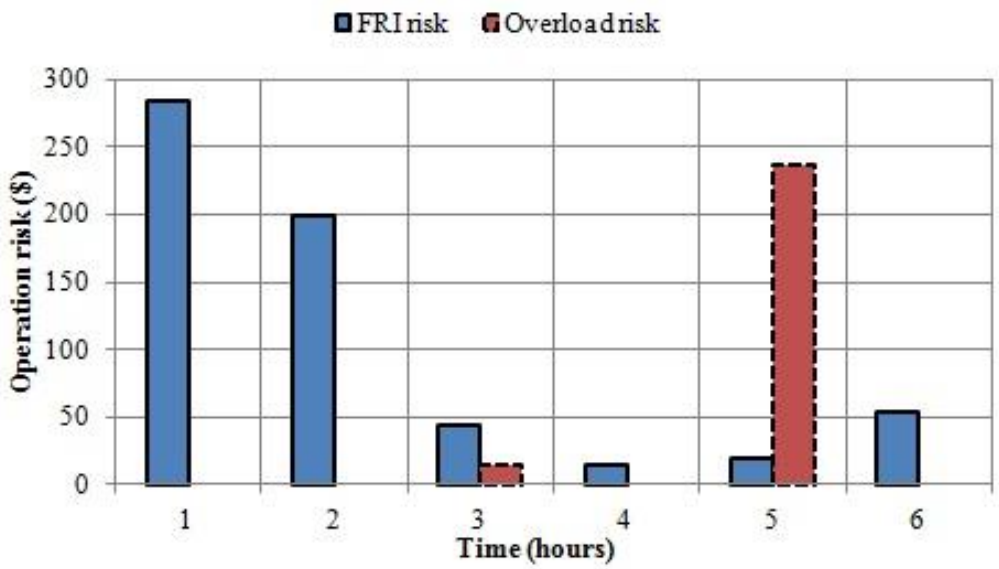

Fig. 4.7. Operational risks associated with the loss of the interconnection link.

Fig. 4.8 shows the operational risk contours at time interval t = 2 with different interconnection flows and WPG outputs. Each contour represents a set of operating points, which have the same value of operational risks, FRI risks in Fig. 4.8(a) and overload risks in Fig. 4.8(b), respectively. As can be seen, when the interconnection flow is zero and WPG is 0.8 p.u., the FRI risk is $200 and the overload risk is almost zero; this is consistent with the results shown in Fig. 4.7 for time interval t = 2. If the risk threshold of $100 (in terms of expected load interruption cost) is chosen as the maximum allowable FRI risk for operation in the planning period, the wind generation output must be curtailed to 0.67 p.u. and the interconnection power flow must be set within the range between -150 MW (the negative sign indicates that the interconnection operates in the exporting mode) to 0 MW.

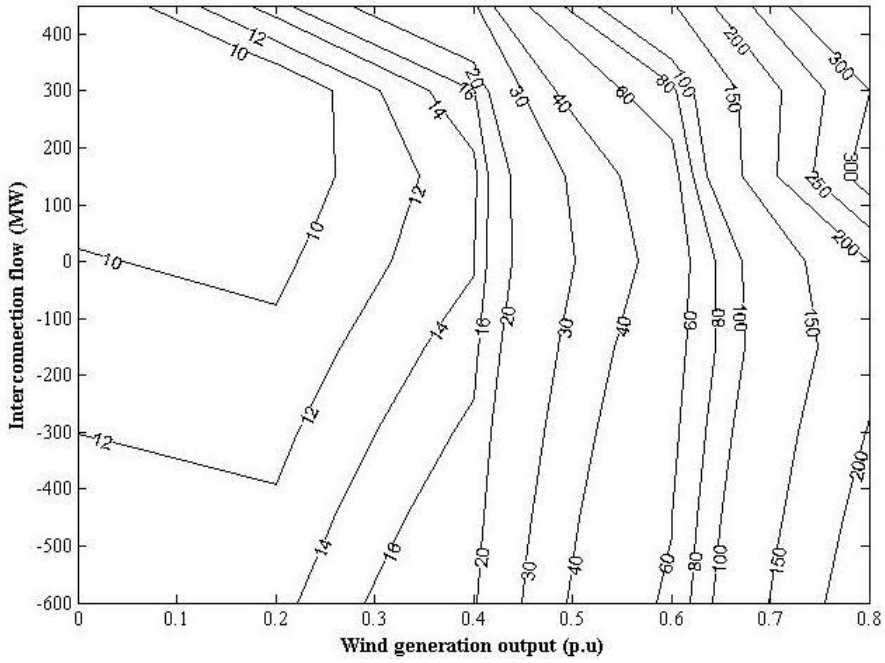

(a)

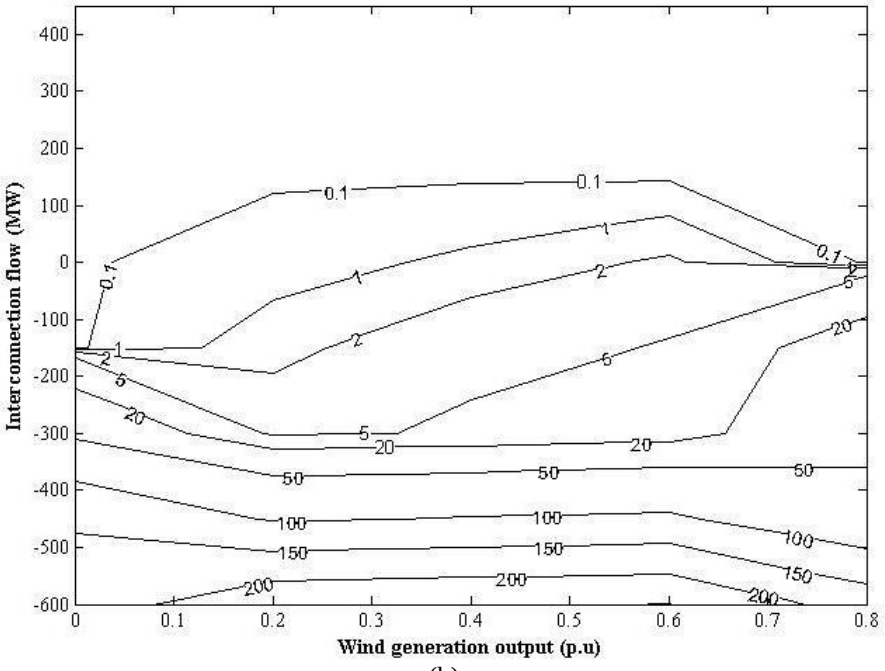

(b)

Fig. 4.8. Operational risk contours at time interval t = 2. (a) FRI risks. (b) Overload risks. (Negative values of interconnection flow indicate exporting and positive values indicate importing).

If we want to operate at a full range of the interconnection power flow (from -600 MW to 450 MW), the wind generation output must be further curtailed to 0.52 p.u., as can be seen in Fig. 4.8(a). If the same risk threshold applies to overload risks, the interconnection power flow must be limited to -500 MW at maximum wind generation output (0.8 p.u.), as shown in Fig. 4.8(b). Fig. 4.8 also shows that the wind generation level affects the FRI risk significantly, but has little impact on the overload risk. In contrast, the interconnection power flow has large effect on the risk of overload. It should be noted that the risk threshold is based on a management decision. It is system-specific and depends on the criteria system operators use in their decision-making process. The risk threshold can vary under different operating conditions and time intervals in the same system.

4.4.2.2 Impact of the increasing WPG on operational risks

To evaluate the impact of increasing WPG penetration on the system operational risks, two additional wind farms with the installed capacity of 100 MW each are connected to Bus 7. These two wind farms are assumed to have the same outage replacement rate and wind speed conditions at any time interval as the other two farms connected to Bus 2 and Bus 9, respectively. Fig. 4.9 compares the system operational risks at time interval t = 3 with two wind generation scenarios: 300 MW (two wind farms – solid curves) and 500 MW (four wind farms – dash curves). As can be seen, in the 300 MW scenario, when the interconnection flow is zero, the FRI and overload risks are around \$44 and \$14, respectively. These values are consistent with the results shown in Fig. 4.7 for time interval t = 3. In addition, Fig. 4.9 demonstrates that the increased wind penetration leads to a significant increase in FRI risks, but a slight decrease in overload risks. The reason is that the higher the wind penetration, the higher the WPG forecasting errors, which result in a larger generation-load mismatch and hence, higher FRI risks. Meanwhile, due to the increased wind generation capacity, local loads are more likely to be supplied by local generators, and therefore the loading of transmission lines is likely to reduce.

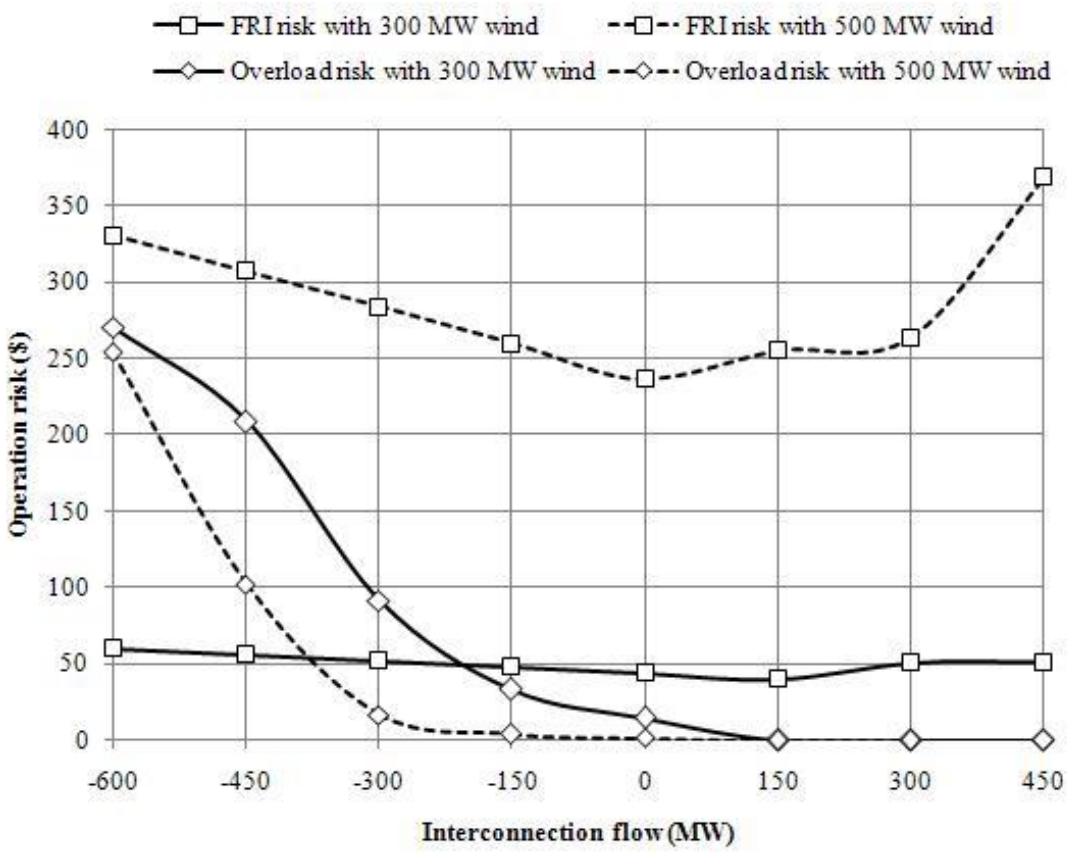

Fig. 4.9. Operational risks at time $t = 3$ when the installed wind generation capacity increases from 300 MW to 500 MW.

4.4.2.3 Frequency response inadequacy risk and primary reserves

As can be seen from the results in the previous sections, the FRI risk is considerably large, especially when the load level is low and the wind generation output is high, or the installed WPG capacity increases. This indicates that 150 MW of primary reserve, which is equal to the size of the largest generator, is not sufficient to deal with possible generation-load mismatches caused by either forecast errors or the loss of a generating unit, or both. In recent years, several authors from both industry and academia stated that operating reserve requirements need to be set dynamically to cope better with the uncertain characteristics of a power system including wind generation uncertainty [52, 58, 60]. It is generally agreed that large integration of WPG will result in an increase in the required amount of operating

reserves to maintain system reliability. However, the cost of providing reserves is far from negligible and should be taken into account when determining the reserve requirements [58]. The risk assessment approach proposed in this paper can assist a system operator in determining reserve requirements dynamically.

As an example, let us consider the system with different levels of primary reserves at time interval t = 2 (Fig. 4.7). The power exchanged through the interconnection link is set to zero. We define the expected operation cost as the sum of the FRI risk and the cost of providing the reserve. The amount of primary reserve needs to be determined to achieve the minimum expected operation cost. Fig. 4.10 shows the FRI risks and the expected operation costs with two different reserve prices. As can be seen, the minimum operation cost is \$200 approximately with 200 MW of reserve and \$0.87/MWh reserve cost, while it is \$580 with 180 MW of reserve and \$2.81/MWh reserve cost.

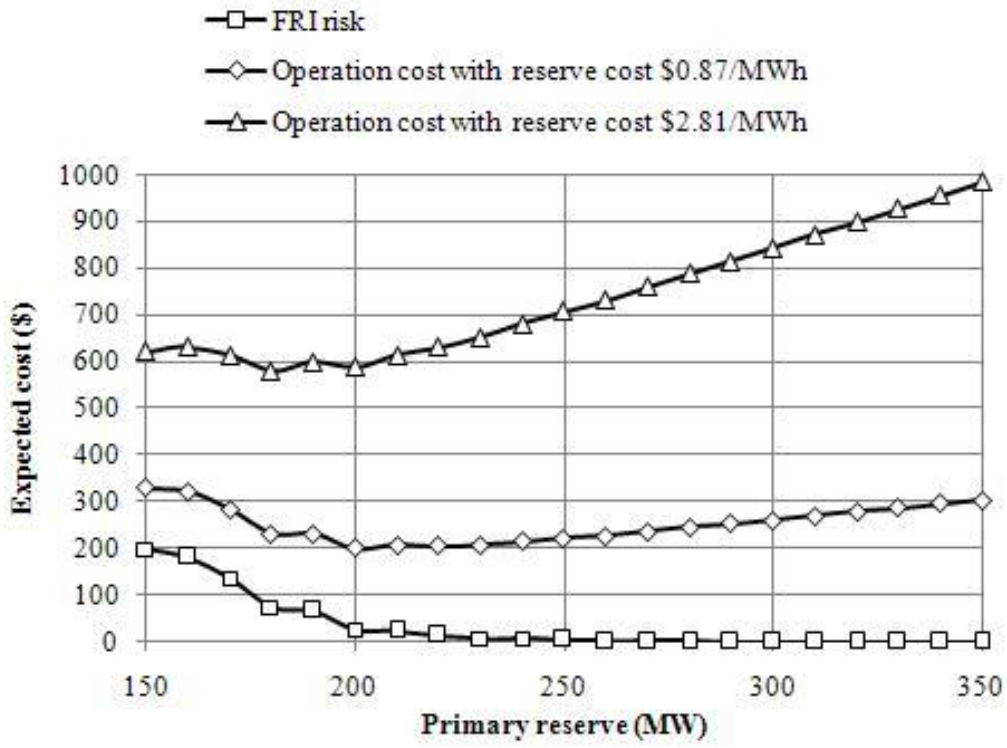

Fig. 4.10. FRI risks and estimated operation costs at time *t = 2* with different primary reserve amount.

4.5 Conclusion

This chapter presented a novel approach to quantitative risk evaluation of wind integrated power systems for short-term operation planning. A risk index representing both the likelihood and consequences of contingencies as well as system uncertainties caused by WPG and load forecasting errors was used to assess the system operation risk. The consequences of system failures were estimated using expected load interruption costs.

In the case study presented, the proposed approach was used to evaluate the operation risk of the nine-bus power system with characteristics similar to the Tasmanian power network. The results showed that the integration of WPG significantly affected the system operation risk, especially risks associated with frequency response inadequacy. Impacts of different factors including load and WPG forecast uncertainties, wind power penetration levels, and operating reserves on the operation risk were investigated. It also showed that the proposed approach could assist system operators in operation planning decision making such as setting constraints for wind generation curtailments and determining operating reserves.

Chapter 5

Development of Mathematical Model for System Frequency Responses

5.1 Introduction

One of the main tasks in a power system is to maintain the balance between the electrical power produced by generators and the power consumed by loads, including system loses. If for some reasons such as load changes or generation variations, this balance is not maintained, it will lead to a frequency excursion. A frequency drop could lead to large magnetizing currents in induction motors and transformers. Large frequency excursions may also have serious impacts on the power system operation and the reliability of power supply.

This chapter presents the development of a mathematical model for system frequency trajectories in load-generation imbalance events which have been used in Chapter 4 to quantify system operation risk. Section 5.2 presents the fundamental dynamic model of frequency in an electrical power system. Section 5.3 presents an overview of power system frequency control. Section 5.4 shows the development of mathematical model for frequency dynamic taking into account the system frequency control services. Section 5.5 presents a number of case studies to validate the developed frequency models. Finally, some remarks are presented in Section 5.6 to conclude the chapter.

5.2 Fundamental dynamic model of system frequency

The swing equation of a rotating machine is [78]

$$J\frac{d\omega}{dt} = T_m - T_e \tag{5.1}$$

where

J is the moment of inertia of the rotating machine

ω is the angular velocity

T_m is the mechanical torque

T_e is the electrical torque

Please note that in the above equation, T_m and T_e are positive for generators and negative for motors. As the relation between power and torque is

$$P = \omega T \tag{5.2}$$

Equation (5.1) can be rewritten as

$$J\omega \frac{d\omega}{dt} = P_m - P_e \tag{5.3}$$

where

P_m is the mechanical power

P_e is the electrical power

For a rotating machine, inertia is often expressed by an inertia constant H defined as the kinetic energy at rated speed divided by the apparent power rating of the machine [78]

$$H = \frac{\frac{1}{2}J\omega_0^2}{S} \tag{5.4}$$

where

ω_0 is the rated angular velocity

S is the apparent power rating

The moment of inertia J in terms of H is

$$J = \frac{2H}{\omega_0^2}S \tag{5.5}$$

Substituting Equation (5.5) into Equation (5.3) gives

$$\frac{2HS}{\omega_0^2}\omega\frac{d\omega}{dt} = P_m - P_e \tag{5.6}$$

Equation (5.6) can be rewritten in terms of frequency instead of angular velocity. Substituting $\omega = 2\pi f$ gives

$$\frac{2HS}{f_0^2}f\frac{df}{dt} = P_m - P_e \tag{5.7}$$

In order to obtain a linear approximation of Equation (5.7), we assume that

$$f\frac{df}{dt} = f_0\frac{df}{dt} \tag{5.8}$$

This is a valid, widely accepted assumption for realistic frequency deviation in power systems [81, 82]. As a result

$$\frac{df}{dt} = \frac{f_0}{2HS}(P_m - P_e) \tag{5.9}$$

A power system can be considered as a collection of generating units and loads, and a simplification can be made if it is assumed that power flows freely and instantaneously between them and the same system frequency occurs throughout the power system. In practice, the combined effect of the interconnecting network and generating unit excitation system dynamics adds a small oscillatory component to the frequency trajectory, but this effect is ignored because it usually decays within a few seconds. Therefore, the fundamental frequency dynamics of the system can be described by the below equation

$$\frac{df}{dt} = \frac{f_0}{2\sum HS}\left(\sum P_m - \sum P_e\right) = \frac{f_0}{2\sum HS}(G_{total} - L_{total}) \tag{5.10}$$

where

f_0 is the nominal system frequency

$\sum HS$ is the aggregate effective inertia of all generating units and motors in the power system

$\sum P_m$ is the sum of all mechanical power,

$\sum P_e$ is the sum of all electrical power outputs

G_{total} is the total generation

L_{total} is the total load including network losses

In general, both G_{total} and L_{total} are functions of frequency and time. If the balance between generation and load is maintained, the system frequency will be kept constant at f_0. When a disturbance occurs such as a loss of generator or a step change in load, there will be an imbalance between generation and load causing a frequency deviation. The system generation and load can be written as

$$\begin{aligned} G_{total}(f,t) &= G_0 + \Delta G(f,t) \\ L_{total}(f,t) &= L_0 + \Delta L(f,t) \end{aligned} \tag{5.11}$$

where

G_0 and L_0 are the generated power and load in steady state, respectively

ΔG and ΔL are the deviations in generation and load from the steady state values

Since the system is in equilibrium prior to the disturbance, hence

$$G_0 = L_0 \tag{5.12}$$

As a result, Equation (5.10) can be rewritten as

$$\frac{df}{dt} = \frac{f_0}{2\sum HS}[\Delta G(f,t) - \Delta L(f,t)] \tag{5.13}$$

It is the fundamental dynamic model of the system frequency.

5.3 Power system frequency control

After a frequency deviation occurs, rotating machines in the power system immediately release their kinetic energy to arrest the change in frequency. This is called inertial responses. If the frequency exceeds its normal operating band, the primary frequency control will be activated to ensure that the frequency is maintained within its short-term acceptable operating limits [83]. The primary control is often

deployed within few seconds and provided by generator governor response and automatic disconnection of interruptible load.

Secondary control is deployed through Automatic Generation Control (AGC) within tens of seconds to minutes after the frequency disturbance occurs. It takes care of the remaining frequency deviation and brings the frequency back to its nominal value. Tertiary control provided by fast start-up generators is later manually deployed to replace the secondary control or complement it if the secondary control reserves are not sufficient for restoring the frequency [84].

If at any time the frequency goes out of the associated operating limits, additional measures such as automatic under frequency load shedding (UFLS) are carried out to bring the frequency back to its limits. The frequency control structure described above is illustrated in Fig. 5.1 and its time spans are shown in Fig. 5.2 [14].

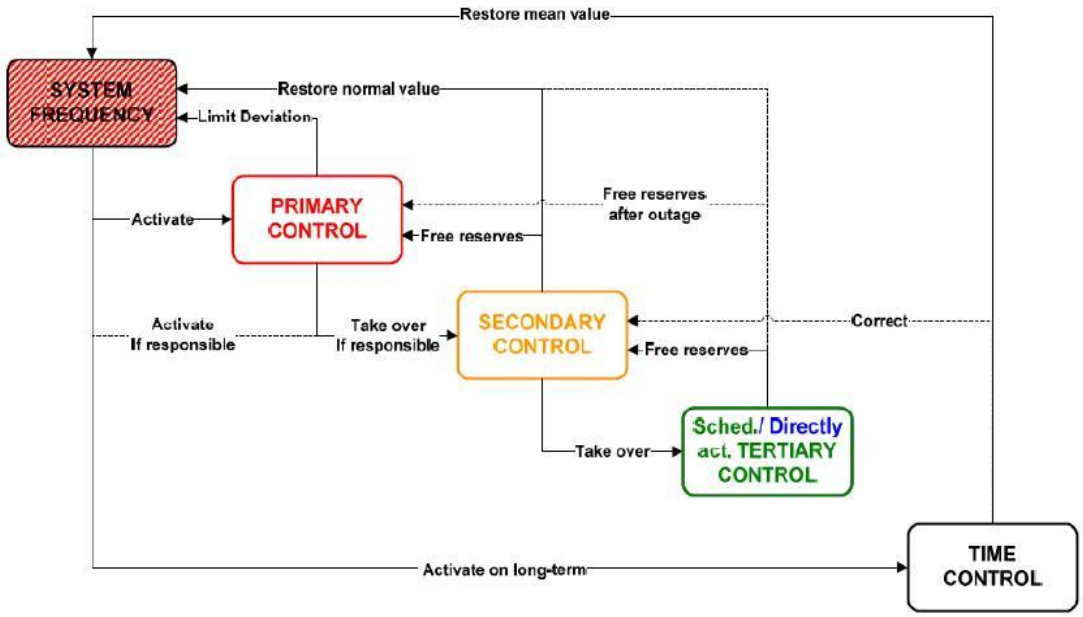

Fig. 5.1. System frequency control structure.

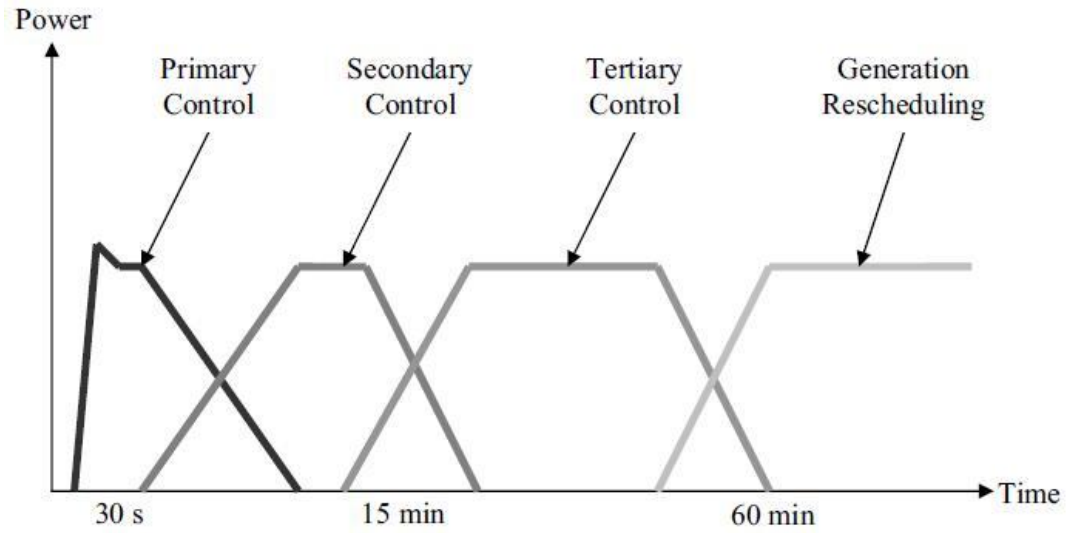

Fig. 5.2. Time spans of frequency control.

5.4 Development of mathematical models for frequency responses

5.4.1 Load relief

In a power system, a frequency dependency of the aggregated system load can be clearly observable. When the frequency decreases, motor loads connected to the power system will slow down. As the amount of power consumed by these machines is proportional to their rotational speed, the demand for power seen by the power system will thus fall as frequency falls. Other loads may also consume less power as the frequency decreases. Conversely, if the frequency increases, the power demand for power will increase. The change in demand for a given frequency deviation is thus related to the number of motors connected to the power system, and the size of the frequency deviation. This effect is called as "load relief" and has a stabilizing effect on the system frequency f. It can be described as follow

$$\Delta L = L - L_0 = -kL_0\left(1 - \frac{f}{f_0}\right) \tag{5.14}$$

where k is the load relief factor. Now we will consider the frequency dynamic model for common generation-load disturbances.

5.4.2 Frequency dynamic model for a loss of generation or load

If a loss of generation "g" occurs at time $t = 0$, the frequency dynamic model is given by combining Equation (5.13) with

$$\begin{aligned} \Delta G &= -g \\ \Delta L &= -kL_0\left(1 - \frac{f}{f_0}\right) \end{aligned} \tag{5.15}$$

we have

$$\frac{df}{dt} = \frac{f_0}{2\sum HS}\left[-g + kL_0\left(1 - \frac{f}{f_0}\right)\right] \tag{5.16}$$

This can be solved for variable *t* as

$$t = -\frac{2\sum HS}{kL_0}\ln\left[1 - \left(1 - \frac{f}{f_0}\right)\frac{kL_0}{g}\right] \tag{5.17}$$

Equation (5.17) can then be solved for frequency as

$$f = f_0\left[1 - \frac{g}{kL_0}\left(1 - e^{\frac{-t}{T_s}}\right)\right] \qquad \text{for } t \geq 0 \tag{5.18}$$

where T_s is the system time constant given by

$$T_s = \frac{2\sum HS}{kL_0} \tag{5.19}$$

Similarly, if a loss of load "l" occurs at time $t = 0$, the frequency dynamic model is given by

$$f = f_0\left[1 + \frac{l}{k(L_0 - l)}\left(1 - e^{\frac{-t}{T_s}}\right)\right] \qquad \text{for } t \geq 0 \tag{5.20}$$

5.4.3 Frequency dynamic model for a ramp of generation

If a ramp of generation starting at time $t = 0$ and levelling at value "r" at time $t = t_1$ occurs, the frequency dynamic model is

$$\frac{df(t)}{dt} = \frac{f_0}{2\sum HS}\left[r(t) + kL_0\left(1 - \frac{f(t)}{f_0}\right)\right] \tag{5.21}$$

where

$$r(t) = \frac{r}{t_1} \times [t \times u(t) - (t - t_1) \times u(t - t_1)] \tag{5.22}$$

$$u(t) = \begin{cases} 0 \; if \; t \leq 0 \\ 1 \; if \; t > 0 \end{cases} \tag{5.23}$$

Substituting Equation (5.19) into Equation (5.21) gives

$$T_s \frac{df(t)}{dt} = \frac{f_0}{kL_0} \times r(t) + f_0 - f(t) \tag{5.24}$$

Using Laplace transform for Equations (5.22) and (5.24) we have

$$R(s) = \begin{cases} \frac{r}{t_1} \times \frac{1}{s^2} \; if \; 0 \leq t \leq t_1 \\ \frac{r}{t_1} \times (1 - e^{-t_1 s}) \times \frac{1}{s^2} \; if \; t_1 < t \end{cases} \tag{5.25}$$

$$T_s(sF(s) - f_0) = \frac{f_0}{kL_0} \times R(s) + \frac{f_0}{s} - F(s) \tag{5.26}$$

Equation (5.26) can be rewritten as

$$F(s) = \frac{1}{T_s s + 1} \times \left(T_s + \frac{1}{s} + \frac{1}{kL_0} \times R(s) \right) \times f_0 \tag{5.27}$$

Substituting Equation (5.25) into Equation (5.27) we have

- If $0 \leq t \leq t_1$

$$F(s) = \frac{1}{T_s s + 1} \times \left(T_s + \frac{1}{s} + \frac{1}{kL_0} \times \frac{r}{t_1} \times \frac{1}{s^2} \right) \times f_0$$

$$= f_0 \times \left(\frac{1}{s} + \frac{1}{kL_0} \times \frac{r}{t_1} \times \left(-\frac{T_s}{s} + \frac{1}{s^2} + \frac{T_s}{s + \frac{1}{T_s}} \right) \right) \tag{5.28}$$

Using inverse Laplace transform for Equation (5.28) gives

$$f(t) = f_0 \times \left[1 + \frac{r}{kL_0} \times (T_s \left(e^{-\frac{t}{T_s}} - 1 \right) + t) \times \frac{1}{t_1} \right] \tag{5.29}$$

- If $t > t_1$

$$F(s) = \frac{1}{T_s s + 1} \times \left[T_s + \frac{1}{s} + \frac{1}{kL_0} \times \frac{r}{t_1} \times \frac{1}{s^2} \times (1 - e^{-t_1 s}) \right] \times f_0$$
$$= f_0 \times \left[\frac{1}{s} + \frac{1}{kL_0} \times \frac{r}{t_1} \times \frac{(1 - e^{-t_1 s})}{s^2 (T_s s + 1)} \right] \quad (5.30)$$

Using inverse Laplace transform for Equation (5.30) gives

$$f(t) = f_0 \times \left[1 + \frac{r}{kL_0} \times \left(T_s \left(e^{-\frac{t}{T_s}} - e^{-\frac{t-t_1}{T_s}} \right) + t_1 \right) \times \frac{1}{t_1} \right] \quad (5.31)$$

To conclude, the frequency dynamic model resulted from a linear ramp of generation starting at time $t = 0$ and levelling at value "r" at time $t = t_1$ is

$$f(t) = \begin{cases} f_0 \times \left[1 + \frac{r}{kL_0} \times \left(T_s \left(e^{-\frac{t}{T_s}} - 1 \right) + t \right) \times \frac{1}{t_1} \right] \; if \; 0 \le t \le t_1 \\ f_0 \times \left[1 + \frac{r}{kL_0} \times \left(T_s \left(e^{-\frac{t}{T_s}} - e^{-\frac{t-t_1}{T_s}} \right) + t_1 \right) \times \frac{1}{t_1} \right] \; if \; t > t_1 \end{cases} \quad (5.32)$$

5.4.4 Model simplification

To simplify the frequency dynamic models developed above, we denote

$$\varphi = 1 - \frac{f}{f_0}$$
$$\delta_g = -\frac{g}{kL_0}$$
$$\delta_r = \frac{r}{kL_0} \quad (5.33)$$
$$\delta_l = \frac{l}{kL_0}$$

Equations (5.18), (5.20), and (5.32) can now be rewritten as

$$\varphi(t) = -\delta_g \times \left[1 - e^{-\frac{t}{T_s}} \right] \quad (5.34)$$

$$\varphi(t) = -\delta_l \times \left[1 - e^{-\frac{t}{T_s}} \right] \quad (5.35)$$

$$\varphi(t) = \begin{cases} -\delta_r \times \left[T_s \left(e^{-\frac{t}{T_s}} - 1 \right) + t \right] \times \frac{1}{t_1} \; if \; 0 \le t \le t_1 \\ -\delta_r \times \left[T_s \left(e^{-\frac{t}{T_s}} - e^{-\frac{t-t_1}{T_s}} \right) + t_1 \right] \times \frac{1}{t_1} \; if \; t > t_1 \end{cases} \quad (5.36)$$

In addition, as the frequency models given by Equations (5.34), (5.35), and (5.36) are linear, they can be combined to show a complete frequency trajectory in a frequency excursion event. For example, the frequency trajectory resulted from a loss of generation "g" at time $t = 0$, followed by a generation ramp starting at time $t = t_1$ and levelling at time $t = t_2$ at value "r", is given by combining Equations (5.34) and (5.36) as shown below

$$\varphi = \begin{cases} \delta_g \left(e^{\frac{-t}{T_S}} - 1 \right) & for\ 0 \le t \le t_1 \\ \delta_g \left(e^{\frac{-t}{T_S}} - 1 \right) - \dfrac{\delta_r \left[T_s \left(e^{\frac{-(t-t_1)}{T_S}} - 1 \right) + t - t_1 \right]}{t_2 - t_1} & for\ t_1 \le t \le t_2 \\ \delta_g \left(e^{\frac{-t}{T_S}} - 1 \right) - \dfrac{\delta_r \left[T_s \left(e^{\frac{-(t-t_1)}{T_S}} - e^{\frac{-(t-t_2)}{T_S}} \right) + t_2 - t_1 \right]}{t_2 - t_1} & for\ t_2 \le t \end{cases} \quad (5.37)$$

5.4.5 Frequency dynamic model with frequency control services

In this section, we will develop a complete frequency dynamic model taking into account the frequency control services. Practically, each frequency control service has a particular shape of response such as a step response for load shedding, an exponential response for governor actions, and a more linear response for a hydro unit in spinning reserve mode. In this thesis, we assume that frequency control services can be modelled by a linear ramp response. This model has two advantages. Firstly, it is a simple technology neutral model which can represent any of the real responses with required accuracy. For example, a fast ramp approximates a step response, and a series of ramps of decreasing slope approximates an exponential response. Secondly, the levelling value of the ramp can represent the amount of the corresponding control service. A similar method has been used by Australian Energy Market Operator (AEMO) for dispatch of operating reserves deterministically [85].

Therefore, the complete frequency dynamic trajectory resulted from a loss of generation "g" occurs at time $t = 0$ with the participation of the power system frequency control can be represented by Equation (5.37) where "r" is the amount of the control service. The frequency control is activated at time $t = t_1$ which is the time

when the frequency exceeds the normal operating threshold f_n. It can be determined by solving Equation (5.34) with

$$\varphi(t) = \varphi_n = 1 - \frac{f_n}{f_0} \tag{5.38}$$

as shown below

$$t_1 = t_n = -T_s \ln\left(\frac{\varphi_n + \delta_g}{\delta_g}\right) \tag{5.39}$$

The next step is to check whether the frequency deviation will trigger the under frequency load shedding service by exceeding the UFLS threshold. Firstly, we need to calculate the minimum frequency using Equation (5.37). The frequency f will reach its minimum value f_{min} at time $t = t_{fmin}$ when

$$\frac{df}{dt} = \frac{d\varphi}{dt} = 0 \tag{5.40}$$

- If $t_n \leq t_{fmin} \leq t_2$ Equation (5.40) can be rewritten as

$$\frac{d\varphi}{dt} = -\frac{\delta_g}{T_s} e^{-\frac{t}{T_s}} - \frac{\delta_r}{t_2 - t_1}\left(1 - e^{-\frac{t-t_n}{T_s}}\right) = 0 \tag{5.41}$$

  It then can be solved for variable t as

$$t_{fmin} = T_s \ln\left[e^{\frac{t_n}{T_s}} - \frac{T_r \delta_g}{T_s \delta_r}\right] \tag{5.42}$$

  where

$$T_r = t_2 - t_n \tag{5.43}$$

  and hence

$$f_{min} = f_0\left[1 + \delta_g + \frac{\delta_r}{T_r}\left(t_{fmin} - t_n\right)\right] \tag{5.44}$$

- If $t_{fmin} > t_2$

$$\frac{d\varphi}{dt} = -\frac{\delta_g}{T_s} e^{-\frac{t}{T_s}} + \frac{\delta_r}{t_2 - t_n} e^{-\frac{t}{T_s}} \left(e^{\frac{t_n}{T_s}} - e^{\frac{t_2}{T_s}} \right) = 0 \tag{5.45}$$

Solving this equation we have

$$\begin{aligned} t_{fmin} &= +\infty \\ f_{min} &= f_0(1 - \delta_g + \delta_r) \end{aligned} \tag{5.46}$$

If the minimum frequency calculated in Equation (5.44) or (5.46) is lower than the UFLS threshold f_x, the UFLS will be activated. The determination of t_x – the UFLS activation time is as follow.

- If $t_n \leq t_x \leq t_2$, t_x can be calculated by solving the below equation

$$1 - \frac{f_x}{f_0} = \delta_g \left(e^{\frac{-t_x}{T_s}} - 1 \right) - \frac{\delta_r}{T_r} \left[T_s \left(e^{\frac{-(t_x - t_n)}{T_s}} - 1 \right) + t_x - t_n \right] \tag{5.47}$$

It can be rewritten as

$$g(\tau) = ae^{-\tau} + b\tau + c = 0 \tag{5.48}$$

where

$$\tau = \frac{t_x}{T_s} \tag{5.49}$$

and

$$\begin{cases} a = \delta_g - \dfrac{\delta_r T_s}{T_r} e^{\frac{t_n}{T_s}} \\ b = -\dfrac{\delta_r T_s}{T_r} \\ c = -\delta_g - \dfrac{\delta_r (T_s + t_n)}{T_r} + \dfrac{f_x}{f_0} - 1 \end{cases} \tag{5.50}$$

Equation (5.48) can be solved to find τ numerically using an iterative technique such as Newton-Raphson with

$$\tau_0 = \frac{t_{fmin} + t_n}{2T_s} \tag{5.51}$$

After that t_x will be calculated using Equation (5.49). Assuming that an amount of load "*l*" is shed due to UFLS action at time $t = t_x$, the frequency dynamic model in Equation (5.37) now becomes

$$\varphi = \begin{cases} \delta_g\left(e^{\frac{-t}{T_s}} - 1\right) & for\ 0 \le t \le t_1 \\ \delta_g\left(e^{\frac{-t}{T_s}} - 1\right) - \frac{\delta_r}{T_r}\left[T_s\left(e^{\frac{-(t-t_1)}{T_s}} - 1\right) + t - t_1\right] & for\ t_1 \le t \le t_x \\ \delta_g\left(e^{\frac{-t}{T_s}} - 1\right) - \frac{\delta_r}{T_r}\left[T_s\left(e^{\frac{-(t-t_1)}{T_s}} - 1\right) + t - t_1\right] + & \\ \quad +\delta_l\left(e^{\frac{-(t-t_x)}{T_s}} - 1\right) & for\ t_x \le t \le t_2 \\ \delta_g\left(e^{\frac{-t}{T_s}} - 1\right) - \frac{\delta_r}{T_r}\left[T_s\left(e^{\frac{-(t-t_1)}{T_s}} - e^{\frac{-(t-t_2)}{T_s}}\right) + t_2 - t_1\right] + & \\ \quad +\delta_l\left(e^{\frac{-(t-t_x)}{T_s}} - 1\right) & for\ t_2 \le t \end{cases} \tag{5.52}$$

- If $t_x > t_2$, solving the equation

$$1 - \frac{f_x}{f_0} = \delta_g\left(e^{\frac{-t_x}{T_s}} - 1\right) - \frac{\delta_r}{T_r}\left[T_s\left(e^{\frac{-(t_x-t_1)}{T_s}} - e^{\frac{-(t_x-t_2)}{T_s}}\right) + t_2 - t_1\right] \tag{5.53}$$

give us

$$t_x = T_s \ln\left[\frac{\delta_g + \frac{T_s}{T_r}\delta_r\left(e^{\frac{t_2}{T_s}} - e^{\frac{t_1}{T_s}}\right)}{\delta_g + \delta_r + 1 - \frac{f_x}{f_0}}\right] \tag{5.54}$$

Assuming that an amount of load "*l*" is shed due to UFLS action at time $t = t_x$, the frequency dynamic model in Equation (5.37) now becomes

$$\varphi = \begin{cases} \delta_g\left(e^{\frac{-t}{T_S}} - 1\right) & for\ 0 \le t \le t_1 \\ \delta_g\left(e^{\frac{-t}{T_S}} - 1\right) - \frac{\delta_r}{T_r}\left[T_s\left(e^{\frac{-(t-t_1)}{T_S}} - 1\right) + t - t_1\right] & for\ t_1 \le t \le t_2 \\ \delta_g\left(e^{\frac{-t}{T_S}} - 1\right) - \frac{\delta_r}{T_r}\left[T_s\left(e^{\frac{-(t-t_1)}{T_S}} - e^{\frac{-(t-t_2)}{T_S}}\right) + t_2 - t_1\right] & for\ t_2 \le t \le t_x \\ \delta_g\left(e^{\frac{-t}{T_S}} - 1\right) - \frac{\delta_r}{T_r}\left[T_s\left(e^{\frac{-(t-t_1)}{T_S}} - e^{\frac{-(t-t_2)}{T_S}}\right) + t_2 - t_1\right] + & \\ \quad + \delta_l\left(e^{\frac{-(t-t_x)}{T_S}} - 1\right) & for\ t_x \le t \end{cases} \quad (5.55)$$

Using the same approach, we can check whether the system frequency f will exceed other UFLS thresholds and when to develop the complete frequency dynamic model.

5.5 Simulation results

In this section, we will validate the frequency dynamic models developed in Section 5.3 by comparing with dynamic simulation results using DIgSILENT PowerFactory. Three study cases are considered.

The first case studies the frequency deviation for a generation loss $g_1 = 100\ MW$ in a 50Hz power system with 1000 MW load. The generation loss occurs at time $t_0 = 0$ followed by a ramp starting at time $t_1 = 0.2$ and levelling at time $t_2 = 6.2$ at value $r_1 = 100\ MW$. The load relief factor is $k = 2$. The system aggregate effective inertia after the generation loss is 8000 MWs. Fig. 5.3 compares the frequency trajectory given by Equation (5.37) with the simulation result using DIgSILENT PowerFactory.

The second case studies the frequency deviation for a loss of generation $g_2 = 200\ MW$ in the same 1000 MW system. The generation loss occurs at time $t_0 = 0$ followed by a ramp starting at time $t_1 = 0.2$ and levelling at time $t_2 = 6.2$ at value $r_2 = 200\ MW$. The load relief factor is $k = 2$. The system aggregate effective inertia after the generation loss is 7000 MWs. Fig. 5.4 compares the frequency trajectory given by Equation (5.37) with the simulation result using DIgSILENT PowerFactory.

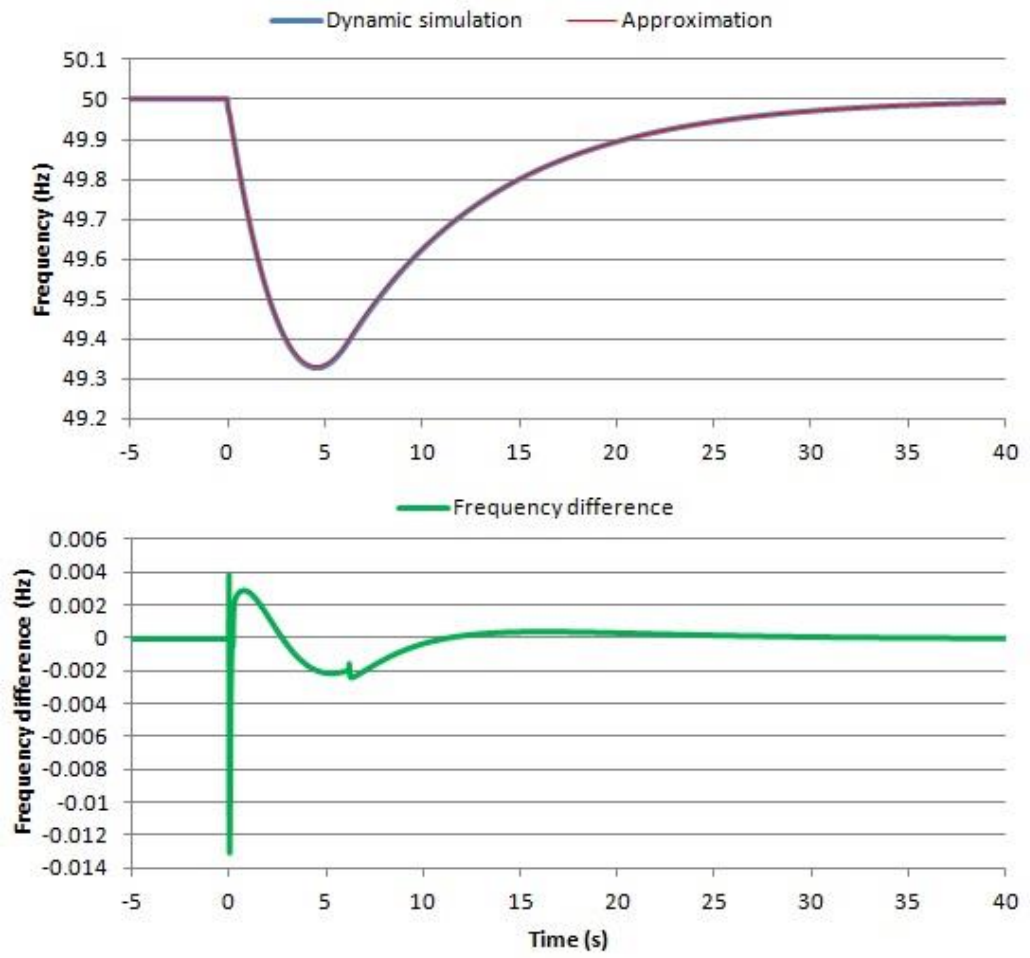

Fig. 5.3. Comparison of frequency trajectories for a loss of 100 MW generation.

The third case studies a more complex frequency deviation. It considers a loss of generation $g_3 = 200\ MW$ occurring at time $t_0 = 0$ in the 1000 MW system. The load relief factor is $k = 2$ and the system aggregate effective inertia after the generation loss is 6000 MWs. The minimum frequency for normal operation is $f_n = 49.85\ Hz$. If the frequency exceeds this limit, the system frequency control service will be activated and fully deployed after 6 seconds. The amount of this service is $r_3 = 100\ MW$. There are two under frequency load shedding threshold $f_{x1} = 48.7\ Hz$ and $f_{x2} = 48.34\ Hz$. The amount of load will be shed for each UFLS threshold is $l = 50\ MW$.

Using our developed method presented in Section 5.3.5, the activation time of the frequency control service will be $t_n = 0.18\ s$ and the frequency deviation will

trigger the two UFLS thresholds at $t_{x1} = 1.96\ s$ and $t_{x2} = 3.90\ s$. Fig. 5.5 compares the developed frequency dynamic model with the simulation result using DIgSILENT PowerFactory.

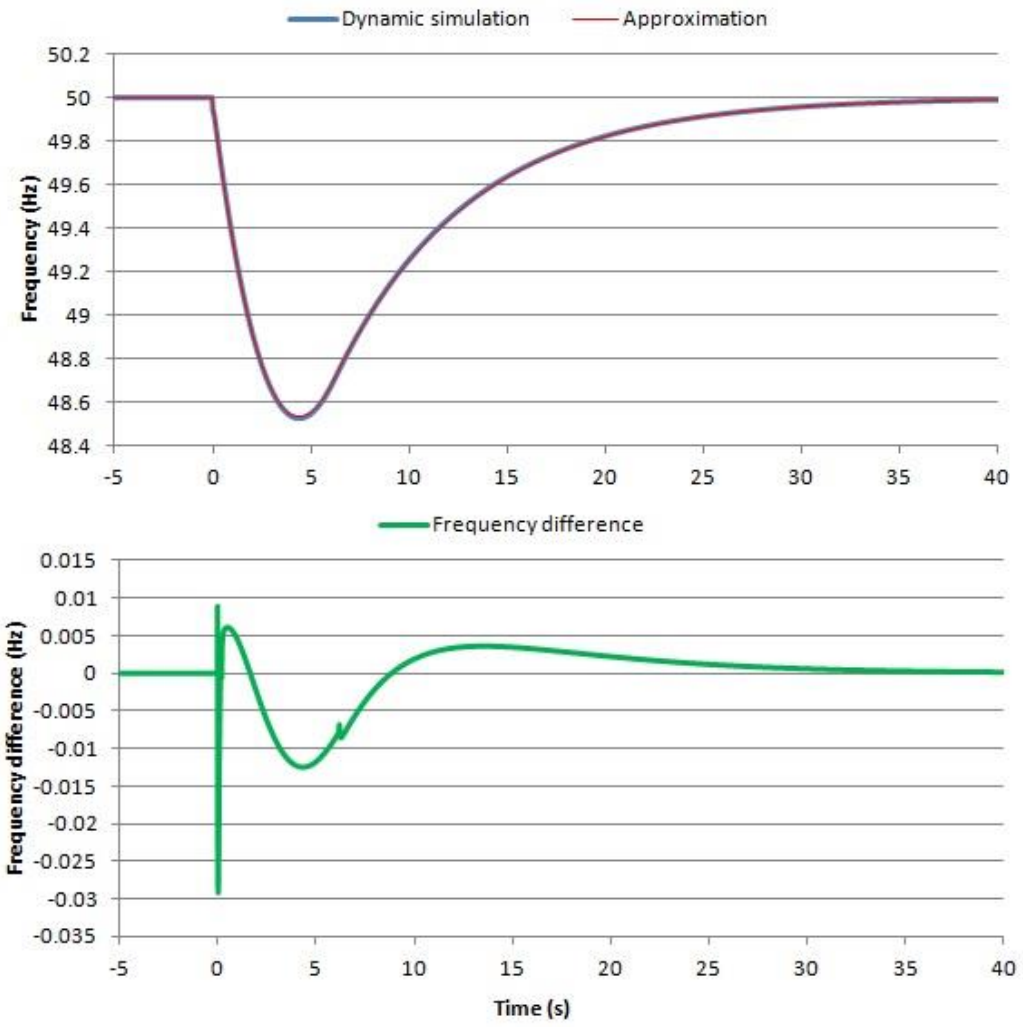

Fig. 5.4. Comparison of frequency trajectories for a loss of 200 MW generation.

The above results demonstrate the validity of the approximated frequency dynamic models. Please note that the spikes in the frequency differences are caused by time intervals used in numerical integration.

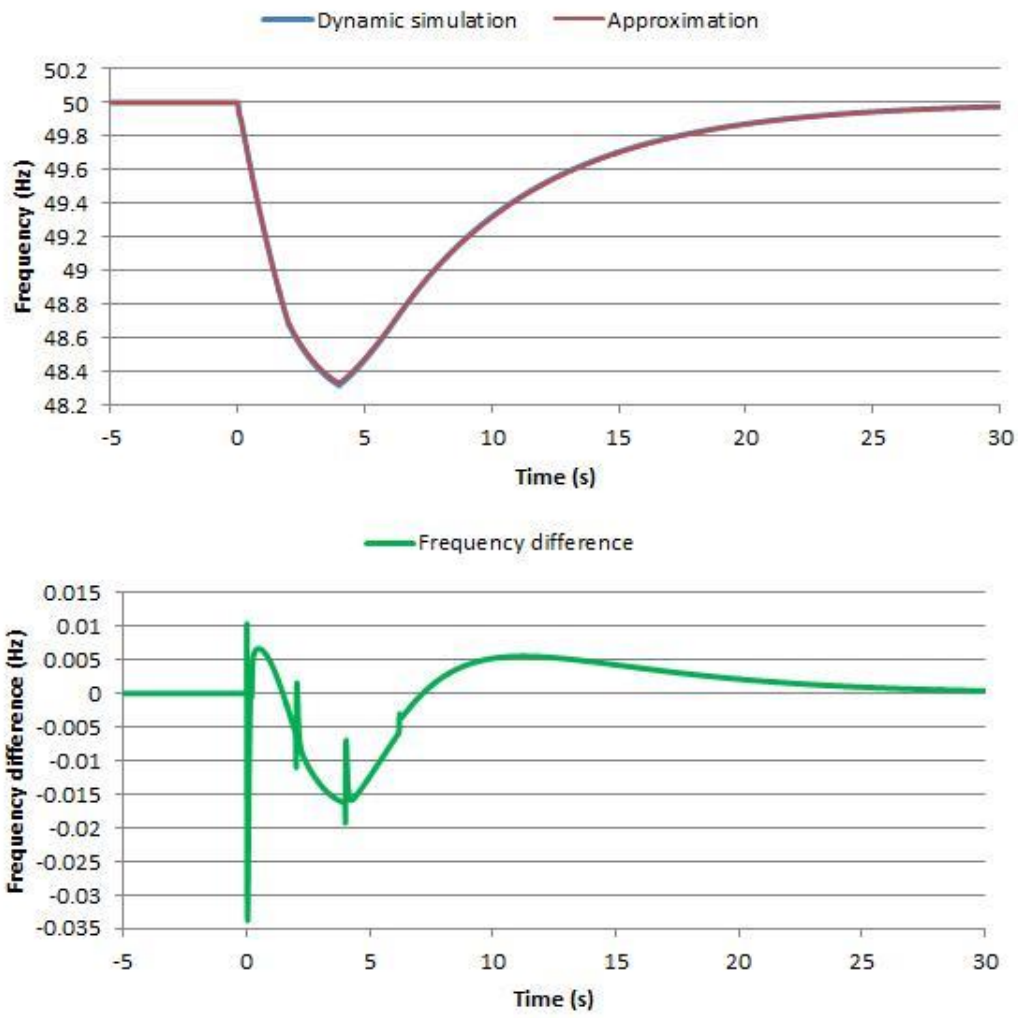

Fig. 5.5. Comparison of frequency trajectories for a loss of 200 MW generation with system frequency control services.

5.6 Conclusions

This chapter presented the development of the mathematical model for frequency responses in generation-load imbalance events. Firstly, the fundamental dynamic model of the system frequency was built based on the traditional swing equation. Secondly, different factors affecting frequency trajectories were studied and modelled including system disturbances (e.g., loss of load or loss of generator), load relief factor, the inertial response of rotating machines, and various types of system

frequency support services. Finally, these models were combined to create the comprehensive frequency model.

The developed mathematical model has been validated through a number of case studies. In these case studies, the frequency profiles obtained using the developed model were compared to the dynamic frequency trajectories obtained from DIgSILENT PowerFactory simulation software. The results showed that the mathematical model can represent the system frequency accurately taking into consideration various types of frequency control services. The developed method helps to reduce the overall computing and simulation time as well as provides the platform to incorporate the adequacy assessment of system frequency responses with the steady-state under voltage and overload evaluations as presented in Chapter 4. It may also play a key role in determining primary reserve level as presented in Chapter 6.

Chapter 6

Risk Assessment of Primary Frequency Response and Reserve Requirement for Wind Integrated Power Systems

6.1 Introduction

This chapter presents an application of the risk-based approach proposed in Chapter 4 to determine the operating reserve requirements in the presence of high WPG penetration. A case study is carried out to evaluate the performance of the proposed approach.

Variability and uncertainty are not unique to wind generation. They also exist in aggregate power demand and supply resources and have always posed challenges for power system operators. Future demand cannot be perfectly predicted, motor loads and generator outputs can vary substantially in different time frames, and large power system equipment can fail at any given time without notice. Power system operators secure different amounts and types of operating reserves to compensate for these characteristics in order to serve load reliably and keep the system frequency stable. There are many different terms, definitions, and rules concerning what operating reserves entail. In this thesis, the term operating reserves is defined as the real power capability that can be given or taken in the operating timeframe to assist in generation and load balance and frequency control.

The types of operating reserves can be differentiated by the type of event they respond to, the timescale of the response and the direction (upward or downward) of the response. The first characterization of a reserve is the type of event it is responding to. Some forms of operating reserve are kept for continuous needs (non-events). Other operating reserves can be used to respond to either contingency events or longer timescale events. Contingencies are instantaneous failures such as the loss

of a generator or failure of a transmission line. Longer timescale events can include net load ramps and forecast errors that occur over a longer amount of time.

In addition to the type of event, reserves can be categorised by the response time required and the physical capabilities needed of the responding participant. For instance, some reserves are required to be generating at partial load to provide spinning reserve, others require AGC, and still others require portions of their reserve to be directly responsive to frequency deviations. According to NERC the difference between spinning and non-spinning reserves is that spinning reserves must be synchronised to the system while non-spinning reserves are not necessarily synchronised. Spinning reserves respond more quickly as they are already synchronised to the system. AGC is a capability whereby a centralised party (system operator) sends control signals directly to the resource on the desired output. Frequency responsive capabilities include governor systems that automatically adjust input when frequency deviations are sensed.

Reserves may also be categorised by whether more or less supply is needed. Upward response is required when there is less generation than load and can be attained by additional generating power or a reduction in participating loads. Downward response is required when there is more generation than load and can be attained by a reduction in generating power or an increase in participating loads. In this thesis, we use the response time to classify operating reserves into three categories including primary, secondary, and tertiary reserves as presented in Section 5.2.

As mentioned earlier in Chapter 2, wind energy is a variable resource with limited availability that changes in time (variability) and despite significant improvement of wind power forecasting it cannot be accurately predicted due to high uncertainty associated with future wind power values. At some stages, this variability and uncertainty may lead to significant load-generation imbalances resulting in large frequency deviations, which in turn, may cause unwanted load shedding (or, in some cases, lead to a system black-out). In addition, due to the asynchronism characteristic

of WPG, large wind penetration may also deteriorate the adequacy of PFR and the current practices used for determining primary reserves under low system inertia and insufficient number of machines providing frequency control, especially in small and isolated power systems. The adequacy of PFR is defined as the capability of power system reserves to prevent frequency from dropping below a certain limit [12].

The total system inertia plays an important role to limit RoCoF as well as frequency nadir. Increasing integration of non-synchronous converter-based generations such as WPG may reduce the inertial response leading to an increase in RoCoF, leaving insufficient time for PFR to deploy and arrest frequency deviations. If RoCoF is high enough, it can trigger the generator's RoCoF protection tripping additional generators, which in turn increases the severity of the frequency deviation, and may lead to the system blackout. Fig. 6.1 shows an example of how inertia affects system frequency responses [86]. Low inertia also increases the phase shift during system disturbances, which in turn may affect operation of power electronics in particular operation of line commutated converters and phase lock loop (PLL) oscillators with the consequential impact on power generation or HVDC transmission. Therefore, it is important to secure a sufficient provision of system inertia.

This chapter proposes a novel approach to evaluate the adequacy of primary frequency response in a power system with significant WPG. This approach is based on the risk assessment method presented in Chapter 4. Firstly, for fast evaluation of PFR adequacy without performing dynamic simulations the mathematical model of frequency trajectory in frequency excursion events developed in Chapter 5 is used. The evaluated risk of primary frequency response inadequacy is then included in a security-constrained economic dispatch to determine the primary reserve requirement. The effectiveness of the proposed approach is illustrated by its application to a test system under different scenarios.

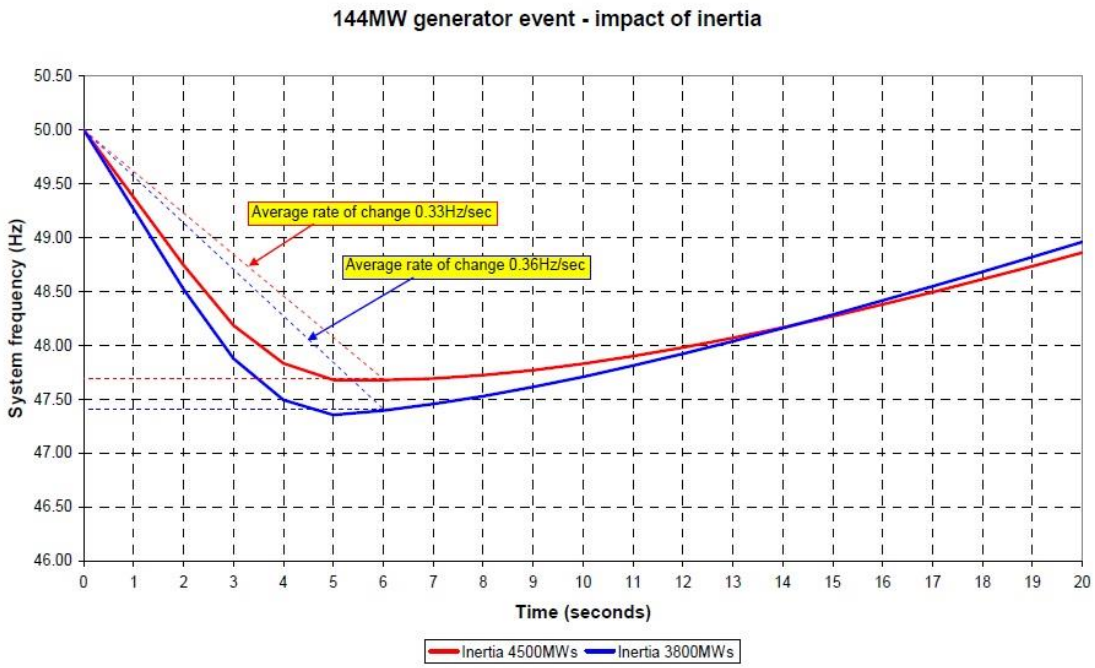

Fig. 6.1. Illustration of inertia impact on system frequency responses.

6.2 Risk assessment of primary frequency response and reserve requirement for power systems with high wind penetration

To evaluate the adequacy of primary frequency response, we use the risk assessment approach presented in Chapter 4. The PFR inadequacy risk is calculated by Equations (4.8)-(4.14). After evaluating the adequacy of PFR, the resulted risk given by Equation (4.8) will then be used to determine the primary reserve requirement by co-optimizing with energy in a security-constrained economic dispatch in order to minimise the expected operation cost (EOC) given by

$$EOC = CoE + Risk + CoPR \tag{6.1}$$

where CoE is the cost of energy – the product of energy price ($/MWh) and energy demand (MWh); and CoPR is the cost of primary reserve – the product of reserve price ($/MWh) and reserve demand (MWh).

6.3 Case study

6.3.1 Case description

A case study is performed to evaluate the proposed risk assessment approach. The test case system S1 is a small islanded power system with characteristics similar to the Tasmanian power network shown in Appendix B. The total installed generation capacity of the system is 2.9 GW with 2.2 GW of hydro, 400 MW of gas, and 300 MW of wind generation. The power demand of S1 is approximately in the range of 800-1700 MW [76]. It is connected to a larger power system S2 (maximum demand 9000 MW) via a single monopolar HVDC link with a capacity to transfer maximum 500 MW of power and minimum 50 MW of power in both direction. The HVDC link is also equipped with a frequency controller allowing it to transfer frequency control services between the two systems subjected to the margins between its power flow and transfer limits.

Figs. 6.2, 6.3 and 6.4 show the system hourly pre-dispatch/forecast data for the next 24 hours sourced from [87]. Due to specific characteristics of the predominantly hydro-power system and its small size, the capability of providing fast frequency response in S1 is limited resulting in high cost of primary reserve, as can be seen in Fig. 6.4. In contrast, the cost of the primary reserve in S2 is much lower due to the dominance of thermal generation units that represent much cheaper sources of service in this system. In addition, the WPG level of S2 is negligible in comparison with the system size. The system inertia and capability of providing fast frequency responses are also strong. As a result, the reserve requirement for S2 is always set to the size of its largest online generator (550MW) and the PFR inadequacy risk of S2 is assumed to be negligible.

The study objective is to determine the interconnection flow (negative for import to and positive for export from S1) and the primary reserve requirement for S1 for each hour so that the operation cost of the two systems is minimised using the

approach proposed in Section 6.2. The results will then be compared with two other methods for primary reserve determination:

- Method A: $Reserve = P_{gen\_max}$, which is the size of the largest online generator. This is one of the most common practices to schedule the amount of operating reserves so that the system will be able to withstand the outage of any single generating unit without the need of load shedding [72].
- Method B: $Reserve = P_{gen\_max} + 3 \times \sigma_{netload}$ as proposed in [72] where $\sigma_{netload}$ is the standard deviation of net-load (demand minus wind generation) forecasting error given by

$$\sigma_{netload} = \sqrt{\sigma_l^2 + \sigma_w^2} \tag{6.2}$$

The main objective of this method is to set the reserve amount so that it can cover the loss of the largest infeed as well as 99.73% of the possible net load forecast errors.

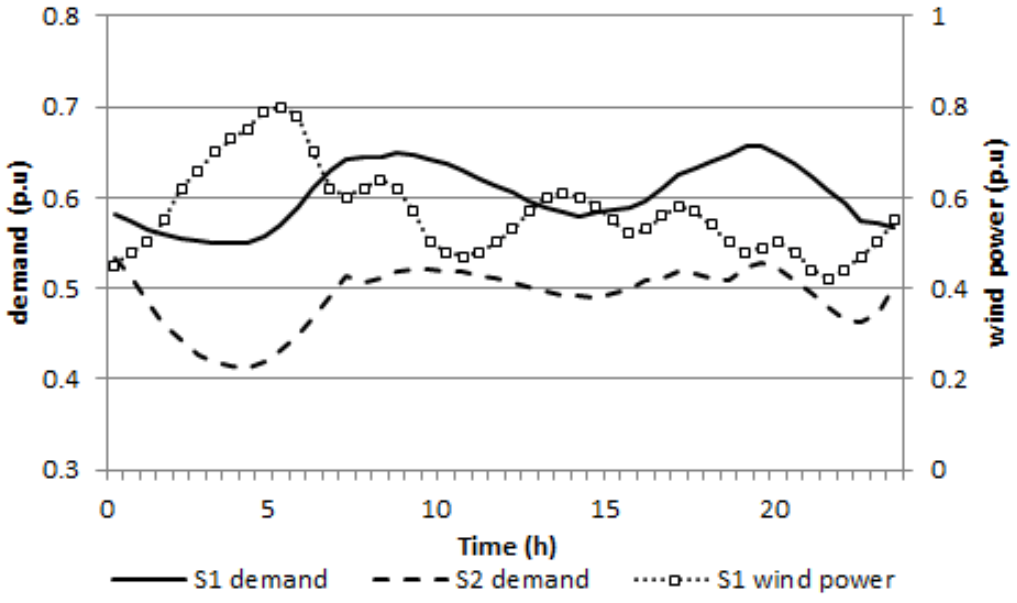

Fig. 6.2. Normalised forecast demand and WPG. The base values of S1 demand, S2 demand and S1 wind power are 1700 MW, 9000 MW and 300 MW, respectively.

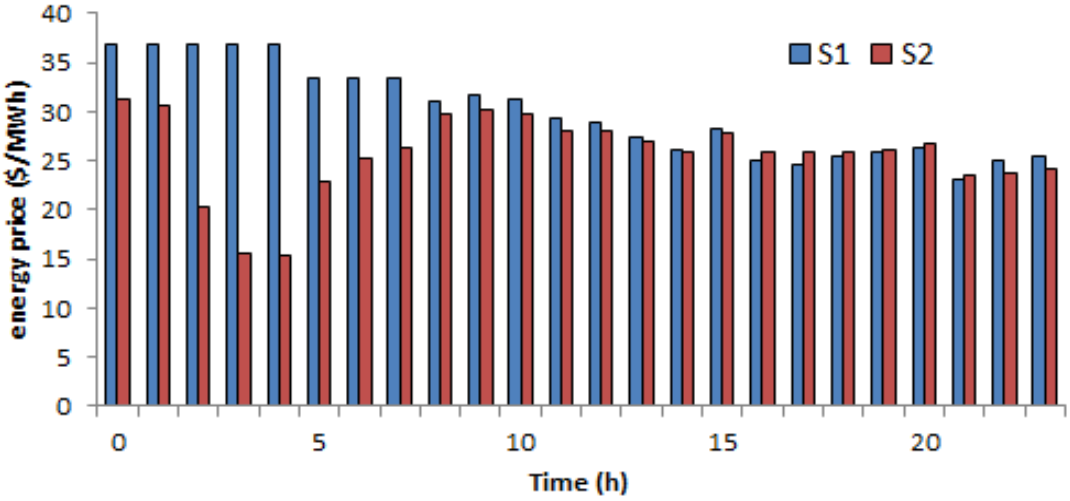

Fig. 6.3. Hourly forecast energy prices.

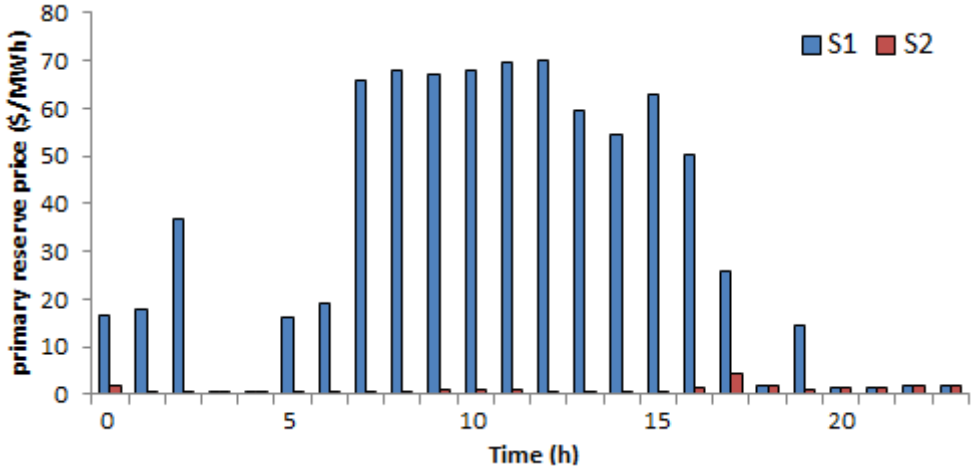

Fig. 6.4. Hourly forecast primary reserve prices.

The contingency probabilities for S1 are calculated as explained in Section 4.3.2. The outage replacement rates of the system components are determined based on the reliability data of the Tasmanian power network provided by TasNetworks. It is assumed that the failure probability of the interconnection link is zero. Load forecast errors are given by Equation (4.11) with a = 1. Wind generation forecast errors are given by Equation (4.10) with $\alpha = 0.01$ and $\beta = 0.16$ based on the data of 1-hour WPG forecast in a region with a diameter of 360 kilometres [73]. Due to the

small size of the test system it is assumed that the wind speeds at all wind farms in S1 are the same at any given moment.

The system nominal frequency is 50Hz. The primary frequency control is activated once the system frequency drops below 49.85 Hz, and it take 6 seconds to reach its maximum value. This corresponds to the fast rise frequency control ancillary service (R6 FCAS) in Australia [78]. There are three under-frequency relay settings for the period of the primary control shown in Table 6.1. These settings are similar to the automatic under-frequency load shedding configuration used in [77]. The load relief factor is k = 1. The UIC is $12,500/MWh, which is the MPC often used in reliability studies in Australia [75].

Table 6.1 Under frequency relay setting

Relay	Load shedding block size (%)	Frequency threshold 1 (Hz)	Time delay 1 (s)	Frequency threshold 2 (Hz)	Time delay 2 (s)
1	10	47.8	0.2	-	-
2	10	47.5	0.2	47.8	10
3	10	47.2	0.2	47.5	2

6.3.2 Result evaluation

6.3.2.1 Determination of reserve requirement

Fig. 6.5 compares the hourly dispatch outcomes in terms of the EOC for the next 24 hours obtained using the proposed optimised approach against Method A and Method B. As can be seen, the optimised approach provides the least expensive solution for all 24 hours and can save up to 1.5% of EOC compared to the other two methods. This saving is rather modest due to a number of reasons. Firstly, as the size of S2 is much bigger than S1, its CoE accounts for more than 80% of the total EOC. Secondly, the saving is achieved by optimizing the primary reserve requirement and PFR inadequacy risk for S1 only, whereas the primary reserve amount of S2 is fixed and its PFR inadequacy risk is negligible as explained in Section 6.3.1. If the WPG

level in S2 is large enough, the same optimization approach can be applied to S2 and bigger saving can be achieved. Meanwhile Method A (which sets the primary reserve amount equal to the largest online generator) results in the most expensive solution in 15 hours.

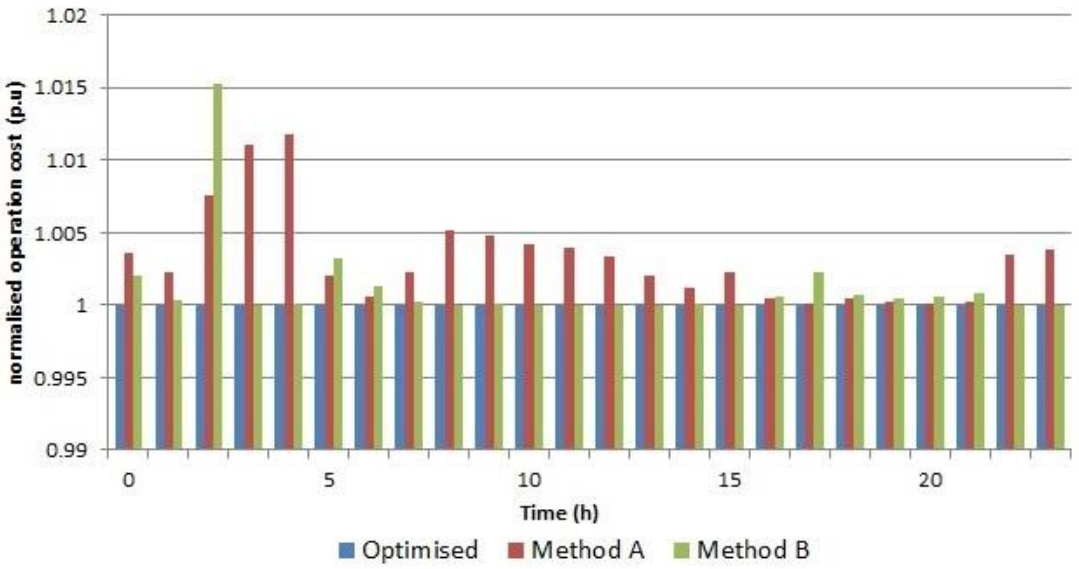

Fig. 6.5. Hourly expected operation costs obtained with the three approaches. These costs have been normalised based on the expected cost obtained with the proposed optimised approach.

Fig. 6.6 shows the hourly dispatch outcomes including the interconnection flow and the S1 primary reserve provision. As can be seen, the energy price plays an important role in determining the interconnection flow. For example, from hour 16 to 21 the interconnection flow is set to its maximum exporting level of 500 MW (S1 exports energy to S2) to take the advantage of cheaper energy prices in S1. At this level of export, S1 can also access lower cost source of primary reserve in S2 as the HVDC interconnection link can transfer up to 450 MW of reserve from S2 to S1. On the other hand, from hour 0 to 9, energy is imported from S2 to S1 as the energy price in S2 during this period is much lower than in S1.

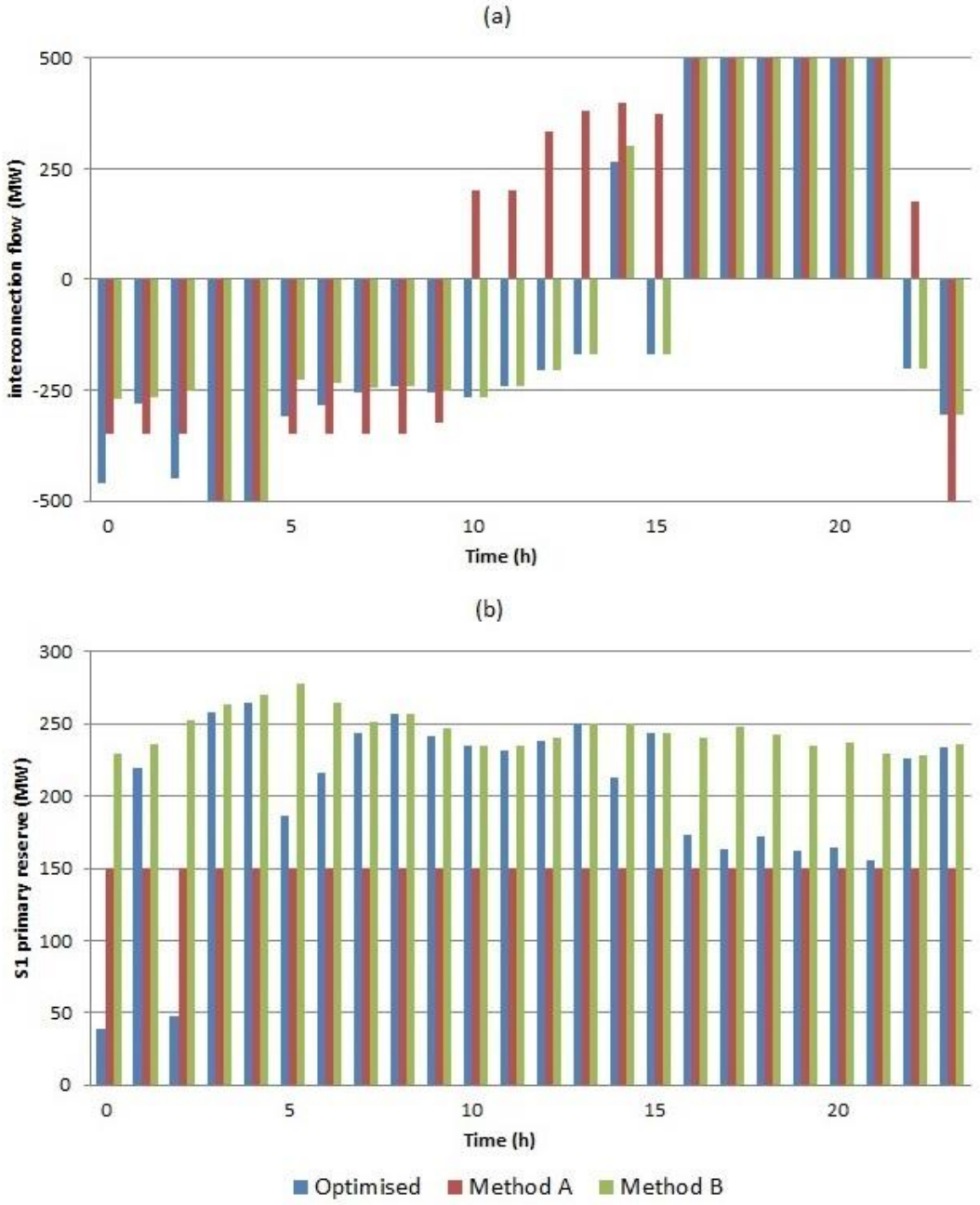

Fig. 6.6. (a) Interconnection flows and (b) S1 primary reserve provisions obtained with the three approaches.

However, the amount of power imported might be limited to provide room for transferring reserve from S2 to S1 when needed as reserve price in S1 is often much higher than in S2. For example, during hour 2, the interconnection flow is set at

279.55 MW, 350 MW and 264.03 MW to provide room for 219.45 MW, 150 MW and 235.97 MW of reserve, respectively, using the optimised approach, Method A and Method B, respectively. In contrast, during the next two hours, 3 and 4, the interconnection flow is set to its maximum importing level of 500 MW (S1 imports 500 MW from S2) using any of the three approaches as the difference between the reserve prices in S1 and S2 is very small compared to the difference between the energy prices in the two systems. During hour 15 the interconnection flow does not follow the sign of the difference in the energy prices. In this period, although the energy price in S2 is lower than in S1, the interconnection flow is set to be positive or in other words, S1 exports energy to S2. The reason is that during this period the difference in energy price between the two systems is very small while the cost of reserve and the PFR inadequacy risk in S1 are high.

Fig. 6.6 also shows that the reserve does not always need to cover the loss of the largest generator. For example, during hour 0 and 2, the optimised reserve amounts for S1 are 39.02 MW and 47.93 MW, respectively. The reason is that during these periods, the cost of providing primary reserve in S1 is higher than the benefit of having additional reserve. In contrast, in a number of cases, such as from hour 7 to 13, the S1's primary reserve is set very close to its maximum value to reduce the system PFR inadequacy risk.

6.3.2.2 Impact of the installed wind power capacity

Fig. 6.7 shows how the total expected cost of operation for the next 24 hours obtained with the optimised approach varies as a function of the installed wind power capacity. It is assumed that the pre-dispatch data are still the same while the installed capacity varies. These results show that the total operation cost increases as the installed capacity increases. This is a rather expected result as higher installed wind power capacities would lead to higher wind forecasting errors, and hence to higher system uncertainty. This may also reduce the number of synchronous generators online leading to a decrease in system inertia. As a result, the system PFR inadequacy risk increases and a larger reserve provision is required, as can be seen in Fig. 6.8.

However, we should note that with the higher installed wind power capacity, the energy price may drop [88]-[90], and a hence lower operation cost might be achieved. Additional WPG also reduces CO_2 emissions, which in turn, could be translated into additional economic benefits.

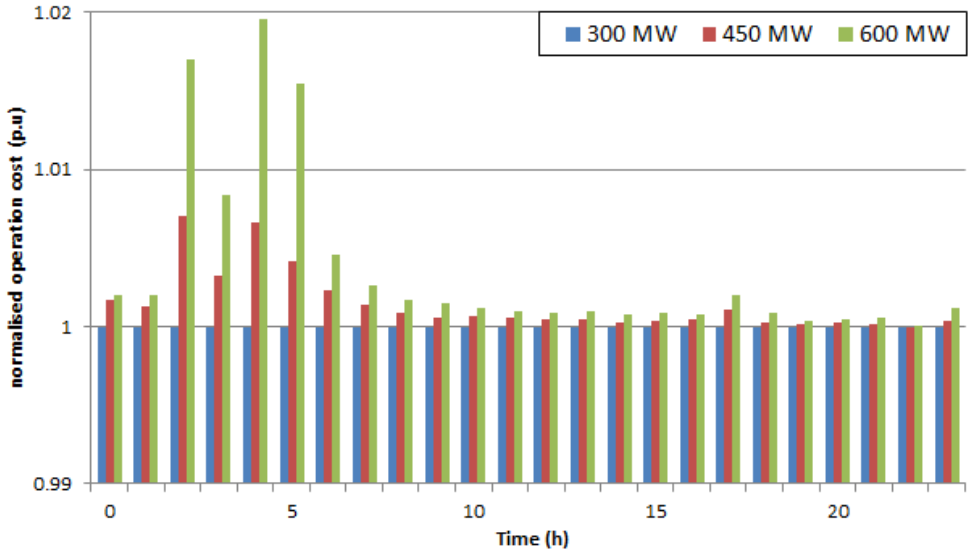

Fig. 6.7. Hourly expected operation costs obtained with the proposed optimization approach for three different levels of installed wind power capacity. These costs are normalised with the base cost = cost associated with the case having 300 MW of installed wind

6.3.2.3 Impact of the system inertia

Fig. 6.9 shows how the total expected cost of operation for the next 24 hours obtained with the optimised approach varied as a function of the system inertia. A minimum level of inertia is secured for each case. In this study, we do not consider the cost of inertia. As can be seen, the operation cost reduces as the minimum system inertia increases. In reality, increasing inertia incurs costs. In order to increase power system inertia, we can either operate generators on low load mode or dispatch synchronous condenser units to the grid. The former method may result in the generators operating away from their efficient rating, which leads to an increase in generation (fuel) cost. It may also increase the maintenance cost and reduce a plant's

lifecycle as it may not have been designed for prolonged operation at low loading. The latter method incurs the cost of running synchronous condensers including energy drawn from the grid and maintenance cost. However, at present no electrical power system in the world has implemented a market or incentive based reward for providing inertia service [14], [91], [92].

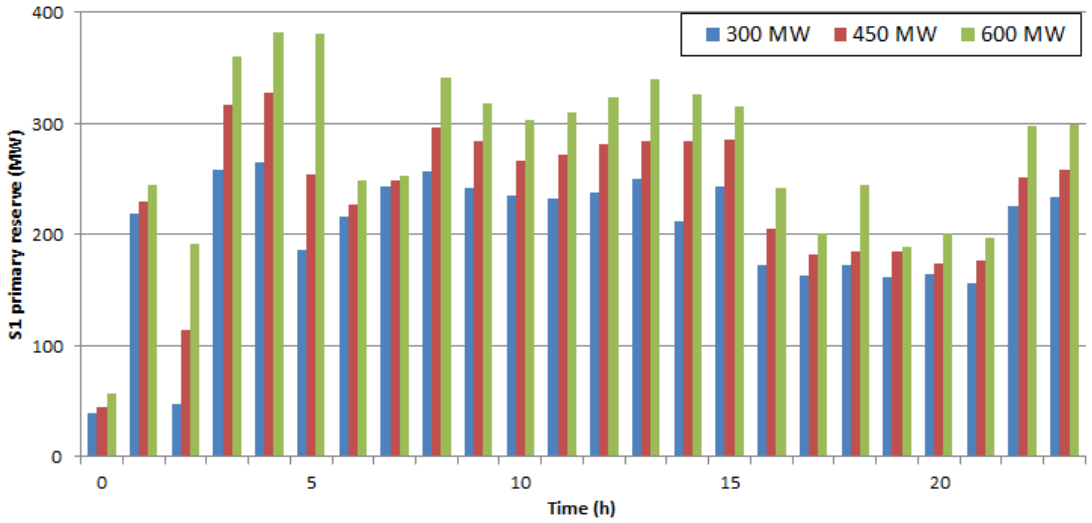

Fig. 6.8. Variation of S1 primary reserve provision as a function of the installed wind power capacity.

Although converter-based wind turbines have no inherent inertial response, they are capable of injecting more active power into the grid using their converter controller in frequency deviation events. There are two types of frequency responses a wind turbine can provide: synthetic inertial and governor-like (frequency droop) responses. The former utilises the kinetic energy stored in the wind turbine (e.g., generator, gearbox and blades). The release of kinetic energy from a wind turbine can be controlled independently from the RoCoF. In theory, it can even deliver a larger inertial response than a traditional synchronous generator. This is a highly desirable characteristic especially for small power systems with limited capacity to supply frequency control ancillary services. In these systems, WPG can provide fast frequency support in the first few seconds after a frequency disturbance occur to improve RoCoF and to buy time for other generators to respond through their

governor systems. In a predominantly hydropower system, this may compensate for the initial reduction in power output, which is caused by pressure reduction due to opening of the wicket gate during the first few seconds [93].

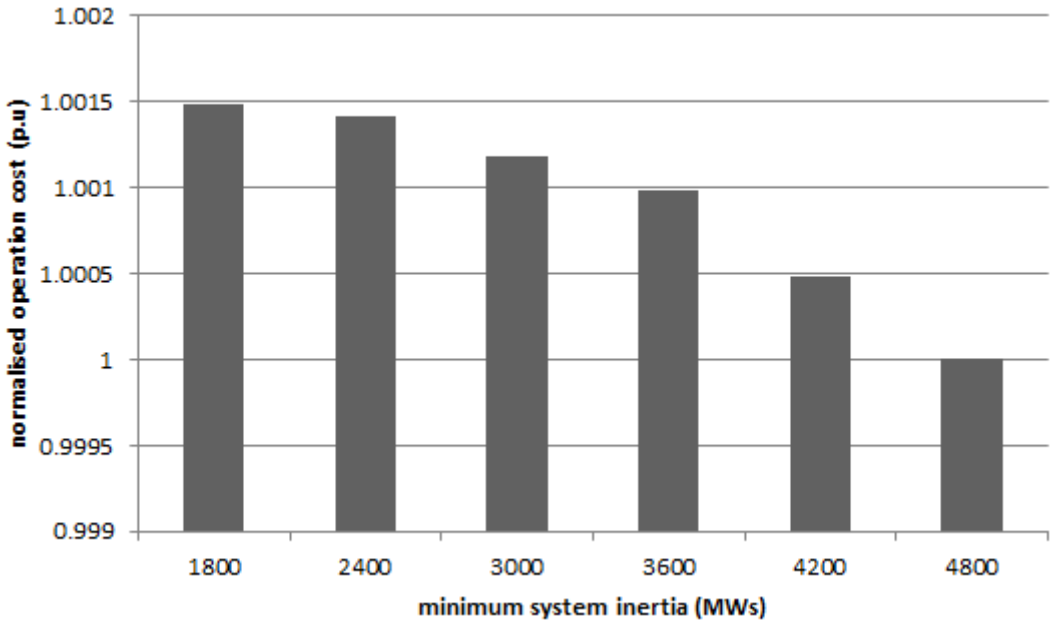

Fig. 6.9. Variation of the total expected operation cost for the next 24 hours as a function of the minimum system inertia. These costs are normalised with the base cost = cost associated with the case of 4800 MWs inertia.

However, if the wind turbine is operating below its rated wind speed when providing the synthetic inertial response, there will be a recovery period in which the turbine power output needs to be reduced for the turbine re-acceleration [23] [94], [95]. This period could delay the system frequency recovery or even cause a second frequency nadir, and hence requires more PFR [96]. Moreover, estimating the aggregated synthetic inertia from WPG is very challenging since there is uncertainty associated with the quantity of wind turbines being online for a given level of system wise wind generation [96], [97]. To achieve governor-like wind turbine responses the turbine is required to operate at a power output which is lower than the maximum output that can potentially be achieved at a given wind speed. In other words, wind power curtailment is required. This means that the turbine needs to operate at a sub-

optimal operating point, which represents additional costs that need to be considered [63]. Further studies are required to assess the benefits of utilizing the frequency response of wind turbines as well as potential consequences before it can be widely implemented in power system operating schemes and considered in new ancillary service market designs.

6.4 Discussion

Increasing penetration of intermittent power generation will inevitably lead to the need to reconsider potential impacts of frequency events on the power system security, especially for small and islanded systems which are more vulnerable to frequency deviations. This is particularly important as frequency violations may become more frequent due to fault-ride-through characteristics of wind turbines, increasing volume of unobservable distributed and PV installations and inevitable forecast errors. The proposed method was applied to a small power system; however, large systems with weak interconnections and high renewable energy penetration can exhibit a similar behaviour under outage conditions making this approach universal.

If the system of interest is part of the large interconnected network, the lost generation will be picked up by a large number of generating units outside the system's immediate control area. In this case, the pickup in generation will appear as an increase in power flow over the tie-line. To represent this situation, we could build a model of our own network, add an equivalent model of the large neighbouring system and place the swing bus in the equivalent system. The generator outside would then be modelled to represent the inertia and fault level of the neighbouring system. The inertia contribution of the neighbouring system would, however, be limited by the power transfer capability of the tie-line under various import/export scenarios. This inertial contribution can be taken into account when calculating the total aggregate effective inertia of the system of interest.

Finally, it should be noted that the proposed method can also be applied to Voltage-Sourced Converter (VSC) and Line-Commutated Converter (LCC) HVDC

schemes that include a frequency controller based either on the frequency error or the frequency differential between two systems. These schemes are capable of injecting significant amount of energy to the system of interest almost instantaneously when this system experiences low frequency conditions. To model this situation, we could represent the HVDC link as an equivalent generator contributing to frequency and voltage control.

6.5 Conclusion

This chapter presented a risk-based approach to assess the adequacy of primary frequency response, and then determined the primary reserve requirement taking into account WPG and load forecast uncertainties. The amount of primary reserve provision was determined so that the total system expected operation cost (i.e., the sum of the actual operating cost and the risk of primary frequency response inadequacy in terms of load interruption cost) was minimised.

A case study was performed to demonstrate the performance of the proposed approach. The results showed that the risk-based approach has potential to deliver lower cost dispatch solution compared with the traditional methods which set the reserve requirement based on the largest generator infeed or a combination of the largest generator and the maximum net load uncertainty. The proposed approach was also able to assess the impact of the installed wind power capacity and the total system inertia on the expected cost of operation. However, since reserve market structures are generally system-specific, the simulation results and conclusions are only reflective of the particular case-study. More studies should be done with different power systems, particularly different generation mix and reserve market structures, to evaluate the effectiveness of the proposed method.

Chapter 7

Conclusions and Suggestions for Future Work

7.1 Conclusions

The increasing penetration of WPG raises a number of challenges in power system operation due to its variability, uncertainty and asynchronism characteristics. The current system operation practices mostly based on deterministic criteria may no longer be adequate to deal with power systems with high penetration of WPG.

This thesis proposed a novel probabilistic risk-based approach to quantitatively assess security of a power system with large penetration of WPG for short-term operation planning. A risk index representing both the likelihood and consequences of contingencies and system uncertainty caused by WPG and load forecasting errors was used to evaluate the system security. The consequences of system failures were estimated using expected cost of load interruption. The proposed security assessment approach is concerned with steady-state voltage and overload evaluations, as well as frequency response adequacy. For illustrating purposes, the proposed approach was used to evaluate operation risks of the simplified model of the Tasmanian power system under a number of operation scenarios. The results showed that the integration of WPG significantly affected the system operation risk, especially risks associated with inadequacy of frequency responses. Impacts of different factors including load and WPG forecasting uncertainties, wind power penetration levels, and operating reserves on the system security were investigated. It also showed that the proposed approach could assist system operators in operation planning such as setting constraints for wind generation curtailments and determining operating reserves.

One of the main contributions of this thesis is the development of mathematical models of frequency trajectories so that the adequacy assessment of system frequency responses can be performed simultaneously with the steady-state voltage and overload evaluations in the overall system security assessment. It takes into account

both the system inertia and frequency control ancillary services. A series of simulations demonstrates the validity of the developed mathematical models. Increasing penetration of intermittent power generation, particularly WPG, will inevitably lead to the need to reconsider potential impacts of frequency events on the system security, especially for small and islanded systems which are more vulnerable to frequency deviations. This is particularly important as frequency violations may become more frequent due to fault-ride-through characteristics of wind turbines, increasing volume of unobservable distributed and PV installations and inevitable forecast errors. The proposed method was applied to a small power system; however, large systems with weak interconnections and high renewable energy penetration can exhibit a similar behaviour under outage conditions making this approach universal.

The proposed risk-based approach is then further developed to formulate an optimised security-constrained economic dispatch to determine the primary reserve requirement in a power system with significant wind generation. Firstly, the adequacy of primary frequency response is assessed. The amount of primary reserve provision is then determined so that the total system expected operation cost (i.e., the sum of the actual operating cost and the operation risk associated with inadequacy of primary frequency response capability in terms of load interruption cost) is minimised. A number of case studies are performed to demonstrate the performance of the proposed approach. The results show that the risk-based approach has potential to deliver lower cost dispatch solution compared with the traditional method setting the reserve requirement based on the largest generator infeed and the combined method which sets the reserve provision as the sum of the largest generator and the net load uncertainty. The proposed approach is also able to assess the impact of the installed wind power capacity and the total system inertia on the expected cost of operation.

To summarise, the main contributions of this thesis are as follows:

1. Development of a novel approach to quantitatively evaluate operation risk associated with steady-state under voltage, line overload and inadequacy of system frequency responses. It takes into consideration both the probability and severity of system uncertainty including random contingencies, load

and WPG forecast errors.

2. Development of an analytical method to represent system frequency approximately (accurately) in generation-load imbalance events without running dynamic simulation. The method helps to reduce the overall computing time and incorporate the adequacy assessment of system frequency responses with the steady-state under voltage and overload evaluations.

3. Development of a cost effective approach to determine operating reserve requirements. The approach co-optimises system operation risks associated with frequency response inadequacy and actual operating cost (i.e., cost of energy and reserve).

7.2 Suggestions for future work

In this section a few ideas that might enhance the proposed approaches are discussed.

1. This thesis does not consider the impact of initial conditions in calculating the probability of random contingencies and operating conditions (i.e., load and wind generation forecast errors). It is therefore more applicable for hourly operating decisions for the next day. The next step is to take into account the impact of initial conditions so that the methodology presented in this work can be used for operating decisions in real time knowing the initial condition.

2. In the case studies presented it was assumed that the random contingencies occur at a given period of time and that they do not extend beyond that period. This is, however, optimistic in real systems, and hence a more advanced model taking into account the multi-period effect of the contingencies could be used to improve the proposed approaches.

3. In this thesis, a wind farm is considered as a single generator with aggregated capacity in calculating its contingency probability for the sake

of simplicity. However, alternative approaches could be used to enhance the accuracy of the proposed method, e.g., using equivalent outage replacement rate of individual wind turbines.

4. In addition, advanced models of wind power forecast errors could be used to improve the performance of the proposed method.

5. The case studies presented in this thesis are based on the Tasmanian power network which is a small island system connected to a much larger system via an HVDC link. Therefore, the correlation between wind farms is assumed to be 100% (i.e., the wind speeds are the same at any wind farm). Large systems with more complex WPG scenarios and different wind correlations should be studied. Different generation mix and reserve market structures should also be considered.

6. The proposed security assessment method is also applicable to systems with AC interconnection lines. In that case, the external system will be taken into consideration as a slack bus with infinite inertia which is connected to the test system via tie-lines. But the inertia contribution of the external system to the test system's frequency control is limited by the tie-lines capability at various import/export scenarios. This inertia contribution will be taken into account when we calculate the total aggregate effective inertia of the test system.

7. In this work, we assume that frequency control services can be modelled by a linear ramp response. Practically, each frequency control service has a particular shape of response such as a step response for load shedding or an exponential response for governor actions. Future work may take this into account to better evaluate the adequacy of system frequency responses. The wind turbine capability of providing frequency support might also be taken into consideration.

8. In reality, operating reserves cater for both random generator outages and outage of any network component such as transmission line. For example,

in some topologies the outage of transmission lines might limit the operating reserves even though enough spare generation capacity is scheduled. Therefore, the impact of the transmission system on the power flows throughout the network and on the operation risk must be considered. An optimal power flow should be included with the proposed reserve determination approach to achieve the overall optima considering the transmission constraints. Generator ramping capability should also be considered.

9. The VOLL value takes a very important role in the results of the proposed approaches. In the thesis, this value is assumed to be constant. However, in reality it should be presented as a distribution curve as there is always a stack with more expensive available generation and depending on actual shortage the price might be much lower.
10. Future work will be interesting to include PV integration (along with WPG) for similar study.

Appendix A

Basic Probability Concepts

A.1 Random variable and its distribution

A random event can be represented using a random variable. Given a continuous random variable *X*, the probability of *X* being not larger than a real number *x* is a function of *x*. This function is called the cumulative distribution function *F(x)* of the random variable *X*, which can be expressed in the following form:

$$F(x) = \int_{-\infty}^{x} f(x)dx \tag{A.1}$$

where $f(x)$ is the probability density function. Obviously

$$f(x) = \frac{dF(x)}{dx} \tag{A.2}$$

The probability of *X* lying between *a* and *b* is given by

$$P(a \le X \le b) = \int_{a}^{b} f(x)dx \tag{A.3}$$

For a discrete random variable, its probability density function can be expressed as

$$p_k = P(X = x_k) \quad k = 1,2,\ldots \tag{A.4}$$

and its cumulative probability distribution function is

$$F(x_k) = P(X \le x_k) \quad k = 1,2,\ldots \tag{A.5}$$

The relationship between the density and cumulative distribution functions of a discrete random variable is given by

$$F(x_k) = \sum_{i \le k} p_i \quad k = 1,2,\ldots \tag{A.6}$$

$$p_k = F(x_k) - F(x_{k-1}) \tag{A.7}$$

A.2 Four important distributions in risk assessment

A.2.1 Exponential distribution

The exponential distribution is a single-parameter distribution. Its density function is given by

$$f(x) = \lambda e^{-\lambda x} \qquad (x \geq 0) \tag{A.8}$$

The cumulative distribution function is given by

$$F(x) = 1 - e^{-\lambda x} = \lambda x - \frac{(\lambda x)^2}{2!} + \frac{(\lambda x)^3}{3!} - \cdots \tag{A.9}$$

These two functions are shown in Figs. A.1 and A.2. When $\lambda x \ll 1$, Equation (A.9) is approximated by

$$F(x) = \lambda x \tag{A.10}$$

The mean and variance of the exponential distribution are $1/\lambda$ and $1/\lambda^2$, respectively.

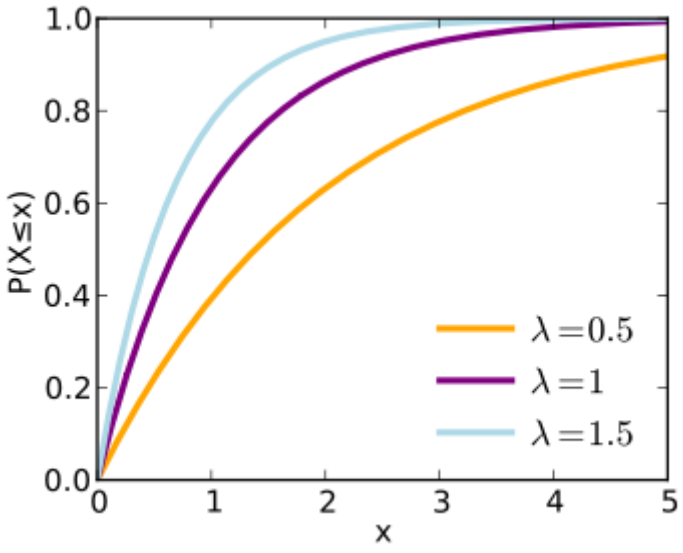

Fig. A.1. Cumulative distribution function of exponential distribution.

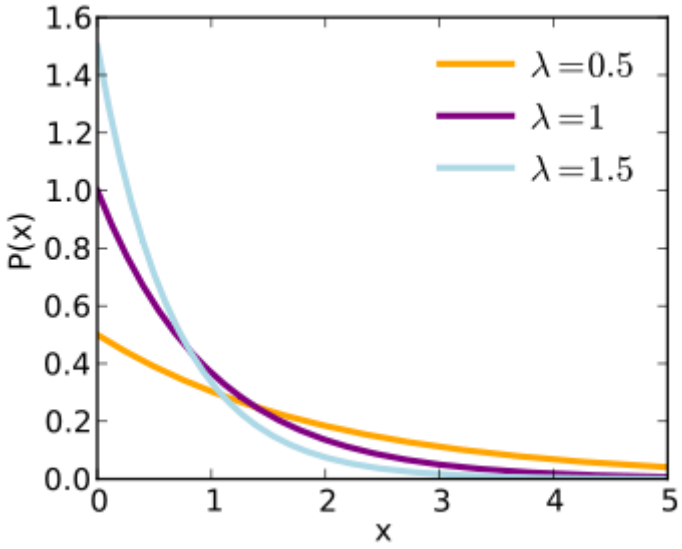

Fig. A.2. Probability density function of exponential distribution.

A.2.2 Normal distribution

The density function of normal distribution is given by

$$f(x) = \frac{1}{\sigma\sqrt{2\pi}} \exp\left[-\frac{(x-\mu)^2}{2\sigma^2}\right] \qquad (-\infty \le x \le \infty) \qquad (A.11)$$

where μ and σ^2 are the mean and variance of the normal distribution. By using the following substitution,

$$z = \frac{x-\mu}{\sigma} \qquad (A.12)$$

Equation (A.11) can be rewritten as

$$f(z) = \frac{1}{\sqrt{2\pi}} \exp\left[-\frac{z^2}{2}\right] \qquad (-\infty \le z \le \infty) \qquad (A.13)$$

This is the density function of the standard normal distribution. Fig. A.3 shows the probability density function of the normal distribution.

There is no explicitly analytical expression for the cumulative distribution function of the normal distribution. The area *Q(z)* under the standard normal density function shown in Fig. A.4 can be found from the following polynomial approximation for $z \ge 0$:

$$Q(z) = f(z)[b_1 t + b_2 t^2 + b_3 t^3 + b_4 t^4 + b_5 t^5] \quad (A.14)$$

where

$$t = \frac{1}{1 + rz}$$

$$r = 0.2316419$$

$$b_1 = 0.31938153$$

$$b_2 = -0.356563782$$

$$b_3 = 1.781477937$$

$$b_4 = -1.821255978$$

$$b_5 = 1.330274429$$

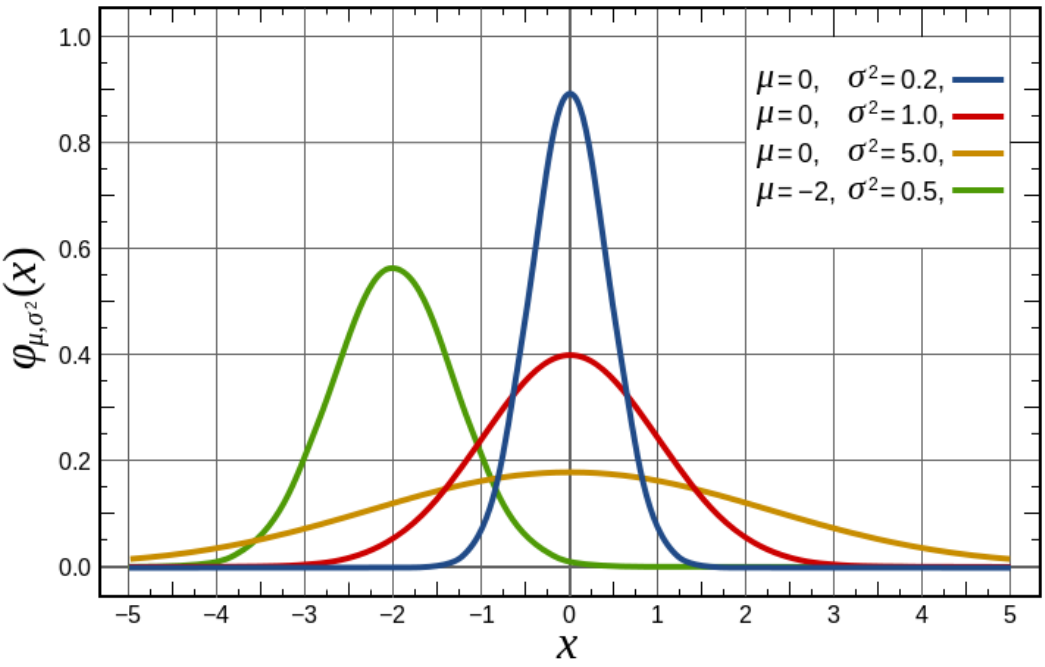

Fig. A.3. Probability density function of normal distribution.

The maximum error of Equation (A.14) is smaller than 7.5×10^{-8}. Fig. A.5 shows some examples of the cumulative distribution function of the normal distribution.

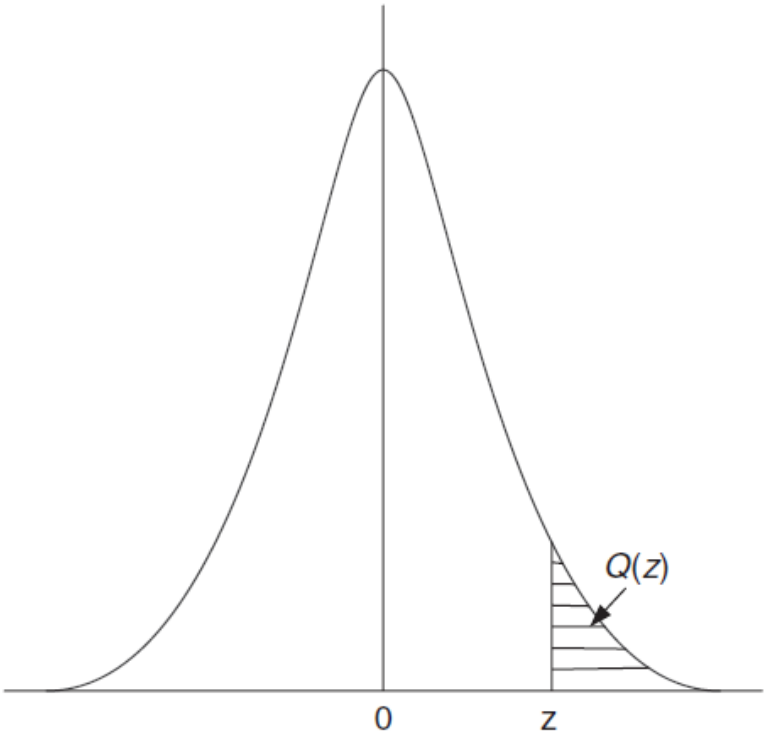

Fig. A.4. Area under standard normal density function.

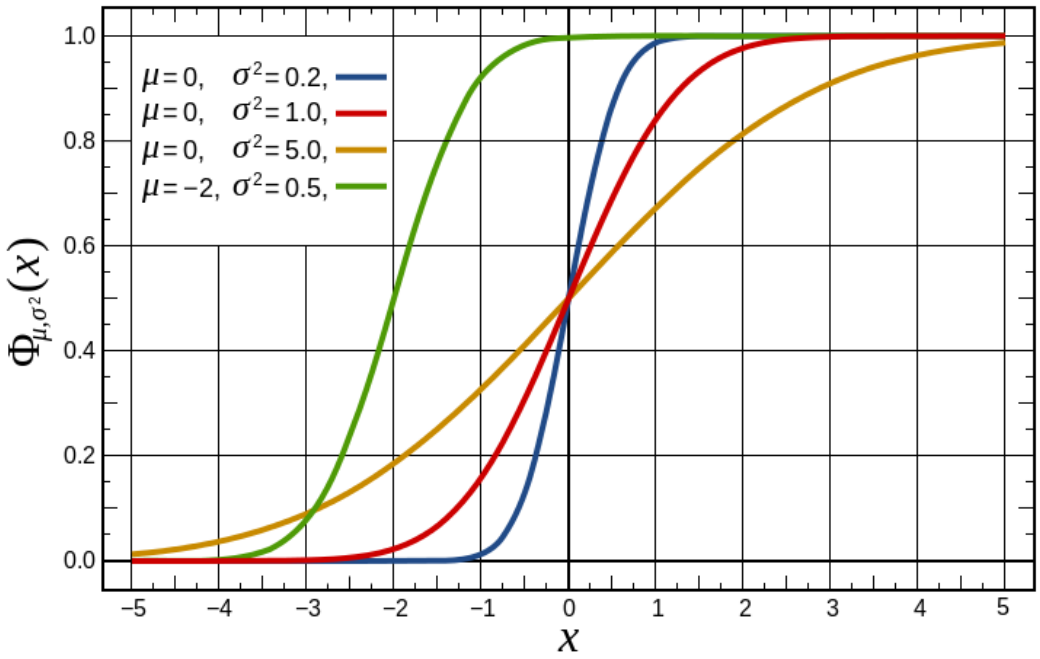

Fig. A.5. Cumulative distribution function of normal distribution.

A.2.3 Log-normal distribution

The density function of the log-normal distribution is

$$f(x) = \frac{1}{x\sigma\sqrt{2\pi}} \exp\left[-\frac{(\ln x - \mu)^2}{2\sigma^2}\right] \qquad (x > 0) \qquad (A.15)$$

It is important to recognise that μ and σ^2 are not the mean and variance of the log-normal distribution. The mean, *E(x)*, and variance, *V(x)*, of the log-normal distribution are given by

$$E(x) = \exp(\mu + \frac{\sigma^2}{2}) \qquad (A.16)$$

$$V(x) = \exp(2\mu + \sigma^2)[\exp(\sigma^2) - 1] \qquad (A.17)$$

If the mean and variance of the log-normal distribution are pre-specified, the parameters μ and σ^2 in Equation (A.17) are calculated by

$$\mu = \ln\left[\frac{E^2}{\sqrt{(V + E^2)}}\right] \qquad (A.18)$$

$$\sigma^2 = \ln\left[\frac{V + E^2}{E^2}\right] \qquad (A.19)$$

Examples of the probability density and cumulative distribution functions of the log-normal distribution are shown in Figs. A.6 and A.7, respectively.

A.2.4 Weibull distribution

The density function of Weibull distribution is given by

$$f(x) = \frac{kx^{k-1}}{\lambda^k} exp\left[-(\frac{x}{\lambda})^k\right] \qquad (\infty > x \geq 0, k > 0, \lambda > 0) \qquad (A.20)$$

The cumulative distribution function is

$$F(x) = 1 - exp\left[-(\frac{x}{\lambda})^k\right] \qquad (\infty > x \geq 0, k > 0, \lambda > 0) \qquad (A.21)$$

Figs. A.8 and A.9 show examples of these two functions.

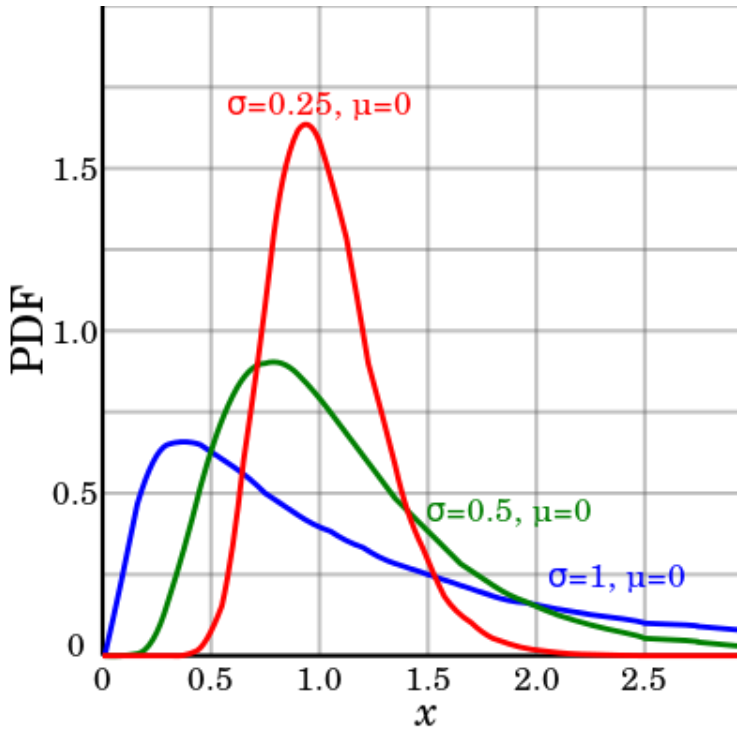

Fig. A.6. Probability density function of log-normal distribution.

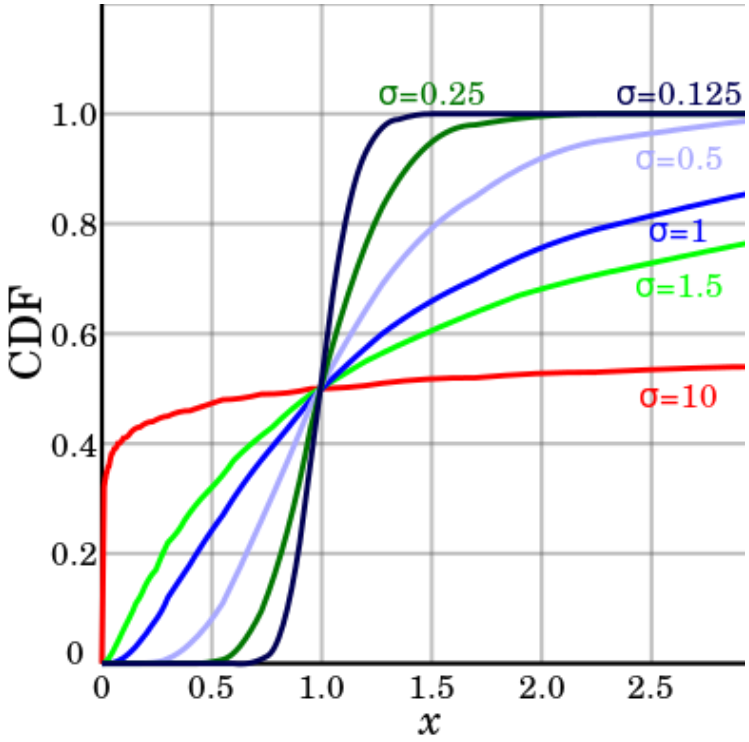

Fig. A.7. Cumulative distribution function of log-normal distribution.

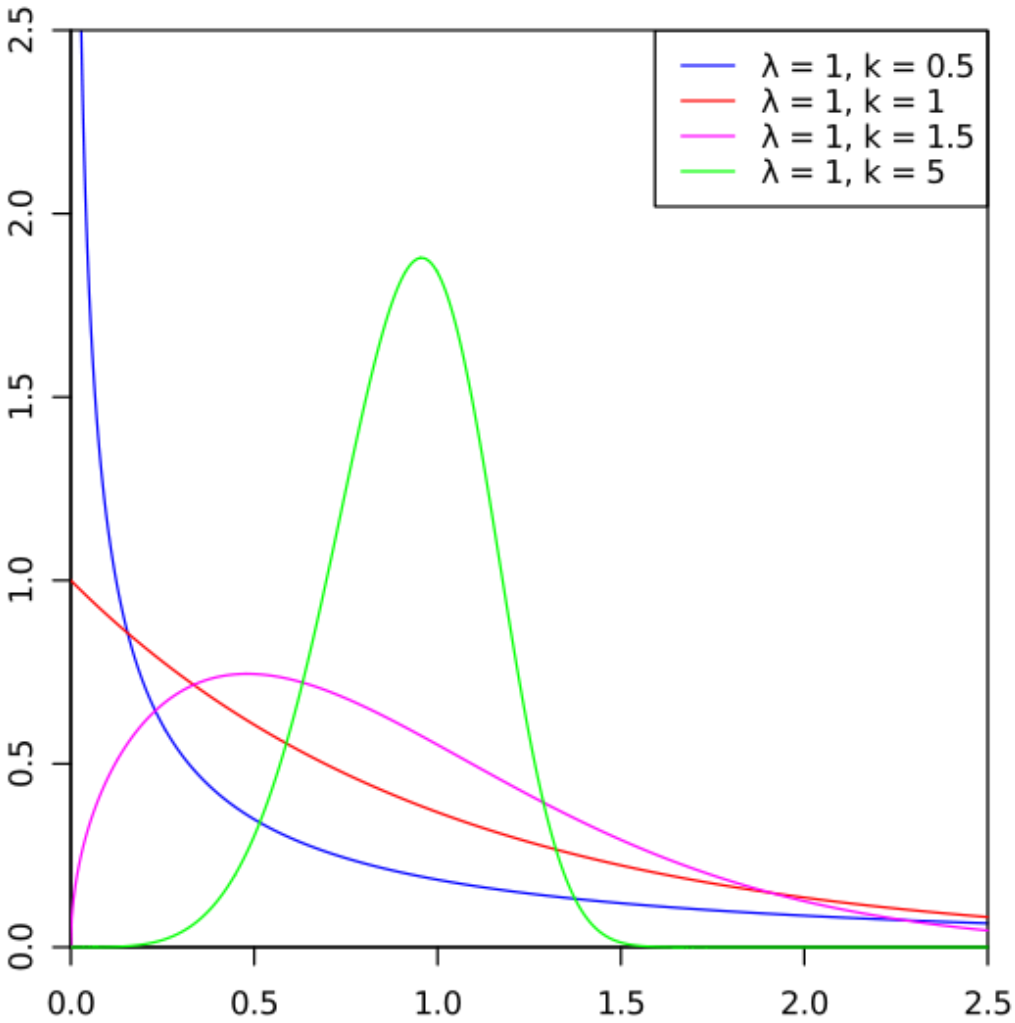

Fig. A.8. Probability density function of Weibull distribution.

The mean and standard deviation of the Weibull distribution can be calculated from the scale λ and shape k parameters as follows:

$$\mu = \lambda\Gamma\left(1+\frac{1}{k}\right) \tag{A.22}$$

$$\sigma^2 = \lambda^2\left[\Gamma\left(1+\frac{2}{k}\right) - \Gamma^2\left(1+\frac{1}{k}\right)\right] \tag{A.23}$$

where Γ is the gamma function which is defined as

$$\Gamma(x) = \int_{-\infty}^{\infty} t^{x-1}e^{-t}dt \tag{A.24}$$

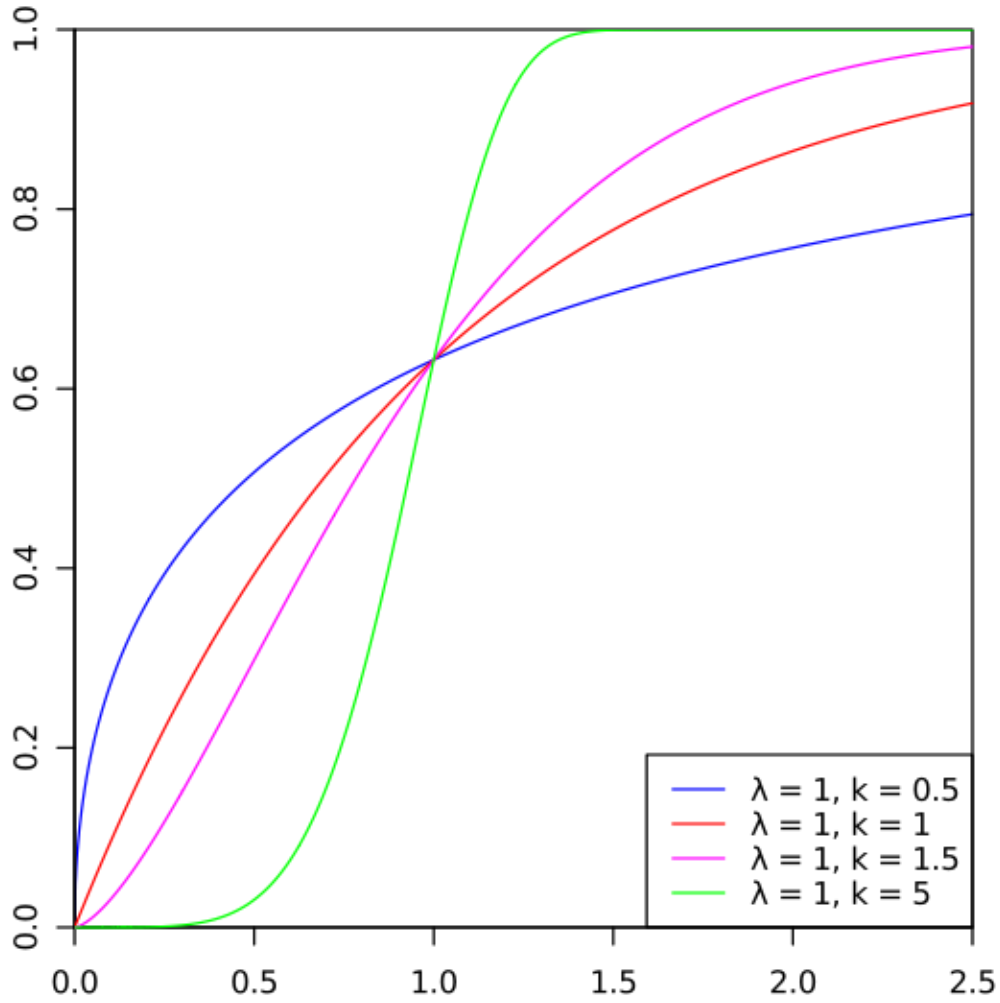

Fig. A.9. Cumulative distribution function of Weibull distribution

There is no analytical expression for the scale λ and shape k using the mean μ and the standard deviation σ but the following method can be used. By eliminating λ from Equations (A.31) and (A.32) we have

$$\frac{\Gamma\left(1+\frac{2}{k}\right)}{\Gamma^2\left(1+\frac{1}{k}\right)} = 1 + \frac{\sigma^2}{\mu^2} \qquad (A.25)$$

Using an approximate expression of the gamma function [98], Equation (A.25) can be rewritten as

$$\frac{(1+\frac{2}{k})^{(0.5+\frac{2}{k})}\times e^{-(1+\frac{2}{k})}\times\left[1+\frac{1}{12}(1+\frac{2}{k})\right]}{\sqrt{2\pi}\left[(1+\frac{1}{k})^{(1+\frac{2}{k})}\times e^{-(2+\frac{2}{k})}\times\left[1+\frac{1}{12}(1+\frac{1}{k})\right]^2\right]}=1+\frac{\sigma^2}{\mu^2} \qquad (A.26)$$

Equation (A.26) can be solved to obtain k using a bifurcation algorithm. Then λ is calculated from Equation (A.23) using k and σ.

A.3 Numerical characteristics

Random variables can be simply described using one or more parameters that are called numerical characteristics. The most useful numerical characteristics in risk evaluation are the mathematical expectation (mean), variance or standard deviation, covariance, and correlation coefficients. As a matter of fact, a risk is a mean value, whereas a standard deviation of an estimate is often used as an indicator of the accuracy in Monte Carlo simulation.

A.3.1 Mathematical expectation

If a random variable X has the probability density function $f(x)$ and the random variable Y is a function of X, that is, $y=y(x)$, then the mathematical expectation or mean value of Y is defined as

$$E(X)=\int_{-\infty}^{+\infty}y(x)f(x)dx \qquad (A.27)$$

As a special case of the general definition, the mean of the random variable X is

$$E(X)=\int_{-\infty}^{+\infty}xf(x)dx \qquad (A.28)$$

For a discrete random variable, Equations (A.27) and (A.28) can be rewritten as

$$E(Y)=\sum_{i=1}^{n}y(x_i)p_i \qquad (A.29)$$

$$E(X)=\sum_{i=1}^{n}x_ip_i \qquad (A.30)$$

A.3.2 Variance and standard deviation

The variance of a random variable *X* with the probability density function *f(x)* is given by

$$V(X) = E\{[X - E(X)]^2\} = \int_{-\infty}^{+\infty} [X - E(X)]^2 f(x) dx \qquad (A.31)$$

The variance is an indicator for the dispersion degree of possible values of *X* from its mean. The square root of the variance is known as the standard deviation and is often denoted as $\sigma(X)$. If *X* is a discrete random variable, its variance is given by

$$V(X) = \sum_{i=1}^{n} [x_i - E(X)]^2 p_i \qquad (A.32)$$

A.3.3 Covariance and correlation coefficients

Given an *N*-dimension random vector $(X_1, X_2, \ldots, X_N)$, the covariance between any two elements X_i and X_j is defined as

$$c_{ij} = E\{[X_i - E(X_i)][X_j - E(X_j)]\} = E(X_i X_j) - E(X_i)E(X_j) \qquad (A.33)$$

The covariance is often expressed as $cov(X_i, X_j)$. The covariance between an element and itself is its variance

$$cov(X_i, X_i) = V(X_i) \qquad (A.34)$$

The correlation coefficient of X_i and X_j is defined as

$$\rho_{ij} = \frac{cov(X_i, X_i)}{\sqrt{V(X_i)V(X_j)}} \qquad (A.35)$$

The absolute value of ρ_{ij} is smaller or equal to 1.0. If $\rho_{ij} = 0$, then X_i and X_j are not correlated. If $\rho_{ij} > 0$, then X_i and X_j are positively correlated. If $\rho_{ij} < 0$, then X_i and X_j are negatively correlated.

Appendix B

Single Line Diagram of Tasmanian Power Network

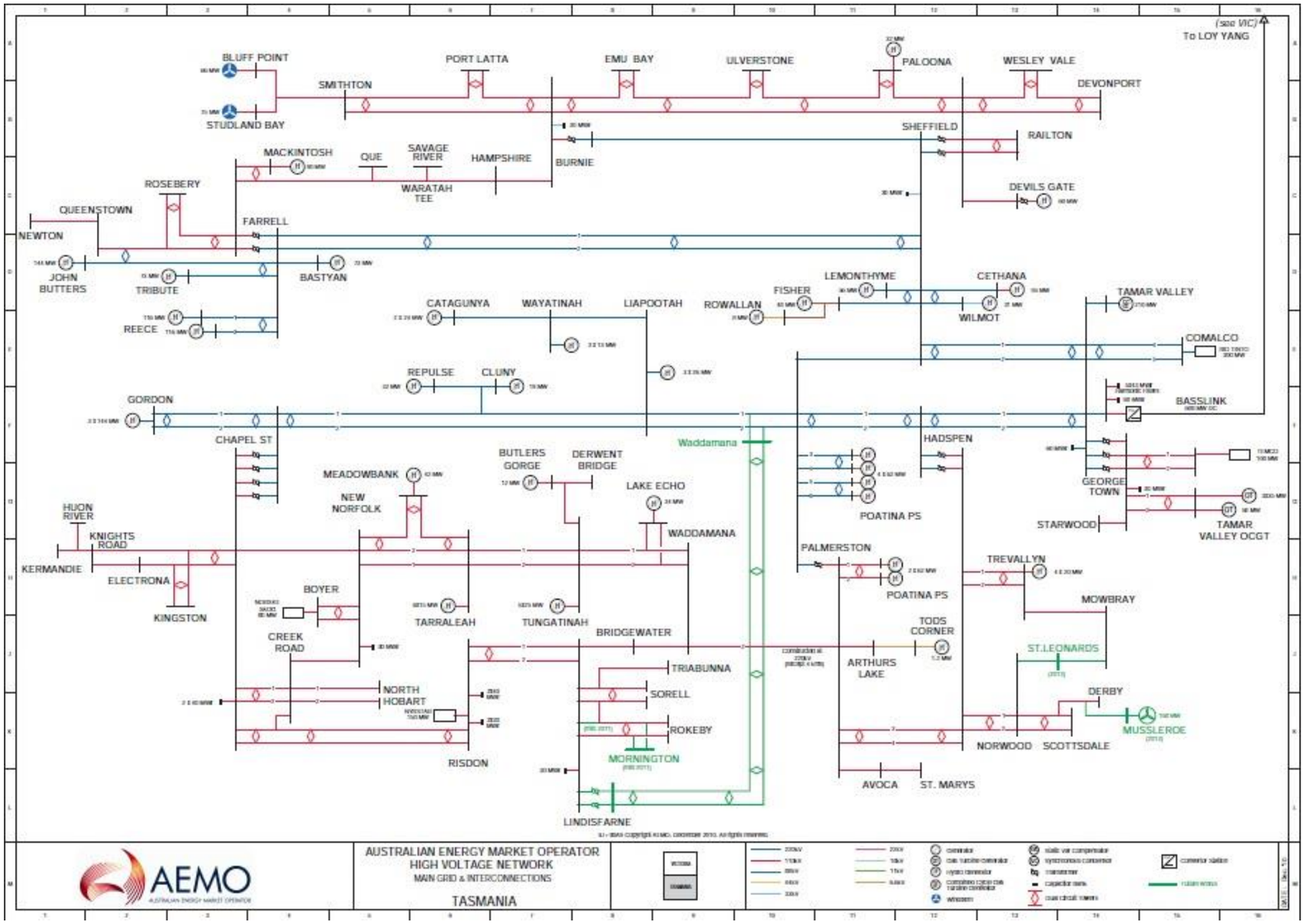

List of References

[1] World Wind Energy Association (WWEA), "2014 Half-year report," 2014.

[2] American Wind Energy Association (AWEA), "U.S. Wind industry thrid quarter 2014 market report," Oct. 2014.

[3] European Wind Energy Association (EWEA), "Wind in power: 2013 European statistics," Feb. 2014.

[4] Australian Energy Market Operator (AEMO) and ElectraNet, "Renewable energy integration in South Australia," Oct. 2014.

[5] Australian Energy Market Operator (AEMO), "Integrating renewable energy - Wind integration studies report," 2013.

[6] CIGRE Working Group C4.601, "Review of the current status of tools and techniques for risk-based and probabilistic planning in power systems," Oct. 2010.

[7] W. Li and J.Q. Zhou, "Probabilistic reliability assessment of power system operations," *Electric Power Components and Systems*, vol. 36, pp. 1102-1114, 2008.

[8] J. D. McCalley, S. Asgarpoor, L. Bertling, R. Billinton, H. Chao, J. Chen, et al., "Probabilistic security assessment for power system operations," in *Proc. 2004 Power Engineering Society General Meeting*, 2004.

[9] CIGRE Working Group C4.601, "Review of on-line dynamic security assessment tools and techniques," 2007.

[10] F. Xiao and J. D. McCalley, "Risk-based multi-objective optimization for transmission loading relief strategies," in *Proc. 2007 IEEE PES General Meeting*, 2007.

[11] Wenyuan Li, "Risk assessment of power systems: Models, methods, and applications," Vancouver, Canada, John Wiley & Sons, 2004.

[12] Electric Power Reserach Institute (EPRI), "Frequency response adequacy and assessment: Global industry practices and potential impact of changing generation mix," Dec. 2012.

[13] T. Acker, "IEA Wind task 24 - Integration of wind and hydropower systems," National Renewable Energy Laboratory (NREL), Dec. 2011.

[14] E. Ela, M. Milligan, and B. Kirby, "Operating reserves and variable generation," National Renewable Energy Laboratory (NREL), Aug. 2011.

[15] D. Jones, S. Pasalic, and M. Negnevitsky, "Determining the frequency stability boundary of the Tasmanian system due to voltage disturbances," in *Proc. 2012 IEEE POWERCON*, Auckland, NZ, 2012.

[16] J. Kennedy, B. Fox, T. Littler, and D. Flynn, "Validation of fixed speed induction generator models for inertial response using wind farm measurement," *IEEE Trans. Power Systems*, vol. 26, pp. 1454-1461, Aug. 2012.

[17] K. Kim, T. Van, D. Lee, S. Song, and E. Kim, "Maximum output power tracking control in variable-speed wind turbine systems considering rotorinertial power," *IEEE Trans. Industrial Electronics*, vol. 60, pp. 3207-3217, Aug. 2013.

[18] L. Ruttledge, N. Miller, J. O'Sullivan, and D. Flynn, "Frequency response of power systems with variable speed wind turbines," *IEEE Trans. Sustainable Energy*, vol. 3, pp. 683-691, Oct. 2012.

[19] Lei Wu and D. G. Infield, "Towards an assessment of power system frequency support from wind plant—Modeling aggregate inertial response," *IEEE Trans. Power Systems*, vol. 28, pp. 2283-2291, Aug. 2013.

[20] Lei Wu and D. G. Infield, "Power system frequency management challenges – a new approach to assessing the potential of wind capacity to aid system frequency stability," *IET Renewable Power Generation*, vol. 8, pp. 733-739, Sep. 2014.

[21] M. F. M. Arani and E. F. El-Saadany, "Implementing virtual inertia in DFIG-based wind power generation," *IEEE Trans. Power Systems*, vol. 28, pp. 1373-1384, May 2013.

[22] M. Wang-Hansen, R. Josefsson, and H. Mehmedovic, "Frequency controlling wind power modeling of control strategies," *IEEE Trans. Sustainable Energy*, vol. 4, pp. 954-959, Oct. 2013.

[23] Electric Reliabilit Council of Texas (ERCOT), "Future ancillary services in ERCOT," 2013.

[24] R. Springer, "Vestas presentation," presented at *the NREL and EPRI Workshop: Active power control from wind power*, Denver, CO, US, Jan. 2011.

[25] R. Allan and R. Billinton, "Probabilistic assessment of power systems," *Proceedings of the IEEE*, vol. 88, pp. 140 - 162, 2000.

[26] R. Billinton and R. Mo, "Deterministic/probabilistic contigency evaluation in composite generation and transmission systems," in *Proc. 2004 Power Engineering Society General Meeting*, 2004

[27] R. Moreno, D. Pudjianto, and G. Strbac, "Future transmission network operation and design standards to support a low carbon electricity system," in *Proc. 2010 IEEE Power and Energy Society General Meeting*, 2010.

[28] C.I.F. Agreira, S.M.F de Jesus, S.L de Figueiredo, C.M. Ferreira, J.A.D. Pinto, and F.P.M. Barbosa, "Probabilistic steady-state security assessment of an electric power system using a Monte Carlo approach," in *Proc. 2006 Universities Power Engineering Conference*, pp. 408 - 411, 2006.

[29] J. Ma, Z. Huang, P.C. Wong, and T. Ferryman, "Probabilistic vulnerability assessment based on power flow and voltage distribution," in *Proc. 2010 IEEE PES Transmission and Distribution Conference and Exposition*, New Orleans, LA, US, 2010.

[30] S. Meliopoulos, D. Taylor, C. Singh, F. Yang, S.W. Kang, and G. Stefopoulos, "Comprehensive power system reliability assessment," Power Systems Engineering Research Center, 2005.

[31] F. Xiao and J. D. McCalley, "Power system risk assessment and control in a Multiobjective framework.," *IEEE Trans. Power Systems*, vol. 24, pp. 78-85, 2009.

[32] F. Xiao and J. D. McCalley, "Risk-based security and economy tradeoff nalysis for real-time operation," *IEEE Trans. Power Systems*, vol. 22, pp. 2287-2288, 2007.

[33] H. Wan, J. D. McCalley, and V. Vittal, "Risk based voltage security assessment," *IEEE Trans. Power Systems*, vol. 15, pp. 1247-1254, 2000.

[34] J. D. McCalley, A. A. Fouad, V. Vittal, A. A. Irizarry-Rivera, B. L Agrawal, and R. G. Farmer, "A risk-based security index for determining operating limits in stability-limited electric power systems," *IEEE Trans. Power Systems*, vol. 12, pp. 1210-1219, 1997.

[35] J. D. McCalley, V. Vittal, H. Wan, Y. Dai, and N. Abi-Samra, "Voltage risk assessment " in *Proc. 1999 IEEE Power Engineering Society Summer Meeting*, 1999.

[36] J. D. McCalley, V. Vittal, and N. Abi-Samra, "An overview of risk based security assessment " in *Proc. 1999 IEEE Power Engineering Society Summer Meeting*, 1999.

[37] M. Ni, J. D. McCalley, V. Vittal, S. Greene, C. Ten, V. S. Ganugula, et al., "Software implementation of online risk-based security assessment," *IEEE Trans. Power Systems*, vol. 18, pp. 1165-1172, 2003.

[38] M. Ni, J. D. McCalley, V. Vittal, and T. Tayyib, "Online risk-based security assessment," *IEEE Trans. Power Systems*, vol. 18, pp. 258-265, 2003.

[39] Y. Dai, J. D. McCalley, N. Abi-Samra, and V. Vittal, "Annual risk assessment for overload security.," *IEEE Trans. Power Systems*, vol. 16, pp. 616-623, 2001.

[40] D. S. Kirschen and D. Jayaweera, "Comparisons of risk-based and deterministic security assessments," *IET Generation, Transmission and Distribution*, vol. 1, pp. 527-533, 2007.

[41] D. S. Kirschen, D. Jayaweera, D. P. Nedic, and R. N. Allan, "A probabilistic indicator of system stress," *IEEE Trans. Power Systems*, vol. 19, pp. 1650-1657, 2004.

[42] D. S. Kirschen, K. R. W. Bell, D. P. Nedic, D. Jayaweera, and R. N. Allan, "Computing the value of security," *IEE Proceedings Generation, Transmission and Distribution*, vol. 150, pp. 673-678, 2003.

[43] M. A. Rios, D. S. Kirschen, D. Jayaweera, D. P. Nedic, and R. N. Allan, "Value of security: Modeling time-dependent phenomena and weather conditions," *IEEE Trans. Power Systems*, vol. 17, pp. 543-548, 2002.

[44] H. Mohammed and C.O. Nwankpa, "Stochastic analysis and simulation of grid-connected wind energy conversion system," *IEEE Trans. Energy Conversion*, vol. 15, pp. 85 - 90, 2000.

[45] Yi Zhang, A.A Chowdhury, and D.O. Koval, "Probabilistic wind energy modeling in electric generation system reliability assessment," *IEEE Trans. Industry Applications*, vol. 47, pp. 1507 - 1514, 2011.

[46] P. Meibom, R. Barth, B. Hasche, H. Brand, C. Weber, and M. O'Malley, "Stochastic optimization model to study the operational impacts of high wind penetrations in Ireland " *IEEE Trans. Power Systems*, vol. 26, pp. 1367 - 1379 2011

[47] R. Billinton, B. Karki, R. Karki, and G. Ramakrishna, "Unit commitment risk analysis of wind integrated power systems," *IEEE Trans. Power Systems*, vol. 24, pp. 930-939, May 2009.

[48] R. Karki, S. Thapa, and R. Billinton, "A simplified risk-based method for short-term wind power commitment," *IEEE Trans. Sustainable Energy*, vol. 3, pp. 498-505, Jul. 2012.

[49] R. Billinton, R. Karki, and A. K. Verma, "Reliability and risk evaluation of wind integrated power systems (Reliable and sustainable electric power and energy systems management)," Wiley, 2013.

[50] F. Bouffard, F.D. Galiana, and A.J. Conejo, "Market-clearing with stochastic security - Part I: Formulation," *IEEE Trans. Power Systems*, vol. 20, pp. 1818 - 1826, 2005.

[51] F. Bouffard, F.D. Galiana, and A.J. Conejo, "Market-clearing with stochastic security - Part II: Case studies," *IEEE Trans. Power Systems*, vol. 20, pp. 1827 - 1835, 2005.

[52] F. Bouffard and F.D. Galiana, "Stochastic security for operations planning with significant wind power generation," *IEEE Trans. Power Systems*, vol. 23, pp. 306 - 316, 2008.

[53] R. Doherty and M. O'Malley, "A new approach to quantify reserve demand in systems with significant installed wind capacity," *IEEE Trans. Power Systems*, vol. 20, pp. 587-595, May 2005.

[54] M. Black and G. Strbac, "Value of bulk energy storage for managing wind power fluctuations," *IEEE Trans. Energy Conversion*, vol. 22, pp. 197-205, Mar. 2007.

[55] G. Dany, "Power reserve in interconnected systems with high wind power production," in *Proc. 2001 IEEE Porto Power Tech Conference*, Porto, Portugal, Sep. 2001.

[56] S. Persaud, B. Fox, and D. Flynn, "Effects of large scale wind power on total system variability and operation: Case study of Northern Ireland," *Wind Engineering*, vol. 27, pp. 3-20, 2003.

[57] M. A. Ortega-Vaquez and D. S. Kirschen, "Assessing the impact of wind power generation on operating costs," *IEEE Trans. Smart Grid*, vol. 1, pp. 295-301, Dec 2010.

[58] M. A. Ortega-Vaquez and D. S. Kirschen, "Estimating the spinning reserve requirements in systems with significant wind power generation penetration," *IEEE Trans. Power Systems*, vol. 24, pp. 114-124, Feb. 2009.

[59] A. Papavasiliou, S.S. Oren, and E.P. O'Neill, "Reserve requirements for wind power integration: A scenario-based stochastic programming framework," *IEEE Trans. Power Systems*, vol. 26, pp. 2197 - 2206 2011

[60] M. A. Matos and R. j. Bessa, "Setting the operating reserve using probabilistic wind power forecasts," *IEEE Trans. Power Systems,* vol. 26, pp. 594-603, May 2011.

[61] M. Vrakopoulou, K. Margellos, J. Lygeros, and G. Andersson, "A probabilistic framework for reserve scheduling and N-1 security assessment of systems with high wind power penetration," *IEEE Trans. Power Systems,* vol. 28, pp. 3885-3896, Nov. 2013.

[62] E. Ela, V. Gevorgian, A. Tuohy, B. Kirby, M. Milligan, and M. O'Malley, "Market designs for the primary frequency response ancillary service—Part I: Motivation and design," *IEEE Trans. Power Systems*, vol. 29, pp. 421 - 431, Jan. 2014.

[63] H. Chavez, M. R. Hezamsadeh, and F. Carlsson, "A simplified model for predicting primary control inadequacy for nonresponsive wind power," *IEEE Trans. Sustainable Energy*, vol. 7, pp. 271 - 278, Jan. 2016.

[64] H. Chavez and R. Baldick, "Inertia and governor ramp rate constrained economic dispatch to assess primary frequency response adequacy," in *Proc. 2012 International Conference on Renewable Energies and Power Quality*, Spain, March 2012.

[65] Liisa Pottonen, "A method for the probabilistic security analysis of transmission grids," *Doctoral thesis*, Department of Electrical and Communications Engineering, Helsinki University of Technology, 2005.

[66] R. Billinton and R. Allan, "Reliability evaluation of power systems", 2nd ed., Springer, 1996.

[67] R. Billinton and R. N. Allan, "Reliability eveluation of engineering systems: Concepts and techniques", 2nd ed., New York and London, Plenum Press, 1992.

[68] R. Billinton and W. Li, "Reliability assessment of electric power system using Monte Carlo methods." New York and London, Plenum Press, 1994.

[69] R. Y. Rubinstein, "Simulation and Monte Carlo method." New York, Wiley, 1981.

[70] A. U. Haque, P. Mandal, and M. H. Nehrir, "A hybrid intelligent model for deterministic and quantile regression approach for probabilistic wind power forecasting," *IEEE Trans. Power Systems*, vol. 29, pp. 1663-1672, 2014.

[71] C. W. Potter and M. Negnevitsky, "Very short-term wind forecasting for Tasmanian power generation," *IEEE Trans. Power Systems*, vol. 21, pp. 965-972, May 2006.

[72] V. Silva, "Value of flexibility in systems with large wind penetration," *Doctoral thesis*, Imperial College London, University of London, London, UK, 2010.

[73] A. Fabbri, T. G. S. Roman, J. R. Abbad, and V. H. M. Quezada, "Assessment of the cost associated with wind generation prediction errors in a liberalized electricity market," *IEEE Trans. Power Systems*, vol. 20, pp. 1440-1446, 2005.

[74] W. Li, "Probabilistic transmission system planning." Singapore, Wiley, 2011.

[75] Reliability Panel AEMC, "Final report: Reliability standard and reliability settings review," The Australian Energy Market Commission, Sydney, Australia, 2010.

[76] Transend Network, "Transend annual planning report 2013," Transend Network, Tasmania, Australia, 2013.

[77] K. Mollah, M. Bahadornejad, and N. Nair, "Automatic under-frequency load shedding in New Zealand power system — A systematic review," in *Proc. 21st Australasian Universities Power Engineering Conference (AUPEC)*, Brisbane, QLD, Australia, Sept. 2011, pp. 1-7.

[78] Australian Energy Market Operator (AEMO), "ESOPP guide - FCAS constraint equations," Dec. 2009.

[79] J. J. Hargreaves and B. F. Hobbs, "Commitment and dispatch with uncertain wind generation by dynamic programming," *IEEE Trans. Sustainable Energy*, vol. 3, pp. 724-734, Oct. 2012.

[80] Australia Energy Market Commission (AEMC), "Rule determination - National electricity amendment (central dispatch and integration of wind and other intermittent generation) rule 2008," May 2008, p. 134.

[81] A. J. Wood and B. F. Wollenberg, "Power generation, operation and control." New York, US, John Wiley & Sons, 1996.

[82] G. Andersson, "Lecture notes - Dynamics and control of electric power systems," ETH Zurich, Feb. 2012.

[83] North American Electric Reliability Corporation (NERC), "Balancing and frequency control," Jan. 2011.

[84] Union for the Co-ordination of Transmission of Electricity (UCTE), "Operation Handbook", 2004.

[85] National Electricity Market Management Company (NEMMCO), "Dispatch of contingency frequency control ancillary services," Dec. 2003.

[86] National Electricity Market Management Company (NEMMCO), "Market ancillary service specifications - Final determination and report," May 2009.

[87] Australian Energy Market Operator (AEMO), " www.aemo.com.au/Electricity/Data".

[88] F. Nieuwenhout and A. Brand, "The impact of wind power on day-ahead electricity prices in the Netherlands," in *Proc. 8th International Conference on the European Energy Market (EEM)*, Zagreb, May 2011.

[89] Hoong Yan See Tao, A. K. Srivastava, R. L. Pineda , and P. Mandal, "Wind power generation impact on electricity price in ERCOT," in *Proc. 2012 IEEE Power and Energy Society General Meeting*, San Diego, CA, July 2012.

[90] J. C. Ketterer, "The impact of wind power generation on the electricity price in Germany," *Energy Economics*, vol. 44, pp. 270-280, July 2014.

[91] J. Riesz and I. MacGill, "Frequency control ancillary services - Is Australia a model market for renewable energy," in *Proc. 12th International workship on large-scale integration of wind power into power systems*, London, Oct. 2013.

[92] Pieter Tielens and Dirk Van Hertem, "The relevance of inertia in power systems," *Renewable and Sustainable Energy Reviews*, vol. 55, pp. 999-1009, Mar. 2016.

[93] Bureau of Reclamation, "Mechanical governors for hydroelectric units - Facilities, instructions, standards, and techniques," Jul. 2002.

[94] M. Fischer, S. Engelken, N. Mihov, and A. Mendonca, "Operational experiences with inertial response provided by type 4 wind turbines," *IET Renewable Power Generation*, vol. 10, pp. 17 - 24, Jan. 2016.

[95] Mohamed Asmine and Charles-Éric Langlois, "Field measurements for the assessment of inertial response for wind power plants based on Hydro-Québec TransÉnergie requirements," *IET Renewable Power Generation*, vol. 10, pp. 25-32, Jan. 2016.

[96] F. Teng and G. Strbac, "Assessment of the role and value of frequency response support from wind plants," *IEEE Trans. Sustainable Energy*, vol. 7, pp. 586 - 595, Apr. 2016.

[97] F. Teng, V. Trovato, and G. Strbac, "Stochastic scheduling with inertia-dependent fast frequency response requirements," *IEEE Trans. Power Systems*, vol. 31, pp. 1557 - 1566, Mar. 2016.

[98] Mathematics Manual Editing Group, "Mathematics manual." Beijing, People's Education Press, 1997.